

UNIVERSIDADE DE SÃO PAULO
CENTRO DE ENERGIA NUCLEAR NA AGRICULTURA

TATIANA NISHIDA MÁXIMO DA CRUZ

Root absorption and effects of ZnO nanoparticles on *Phaseolus vulgaris* plants

Piracicaba
2018

TATIANA NISHIDA MÁXIMO DA CRUZ

Root absorption and effects of ZnO nanoparticles on *Phaseolus vulgaris* plants

Dissertação apresentada no Centro de Energia Nuclear na Agricultura da Universidade de São Paulo, para obtenção do título de Mestre em Ciências

Área de Concentração: Química na Agricultura e no Ambiente

Orientador: Prof. Dr. Hudson Wallace Pereira de Carvalho

Piracicaba

2018

AUTORIZO A DIVULGAÇÃO TOTAL OU PARCIAL DESTE TRABALHO, POR QUALQUER MEIO CONVENCIONAL OU ELETRÔNICO, PARA FINS DE ESTUDO E PESQUISA, DESDE QUE CITADA A FONTE.

Dados Internacionais de Catalogação na Publicação (CIP)
Técnica de Biblioteca - CENA/USP

Cruz, Tatiana Nishida Máximo da

Absorção radicular e efeitos de nanopartículas de óxido de zinco em plantas de *Phaseolus vulgaris*. / Root absorption and effects of ZnO nanoparticles on *Phaseolus vulgaris* plants / Tatiana Nishida Máximo da Cruz; orientador Hudson Wallace Pereira de Carvalho. - - Piracicaba, 2018.

104 p. : il.

Dissertação (Mestrado – Programa de Pós-Graduação em Ciências. Área de concentração: Química na Agricultura e no Ambiente) – Centro de Energia Nuclear na Agricultura, Universidade de São Paulo, 2018.

1. Espectroscopia de raios X 2. Feijão 3. Fisiologia vegetal 4. Fluorescência de raios X
5. Morfologia vegetal 6. Nanopartículas 7. Química analítica 8. Radiação sincrotron I. Título.

CDU 620.3 : (631.811 + 546.47)

Elaborada por:

Marília Ribeiro Garcia Henyei

CRB-8/3631

Resolução CFB Nº 184 de 29 de setembro de 2017

To my wonderful family, and boyfriend,
for all the love and support.

ACKNOWLEDGMENTS

First, I thank God, for protecting and blessing me during these years.

I thank my supervisor, Prof. Dr. Hudson Wallace Pereira de Carvalho, for the guidance, for sharing his knowledge and for the many insightful conversations and comments that helped to improve my academic and scientific development.

I am grateful to Dr. Eduardo de Almeida, for the patience, support and sharing his experience on the development of XRF methodologies.

To Foundation for Research Support of São Paulo State (FAPESP) for granting my scholarship and the financial support for this research.

To Center for Nuclear Energy in Agriculture (CENA) and University of São Paulo for the opportunity to carry out this work. I also would like to thank all the staff for the support at anytime. Specially Prof. Dr. Lavres for supplying the equipment used for SPAD and leaf area analysis; Cleuza Pereira Cabral for sharing her experience and great happiness; Prof. Dr. Victor Vitorello and Profa. Dra. Helaine Carrer for supplying IRGA equipment for physiological analysis.

To LNLS for the beamtimes at XAFS2 beamline, and for the researchers Ana, Santiago and Junior for all the support on the preparation of the facility.

To EMBRAPA for supplying the seeds used on this research.

I would like to thank my lab mates, Joyce, Nadia, Susi, Eduardo, Geovani, Marcos, João, Lucas and Rafael for the cooperation, experimental support, fellowship and fun moments that we had in the laboratory.

My gratitude to Daniele Paschoal for the friendship, support and companionship.

Most important, I thank my family and friends that were always present in the happy and sad moments. Especially I would like to express my gratitude to my parents, Roberto e Meiri, my brother, Mateus, and my boyfriend, Júlio, for all the love, support, incentive and comprehension.

**“You can not hope to build a better world
without improving the individuals.
To that end, each of us must work for his
own improvement”
(Marie Curie, 1867-1934)**

ABSTRACT

CRUZ, T. N. M. da. **Root absorption and effects of ZnO nanoparticles on *Phaseolus vulgaris* plants**. 2018. 104 p. Dissertação (Mestrado) – Centro de Energia Nuclear na Agricultura, Universidade de São Paulo, Piracicaba, 2018.

Nanotechnology has been used in many fields. Nanoparticles are already found as a component of many products. However, the use of nanoparticles in agriculture is still a matter of concern because of its interaction with biological tissues. Aiming to evaluate NPs effects on *Phaseolus vulgaris* plants, this study investigated: how ZnO NPs dispersions are absorbed by plant roots; how it is translocated and accumulated in plant tissues; physiological and morphological effects, and compare results with ZnSO₄ solution. *In vivo* X-ray fluorescence spectroscopy revealed that source, NP size, concentration and coating with surfactants affect Zn release and uptake. Regardless the source, at high doses, there is a gradient of Zn concentration from root to shoot. *In vivo* X-ray absorption spectroscopy showed that Zn is taken up bound mainly to citrate and malate. Entire NPs were observed only in plants whose roots were injured. X-ray fluorescence microanalysis revealed that root to shoot Zn transport can occur through xylem and cortex, and both sources presented the same Zn distribution inside the stems. Infrared gas analysis showed a decrease in the water conductance, photosynthetic and transpiration rate after 48 hours of exposure to ZnO and ZnSO₄ comparing with the control. Root length, shoot height, root dry mass, shoot fresh mass and leaf area were more impaired by Zn concentration than sources.

Keywords: Nanomaterials. Zinc in plants. XRF. Zinc oxide nanoparticles.

RESUMO

CRUZ, T. N. M. da. **Absorção radicular e efeitos de nanopartículas de óxido de zinco em plantas de *Phaseolus vulgaris***. 2018. 104 p. Dissertação (Mestrado) – Centro de Energia Nuclear na Agricultura, Universidade de São Paulo, Piracicaba, 2018.

A nanotecnologia tem sido considerada, em diversos setores, como uma área promissora, e já participa de inúmeras formulações de produtos como um importante componente. Entretanto na agricultura ainda é um motivo de preocupação devido à sua desconhecida interação com tecidos biológicos. Visando avaliar a interação de nanopartículas (NPs) com plantas de *Phaseolus vulgaris*, esse estudo analisou: como dispersões de nanopartículas de ZnO são absorvidas pelas raízes das plantas; como elas são transportadas e acumuladas nos tecidos vegetais; efeito fisiológicos e morfológicos, e compara os resultados com solução de ZnSO₄. Espectroscopia de fluorescência de raios X realizada *in vivo* revelou que a fonte, tamanho da NP, concentração e revestimento com tensoativos afeta liberação e absorção de Zn, e com exceção do ZnSO₄ na maior concentração, existe um gradiente de concentração de Zn da raiz para a parte aérea. Espectroscopia de absorção de raios X mostrou que o Zn é absorvido ligado principalmente a citrato e malato. Foram constatadas NPs no interior de plantas com as raízes danificadas. Microanálises por fluorescência de raios X mostraram que o transporte de Zn das raízes até a parte aérea pode ocorrer através do xilema e do córtex, e ambas fontes apresentaram a mesma distribuição de Zn no interior dos caules. Análises gasosas por infravermelho reportaram uma diminuição na condutância estomática e nas taxas de fotossíntese e transpiração após 48 horas de exposição a ZnO e ZnSO₄ comparando com o controle. Comprimento das raízes, altura da parte aérea, massa seca da raiz, massa fresca da parte aérea e área foliar foram mais prejudicadas pela concentração de Zn do que pela fonte.

Palavras-chave: Nano materiais. Zinco nas plantas. XRF. Nanopartículas de óxido de zinco.

SUMMARY

1. INTRODUCTION	15
1.1.1 Agriculture and Nanotechnology	15
1.1.2. Zinc in plants	16
1.2. Hypothesis.....	18
1.3. Objectives.....	18
1.4. Structure of the thesis	18
2. MECHANISMS OF ABSORPTION AND TRANSPORT OF ZnO NANOPARTICLES BY <i>Phaseolus vulgaris</i> PLANTS via <i>in vivo</i> X-RAY SPECTROSCOPY	21
2.1. Introduction	21
2.2. Experimental	22
2.2.1. Characterization of nanomaterials and dispersions.....	22
2.2.2. <i>In vivo</i> kinetics of Zn absorption	23
2.2.3. μ -XRF and SEM for plant stems	24
2.2.4. <i>In vivo</i> XAS.....	25
2.3. Results and Discussion.....	26
2.3.1. Nanomaterials characterization	26
2.3.2. <i>In vivo</i> kinetics of absorption	27
2.3.3. Spatial distribution of the absorbed Zn	33
2.3.4. <i>In vivo</i> chemical speciation of Zn.....	37
2.4. Conclusions	43
3. PHYSIOLOGICAL EFFECTS AND ROOT-TO-SHOOT ZINC TRANSPORT FROM ZnSO₄ AND ZnO NANOPARTICLES ON <i>Phaseolus vulgaris</i> PLANTS	45
3.1. Introduction	45
3.2. Experimental	47
3.2.1. Characterization of ZnO NPs	47
3.2.2. <i>In vivo</i> Zn monitoring in plants.....	47
3.2.3. Zn quantifying in plants shoots	47
3.2.4. Zn chemical speciation in dispersions and solution	48
3.2.5. IRGA	48
3.3. Results and Discussion.....	48
3.3.1. Zn kinetics in different parts of <i>Phaseolus vulgaris</i> plants	48
3.3.2. Zn content in shoot tissues	52

3.3.3. Chemical environment of Zn in root presence.....	53
3.3.4. Zinc in the petioles, leaves and biological effects	54
3.4. Conclusions	57
4. MORPHOLOGICAL EFFECTS, SPAD INDEX AND NUTRIENT CONCENTRATION IN <i>Phaseolus vulgaris</i> PLANTS EXPOSED TO ZnO NANOPARTICLES: A LONG-TERM EXPOSURE EXPERIMENT	59
4.1. Introduction	59
4.2. Material and Methods.....	60
4.2.1. NP Characterization	60
4.2.2. <i>Phaseolus vulgaris</i> assay design.....	61
4.2.3. Nutritive Solution Monitoring.....	61
4.2.4. Morphological, SPAD analysis and μ -XRF maps	61
4.2.5. Nutrient content on <i>Phaseolus vulgaris</i> tissues.....	63
4.2.6. Data analysis	63
4.3. Results and Discussion.....	64
4.3.1. Effects on morphological aspects and SPAD index	64
4.3.2. Zn content on shoot and root tissues	68
4.3.3. Zn toxicity symptoms.....	70
4.3.4. Correlations between Zn content and morphological effects	72
4.3.3. Nutrient content analysis	73
4.3.4. μ -XRF Zn maps.....	75
4.4. Conclusion.....	77
5. FINAL CONSIDERATIONS AND OUTLOOK	78
REFERENCES.....	80

1. INTRODUCTION

1.1.1 Agriculture and Nanotechnology

The world population is estimated to reach 9.7 billion by 2050, raising serious concerns about global resources demand for energy and food. It is known that the amount of nutrients required by plants is not constant along the life cycle. Thus, simply broadcasting fertilizer before sowing is not an ideal practice, since it can become strongly adsorbed to soil particles and hardly available to plants, leaching down contaminating water table or run off ending in water streams. On the other hand, several fertilizer applications would increase production costs. Hence, innovative technologies are urgently needed aiming at minimizing the human footprint on the planet, extending the life of mineral reserves and at the same time ensuring better living standards.

Like in other fields of knowledge, there is much expectation regarding whether and how agriculture can benefit from nanotechnology¹⁻⁵. In principle, properties of nanomaterials such as tunable surface charge, boosted surface reactivity, multiphase architecture, and higher solubility can be used to design new fertilizers and smart delivery systems for agrochemicals. At the same time, there is a concern regarding their possible negative impacts on the environment⁶⁻⁹.

One of the main concerns refers to whether and how nanoparticles are absorbed, translocate and are stored inside the plants. Are they biotransformed? Do they move through the food web? There are controversies about the topics cited, what is not totally unexpected since exists many plants species and NPs types, varying in size, shape, composition and more features that distinct the interaction of them with the living being.

First of all, when working with NP, it is important to fully characterize it. Some methodologies are currently in use for it. X-ray diffraction (XRD) is known to verify the crystal phase and crystallite size¹⁰. Dynamic light scattering (DLS) can estimate the hydrodynamic radius while the particles are dispersed in liquid media¹¹. Scanning and transmission electron microscope (SEM and TEM, respectively) allow one to observe the shape and size of NPs^{11,12}. The size influence on its surface area, making the zeta potential an important characteristic to measure. Zeta potential can tell us the surface charge¹³ on NPs, which can explain many interactions. The chemical environments of these nanomaterials are also significant, in order to understand the reactions and how these particles are taken up

and translocated. If possible, it is important to verify its chemical environment before and after NP contact biological media. X-ray absorption and X-ray fluorescence spectroscopies can assist one in this characterization^{13,14}. These features can help scientists to explain the NPs interaction with plants.

Regarding NP uptake, transport and accumulation by plants, there are divergent reports on literature. It was already verified that these mechanisms varies according to plant species and NP size, composition and concentration. Many authors report the absorption of entire nanoparticles by roots of plants¹⁵⁻¹⁹. They suggest that NPs can penetrate cells through ion channels, transporters proteins, aquaporins, injuries or bounded to organic compounds^{20,21}. Notwithstanding, others report the NP dissolution on the rhizosphere followed by ionic uptake^{15,22}.

To reach the soot, the nanoparticles that enter via root have cross the Casparian band. This physical barrier that limits the passage of substances¹. The only known way to bypass it is through the cell symplast. However, literature revealed the capacity of some NPs to induce structural changes forming large pores on cell wall. This could facilitate the penetration and translocation of this material²³⁻²⁶.

For most studies in which NP was dissolved into its ionic form, the element was accumulated in the same tissues as bulk particles²¹. On the other hand, there are on literature reports that observed the presence of NP inside pant tissues^{13,27}. NPs are also known as adherent particles, and it is commonly find these material adhere to root surface^{28,29}.

As others common sources of nutrients used in agriculture, NPs might also present beneficial and toxic concentration ranges. It likely varies according to plant species, particle size, concentration and composition. Different plant species exposed to the same NP concentration presented improvement and detrimental effect on seed germination³⁰. Enhancements on seed germination, root and shoot elongation are commonly found in the literature^{31,32}. Although the opposite results are also found^{31,33-35}, mainly when researchers work with high concentrations.

1.1.2. Zinc in plants

Zn is an essential element that is involved in several enzymatic processes³⁶. As every micronutrient, the edge between the beneficial and toxic concentration is sharp. Among the

micronutrients, Zn deficiency is one of the most well mapped and investigated. It is known that 49% of worldwide soils are Zn deficient³⁷. This deficiency afflicts 1 billion people³⁸, which makes it one of the micronutrients with the lowest proper intake³⁹. Generally, Zn is the second most required micronutrient. Aiming at decreasing Zn losses, it is important to figure out the mechanisms that govern its uptake and translocation. Zn is typically uptake as a divalent cation (Zn^{2+}), and its uptake increases as the pH decreases.

Zn deficiency in plants affects their physiological functions and causes a variety of adverse effects on plant growth. For example, one can visually notice the shortening of internodes, leaf chlorosis, eventually reducing crop yield by 20%⁴⁰. Symptoms from Zn deficiency and toxicity are very closely⁴¹.

Although Zn deficiency is very common to observe on agriculture soils, the toxicity can also happen depending on the parent rock and the history of the soil, once residues like sewage sludge can increase the Zn soil content⁴² in a great range. Zn concentration in soils above 110 mg kg^{-1} is toxic to most plant species⁴³. The phytotoxicity varies according to plant species, development stage and type of soil⁴⁴. The most common symptoms of Zn toxicity are: chlorosis, reddening and necrosis of younger leaves; smaller leaf area; vertically oriented leaves and shorter roots^{45,46}. The chlorophyll content and photosynthetic rate are also disturbed by Zn toxicity⁴⁷. Other symptoms can be associated with Fe, P and Ca deficiency, since elevated Zn content can decrease the uptake of these nutrients^{48,49}.

Zn transport is commonly described as the predominant absorption through the symplast pathway^{50,51} assisted by metal transporters. Zn can also be translocated in the apoplastic pathway. In order to reach the xylem, ionic Zn passes through Casparian strips to arrive on the symplastic route. There, Zn can easily move through plasmodesmata and go to shoots by vascular route. Many genes are involved in the processes of Zn transport, as ZIP, NRAMP, YSL, HMA^{52,53}. It seems that their expression varies according to the medium conditions and parts of the plants^{52,54-59}. Some are expressed in roots, others in shoots, and others in both tissues. HMA2 and HMA4 are known to transport Zn in shoots for greater distances in the xylem. It was also observed their presence in the phloem, suggesting that they are also in charge to transport Zn from shoot-to-root^{52,60}.

NPs present the potential can enhance Zn absorption and transport. The size, composition, concentration and surface coating are the most important features of NPs that can be tuned towards nanometer zinc based fertilizers. These aspects are discussed in deep in the next chapters.

1.2. Hypothesis

The roots of *Phaseolus vulgaris*, the model plant employed in this study, can absorb and translocate ZnO nanoparticles. These particles can improve or prevent the plant development according to the dose. Thus, ZnO nanoparticles might consist in interesting sources to the production of Zn fertilizers in the near future.

1.3. Objectives

The main objectives of this work are:

- comprehend the interaction of ZnO NPs with *Phaseolus vulgaris* plants;
- study the mechanisms by which ZnO NPs are absorbed, translocated and where they are accumulated in plants;
- investigate the physiological and morphological effects on plants after being exposure to ZnO NPs;
- uncover the relationship on Zn absorption of with other nutrients uptake;
- Verify what are benefic and toxic concentrations of ZnO NPs to plants, and compare these results with a ZnSO₄.

1.4. Structure of the thesis

This thesis is composed by the general initial introduction above, followed by three chapters written in scientific article layout.

Chapter 2 comprises a short-term study to unravel the *in vivo* absorption and transport of ZnO NPs in the stems of *P. vulgaris* plants, and it is already published in the Environmental Science: Nano entitled as “Shedding light on the mechanisms of absorption and transport of ZnO nanoparticles by plants *via in vivo* X-ray spectroscopy”. Issue 12, pages 2367 to 2376, 2017.

Chapter 3 investigated some physiological effects and ZnO NPs absorption and transport features in the stem, petiole and leaves of *P. vulgaris*, and this report is almost ready to submission peer reviewed scientific journal.

Finally, chapter 4 involves a long-term experiment aiming at verifying the morphological effects of ZnO and ZnSO₄ on *P. vulgaris*. We evaluated the effects of ZnO particle size, concentration and time of exposure on several plant biometric parameters. This chapter will be also soon submitted for a peer reviewed scientific journal.

2. MECHANISMS OF ABSORPTION AND TRANSPORT OF ZnO NANOPARTICLES BY *Phaseolus vulgaris* PLANTS via *in vivo* X-RAY SPECTROSCOPY

Abstract

Several factors have contributed to bring pressure on agriculture. In this context, nanomaterial properties can be explored to design more efficient fertilizers and therefore increase productivity. In the present study, the roots of *Phaseolus vulgaris* were immersed in several nano ZnO dispersions for 48 h. The absorption and transport phenomena were *in vivo* monitored by X-ray fluorescence spectroscopy (XRF) and X-ray absorption spectroscopy (XAS). The nanoparticle size, concentration and coating with surfactants affected the rate of Zn release and therefore its uptake. *In vivo* X-ray absorption spectroscopy showed that *Phaseolus vulgaris* takes up Zn bound to both citrate and malate, while entire nanoparticles were only absorbed when roots were injured. X-ray fluorescence microanalysis unraveled that besides xylem bundles root to shoot Zn transport can take place through the cortex.

Keywords: NPs uptake. Synchrotron. Zn compounds.

2.1. Introduction

In the near future, besides providing food, feed, and fiber, crops will have to supply the biomass that will produce both fuel and raw chemicals used in our everyday life. The increasing human and agricultural animal populations, improvements in life conditions, especially in developing countries, and crude oil scarcity on the horizon, altogether put enormous pressure on agriculture.

Besides light and water, plants require mineral nutrients for growth. In intensive agriculture, these nutrients are depleted from the soil after each harvest. Therefore, they have to be added again in the field to maintain the adequate soil fertility. Some of these nutrient inputs, such as P and K, similar to crude oil, have limited exploitable reserves. Others such as micronutrients, e.g. Mn, Cu or Zn, if not correctly applied, will result in phytotoxicity or cause imbalance in the microbial community associated with plant roots.

In the past ten years, several studies have evaluated the effects of nanomaterials on plant development²⁰. Mineral nutrients, such as Zn^{15-17,61-64}, Cu¹⁸, and Fe⁶⁵, and elements rarely used in agricultural materials, such as Ti²⁵ and Ce^{15,66}, have been investigated under hydroponic and soil cultivation conditions. Some authors reported that nanomaterials can improve^{3,67,68} plant development, whereas others concluded that nanomaterials impair it^{3,6,66-68}. This apparent contradiction may be related to the type of nanomaterial

(composition, shape, and particle size), plant species, and the lack of standardization for experimental procedures in this emerging scientific domain.

One of the most striking knowledge gaps in this area is on how plants take up and transport nanoparticles^{6,20,28}. Despite some studies, it is still unclear whether or how plants take up intact nanoparticles or if they actually absorb soluble ions released by the nanoparticles. Albeit several researchers have reported the ability of plants to uptake entire nanoparticles^{15–18,25,69}, others have found different results^{15,22} and thus this is still a matter of debate²⁸.

In plant tissues, Zn is usually found in concentrations ranging from tens to hundreds of mg kg⁻¹. The most ubiquitous chemical form of Zn applied to plants is the sulphate form³⁶. The main drawback of this compound lies on its high solubility and therefore high rate of absorption, which can lead to phytotoxicity.

One way to circumvent this problem may be by using ZnO nanoparticles. Since they present higher solubility than micro particles and lower solubility than sulphates, the Zn²⁺ ions can be slowly released either by foliar or root absorption. Additionally, if plants could take up small entire nanoparticles, these particles could be dissolved inside the plant, thus supplying nutrients according to the real-time demand without losses by leaching or adsorption to soil particles.

Aiming to contribute to the understanding of the mechanisms of absorption and transport of nanoparticles by plants, this chapter describes how roots of *Phaseolus vulgaris*, also known as kidney or common beans, absorb Zn from ZnO nanoparticles and transport it to the shoot.

2.2. Experimental

2.2.1. Characterization of nanomaterials and dispersions

A total of six ZnO nanomaterials were employed, where three were purchased in powder form: 20 nm (M K Impex Corp, Canada), 40 nm (M K Impex Corp, Canada) and 60 nm (Nanophase, USA). The other three were acquired as aqueous dispersions with surfactants, namely: 40 nm (Nanophase, USA), 60 nm (Nanophase, USA), and 300 nm ZnO (Agrichem Company, Brazil).

These materials were used to prepare 100 and 1000 mg L⁻¹ (weight of Zn in distilled water) aqueous dispersions. To prepare them, the nanoparticles without surfactants were sonicated using an ultrasonic processor (model 705 Sonic Dismembrator, Fisher Scientific, USA) operating at 60 W for three cycles of one minute each.

The crystal phase of the nanomaterials was determined by X-ray diffraction (XRD), using Cu K α radiation in a PW 1877 diffractometer (Philips, Netherlands). The crystallite dimension (D) was determined using the Scherrer equation, corrected by subtracting the instrumental broadening determined by measuring the (111) plane of a Si single crystal.

Scanning electron microscopy (SEM) images were acquired using an Inspect F50 microscope (FEI Company, USA) and employing a Magellan 400 microscope (FEI Company, USA). For these measurements, nano ZnO aqueous dispersions at 100 mg L⁻¹ were spread on carbon tape adhered to a sample holder and dried at room temperature.

Dynamic light scattering (DLS; Zetasizer Nano, Malvern Instruments, UK) was used to evaluate the behavior of the dispersed ZnO nanoparticles. An acrylic cuvette was filled with 80 μ L of the 100 and 1000 mg L⁻¹ nano ZnO dispersions, which were previously dispersed by sonication.

To evaluate the solubility of the nanomaterials, 50 mL each of the 100 and 1000 mg L⁻¹ dispersions was prepared and sonicated as described above. After 48 h, an aliquot of 1 mL was transferred to vials and centrifuged at 14 007 g for 60 min. Then, 15 μ L of the supernatant was pipetted on the top of the 5 μ m thick X-ray polypropylene film. The Zn concentration was determined by energy dispersive XRF (Shimadzu EDX-720, Japan) using external calibration under thin film conditions. The Zn intensities of samples and standards were corrected by using a Ga internal standard.

2.2.2. *In vivo* kinetics of Zn absorption

The roots of *Phaseolus vulgaris* plants at V3 stage were immersed in the 100 and 1000 mg of Zn L⁻¹ of distilled water, from nano ZnO dispersions or ZnSO₄ solutions. The plants were assembled in a sample holder (as shown in Appendix A), then maintained in a growth

room at 27 °C and a 12 h-photoperiod under illuminated LED lamps supplying 250 μmol of photons per m^2 per s. For the XRF measurements, the samples were loaded into the equipment and then returned to the growth room.

The Zn uptake was traced using X-ray fluorescence microanalysis ($\mu\text{-XRF}$; Orbis PC EDAX, USA), where X-rays were generated by a Rh anode operating at 50 kV and 900 μA , using a 1 mm collimator and a Ni filter, to improve the signal-to-noise ratio. The XRF photons were detected by a 30 mm^2 silicon drift detector (SDD), the dwell time was 60 s and the dead time was smaller than 3%. The distance between the sample and the source was 10 mm. No signs of sample damage were observed as a function of the period of analysis. The experiments were repeated twice.

2.2.3. $\mu\text{-XRF}$ and SEM for plant stems

The roots of *P. vulgaris* plants with the first trefoil expanded were immersed in 100 and 1000 mg L^{-1} 40 nm ZnO + surfactant dispersions and aqueous ZnSO_4 . The plants were then maintained in a growth room as the one described on topic 2.2.2. above. After 12 h, 24 h and 48 h, samples were collected. In the base of the crown, the stem was separated from the roots. Then, the stem was flash frozen with liquid N_2 and immediately cut at 2 cm above the root crown using a scalpel. The analyzed sections were 1.4–1.6 mm thick. The tissue cross sections were placed on the top of a Kapton thin film assembled in a 20 mm XRF cup. This was done to minimize the noise originated from X-ray scattering.

Immediately after cutting, the sample was loaded inside the $\mu\text{-XRF}$ equipment. Maps were recorded using a 30 μm X-ray beam focused on the sample by a polycapillary optical element. Matrices of 32 \times 25 or 64 \times 50 pixels were employed in the mapping. X-rays were generated by a Rh anode operating at 50 kV and 600 μA . The distance between the sample and the X-ray source was 10 mm. The XRF photons were detected by a 50 mm^2 SDD detector, the dwell time was 500 ms per point, the total time of analysis was at a maximum of 32 min and the dead time was smaller than 1%.

SEM micrographs were acquired for histological purposes. Stem samples were frozen with liquid N_2 , then transverse sections with a height of 2 cm were cut with a razor blade and immediately immersed in a fixative (2.5% glutaraldehyde in a 0.1 M sodium cacodylate buffer). The samples were subjected to vacuum for 20 min and maintained in the fixative at

4°C, for 48 h, then dehydrated in ethanol (20–100%) and dried through the liquid CO₂ critical point (Leica CPD300). Dried samples were mounted in metal stubs covered with carbon tape and sputter coated with gold (120 nm) (Sputter Coater, Leica EM ACE 600). Observations were performed using a LEO 435 VP (Carl Zeiss, Germany) SEM and digital images were captured.

2.2.4. In vivo XAS

The roots of the plants were immersed in the 1000 mg L⁻¹ dispersions of the above-mentioned nanomaterials. After 48 hours, stem and roots of the plants were analyzed.

The Zn-K edge XAS measurements were carried out during two different beamtimes at the XAFS2 beamline of the Brazilian Synchrotron Light Laboratory (LNLS), in Campinas, Brazil. In this station, synchrotron radiation is generated by a bending magnet dipole, and a cylindrical Rh coated mirror rejected the higher harmonics and vertically collimated the beam. The suitable energy for the Zn K edge was selected by a Si (111) double crystal monochromator. Then, a second Rh coated mirror focuses the X-rays to a spot of nearly 500 μm on the sample position. The detected photon flux density on the sample is *ca.* 2.78×10^9 photons per s per mm² at 7 keV.

The measurements were performed in fluorescence mode using a Canberra 15 element Ge solid state detector. Each near edge X-ray absorption spectrum (XANES) was acquired in 6 minutes and three spectra per point per sample were measured. These spectra were merged, energy calibrated and normalized using the Athena program within the IFEFFIT package⁷⁰. Additionally, the XAS spectra for Zn-malate, Zn-citrate, Zn-histidine, Zn-succinate and Zn-cysteine, Zn-phosphate and Zn-phytate reference compounds synthesized in the laboratory according to the literature⁷¹ were recorded. The spectra of pristine nano ZnO and commercial ZnSO₄ were also recorded. These reference compounds were mixed with cellulose and pelletized.

The spectra recorded for the reference compounds were used in the linear combination analysis carried out from -20 to 50 eV relative to the energy threshold. The disagreement R-factor represents the mean square sum of the misfit of each energy data point. This procedure was carried out using Athena software.⁴² The uncertainties reported for the weight fraction of the components of the linear combination represent the amount by which the fraction could be changed without causing significant changes in the R-factor.

One has to keep in mind that in XAS, the normalization procedure itself can introduce errors in the order of 10%.⁷²

2.3. Results and Discussion

2.3.1. Nanomaterials characterization

Table 1 presents the nominal particle size given by the suppliers, crystallite size ($D_{(hkl)}$) calculated by XRD, nanoparticle diameter observed by SEM, hydrodynamic radius of aggregates in aqueous dispersions determined by DLS and zeta potential. XRD showed that all materials were wurtzite ZnO and the crystallite size varied according to the nominal particle size, except that for 300 nm ZnO (Table 1).

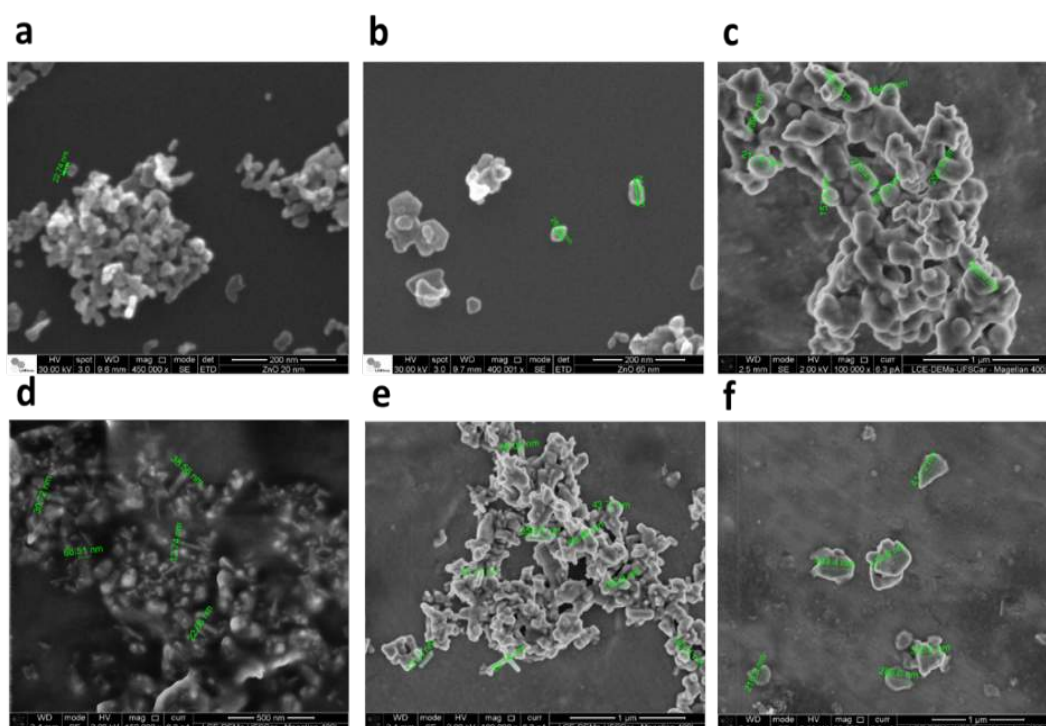
Table 1 - Crystallite size (D) in different planes by XRD, particle diameter by SEM, zeta potential and hydrodynamics radius (nm) of 20, 40, 60, 40 + surfactants, 60 + surfactants and 300 nm +surfactants ZnO nanoparticles

Particle size (nm)	$D_{(hkl)}$			Diameter by SEM (nm)	Zeta Potential (mV)	Hydrodynamic radius (nm)
	(100)	(002)	(101)			
20	14.0	14.5	13.8	23±4	21±4	150±100
40	25.6	47.1	26.0	32±3	20±5	1,500±800
60	47.1	167.1	45.6	160±30	28±5	500±300
40 + surf.	51.8	83.6	48.6	31±8	-15.5	90±30
60 + surf.	68.1	63.4	62.2	67±16	-16.5	100±50
300 + surf.	18.0	20.3	16.3	330±40	-23±5	-----

In spite of the particle size given by the suppliers or estimated by SEM (Figure 1), the particles agglomerate in the dispersions. Dynamic light scattering (DLS) showed that the hydrodynamic radii varied from 90 nm to 1454 nm as shown in Table 1. The ZnO nanoparticles dispersed with surfactants resulted in smaller aggregates than the particles dispersed in water only. The agglomeration behavior of nanoparticles has been reported previously^{16,17,25,61,69,73}. Due to the high concentration and agglomeration, it was not possible

to record the hydrodynamic radius for some of the dispersions. Zeta potentials for the nano ZnO powder dispersed in water were positive, while dispersions with surfactants presented negative potentials.

Figure 1 - Scanning electron microscopy (SEM) micrographs of ZnO nanoparticles. (a) 20 nm, (b) 40 nm and (c) 60 nm, (d) 40 nm + surfactant, (e) 60 nm + surfactant and (f) 300 nm + surfactant

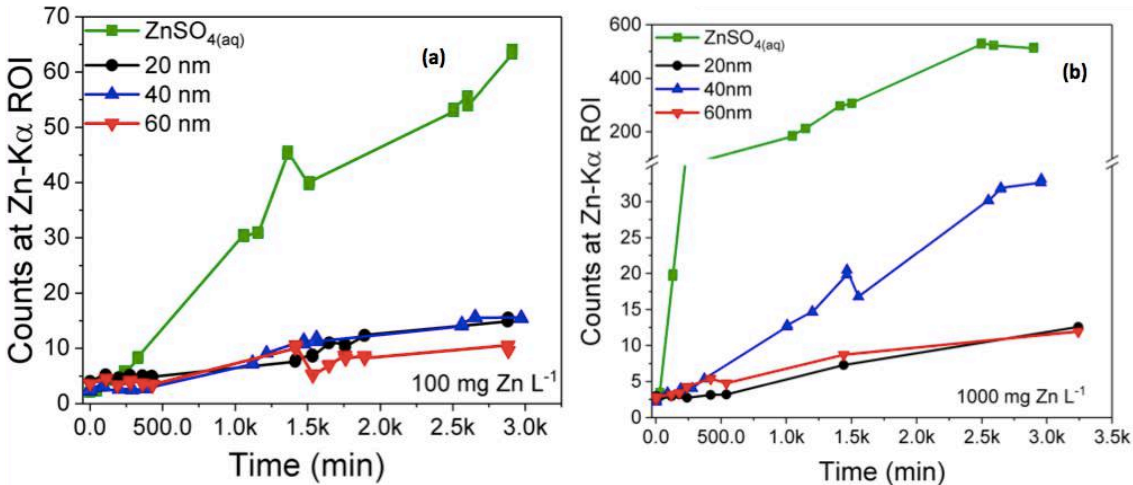


2.3.2. *In vivo* kinetics of absorption

The absorption rate of Zn was *in vivo* monitored by μ -XRF. The effects of the nanoparticle size, the presence/absence of surfactants and the concentration of the dispersion on the uptake velocity were evaluated.

Figure 2 shows the number of counts of Zn-K α photons as a function of time, for plants that were in contact with aqueous nano ZnO dispersions without surfactants at (a) 100 mg L⁻¹ and (b) 1000 mg L⁻¹. For both concentrations, the highest Zn content in the plant was observed for ZnSO_{4(aq)} solutions.

Figure 2 - *In vivo* X-ray fluorescence monitoring the content of Zn in the stem of *Phaseolus vulgaris* whose roots were immersed in aqueous nano ZnO dispersion without surfactant and $\text{ZnSO}_{4(\text{aq})}$ solution. The curves show the number of Zn-K α photon counts for plants exposed to (a) 100 mg Zn L^{-1} and (b) $1000 \text{ mg Zn L}^{-1}$. ROI stands for region of interest

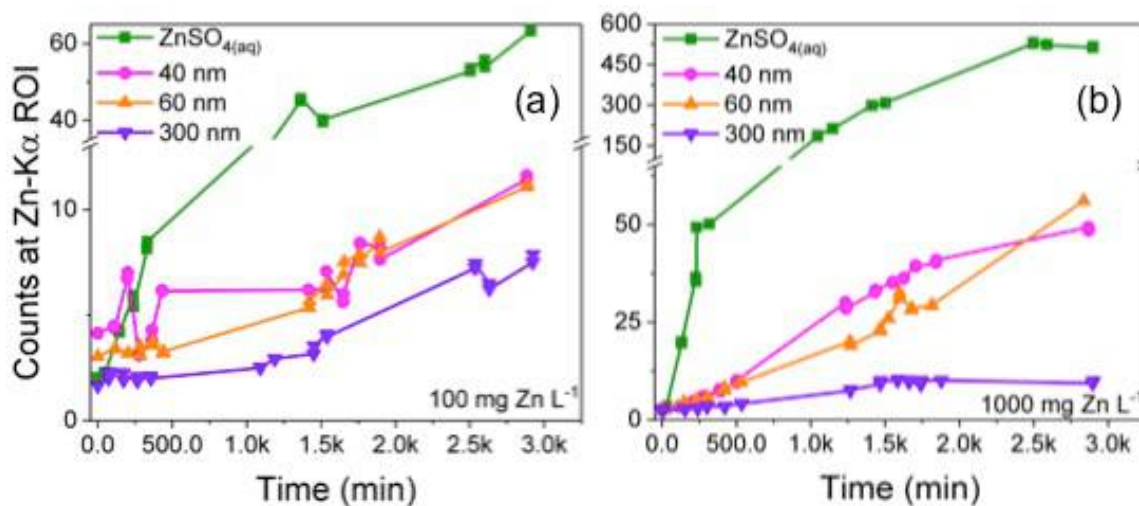


The Zn content in the stem of plants that received ZnO nanoparticles continuously increased during the experiment and did not stabilize. On the other hand, the number of counts for ZnSO_4 at 1000 mg L^{-1} reached a plateau after nearly 2500 minutes. At the end of the exposure period, the plants treated with $1000 \text{ mg L}^{-1} \text{ ZnSO}_{4(\text{aq})}$ presented clearly visual symptoms of intoxication and the leaves became wilted and dried. Conversely, visually these symptoms could neither be detected in plants treated with $100 \text{ mg L}^{-1} \text{ ZnSO}_{4(\text{aq})}$ nor in plants exposed to ZnO nanoparticles in both concentrations.

The number of Zn-K α counts at the end of the experiment showed that the content of Zn in the stem of plants that received ZnO nanoparticles was nearly the same, regardless of the concentration to which the roots were exposed. Except for plants exposed to the 40 nm Zn dispersion, in this case, the Zn content of the 1000 mg L^{-1} dispersion is twice that of the 100 mg L^{-1} dispersion.

Figure 3 presents the number of counts of Zn-K α photons for plants that were in contact with aqueous nano ZnO dispersions with surfactants at (a) 100 mg L^{-1} and (b) 1000 mg L^{-1} .

Figure 3 - *In vivo* X-ray fluorescence monitoring the content of Zn in the stem of *Phaseolus vulgaris* whose roots were immersed in aqueous nano ZnO dispersions with surfactants and $\text{ZnSO}_{4(\text{aq})}$ solution. The curves show the number of Zn-K α photon counts for plants exposed to (a) 100 mg Zn L^{-1} and (b) $1000 \text{ mg Zn L}^{-1}$. ROI stands for region of interest



The Zn content for 40 nm ZnO dispersed with surfactants was dependent on the concentration to which the roots were exposed. While the concentration of ZnO in the dispersion increased by a factor of ten, the Zn content in the stem was incremented by a factor of less than four. The 60 nm ZnO dispersed with surfactants presented the same behavior. The amount of Zn in the plants that received 300 nm ZnO at 1000 mg L^{-1} was approximately 30% higher than that for 100 mg L^{-1} .

The uptake of 1000 mg L^{-1} of 300 nm ZnO dispersed with surfactants reached a maximum after 1500 minutes, and it might be a response from plants with this higher concentration exposure, since the uptake of Zn from the 100 mg L^{-1} dispersion, a lower concentration, continuously increased during the 48 hours of monitoring. The plants exposed to 300 nm ZnO NPs at 1000 mg L^{-1} did not present the same visual symptoms of intoxication from $\text{ZnSO}_{4(\text{aq})}$ at the same concentration.

The analysis of the slopes of the uptake curves showed that the content of Zn in the stem followed a linear function of time (Pearson correlation coefficients are shown in Table 2). Table 2 presents the Zn uptake velocities expressed as counts per minute. The absorption and transport of Zn from $\text{ZnSO}_{4(\text{aq})}$ were faster than those supplied by nano ZnO.

For $\text{ZnSO}_{4(\text{aq})}$, the concentration to which the roots were exposed and the velocity of the uptake were closely correlated. The uptake rate increased by a factor of nine when the concentration was incremented by a factor of ten.

Table 2 - Zn uptake velocity by *P. vulgaris* as function of nanoparticle size and concentration, and Person's R from adjusted slopes. Treatments consisted of 100 and 1000 mg L⁻¹ ZnO nanoparticles and aqueous ZnSO_4

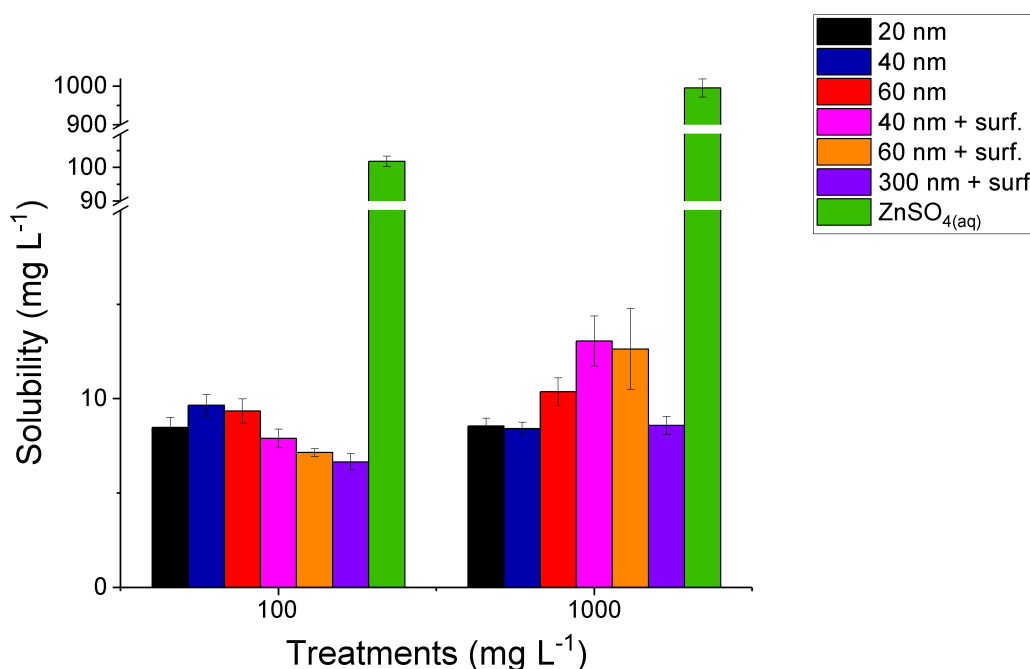
Treatments	100 mg L ⁻¹		1000 mg L ⁻¹	
	Slope x 10 ⁻³ (counts min ⁻¹)	R	Slope x 10 ⁻³ (counts min ⁻¹)	R
$\text{ZnSO}_{4(\text{aq})}$	21.2 ± 1.0	0.95	197.3 ± 5.0	0.99
ZnO 20 nm	3.9 ± 0.2	0.95	3.1 ± 0.2	0.98
ZnO 40 nm	5.1 ± 0.3	0.98	10.9 ± 0.2	0.99
ZnO 60 nm	2.9 ± 0.3	0.95	2.9 ± 0.2	0.95
ZnO 40 nm + surfactant	2.3 ± 0.3	0.83	19.3 ± 0.9	0.96
ZnO 60 nm + surfactant	2.8 ± 0.1	0.96	17.1 ± 0.6	0.97
ZnO 300 nm + surfactant	2.0 ± 0.1	0.91	3.9 ± 0.3	0.87

In the case of nano ZnO dispersed without surfactants, the highest uptake rate was observed for 1000 mg L⁻¹ 40 nm ZnO nm (slope = 10.9 ± 0.2 10⁻³ counts per min), whereas for the same particle size at 100 mg L⁻¹, the velocity was 5.1 ± 0.3 10⁻³ counts per min. For 20 and 60 nm, the amount of Zn absorbed was nearly the same. Thus, the concentration did not affect the absorption rate.

Among the nanomaterials, 40 and 60 nm ZnO dispersed with surfactants presented the highest rate of absorption for the highest concentration. The similarity on their responses might be due to the composition of the surfactants, once they were purchased from the same company. The uptake of Zn from ZnO NPs of 40 nm and 60 nm with surfactants increased as a function of concentration by a factor of ca. eight and six, respectively. Nevertheless, the magnitude of the increment was smaller than that shown by the $\text{ZnSO}_{4(\text{aq})}$. The Zn absorption velocity of 300 nm ZnO was less affected by the concentration. While the concentration of ZnO increased by a factor of ten in the dispersion, the uptake velocity was incremented by a factor of two only.

The dispersions obtained from the ZnO nanoparticles with surfactants were more stable than those prepared with the uncoated particles. At the end of the uptake and solubility experiments, it was noticed that a higher fraction of the nanoparticles without surfactants settled on the bottom of the flask, even with the sonication process. The dissolution of ZnO nanoparticles was evaluated after 48 h and the data are shown in Figure 4. The concentration of Zn in the supernatant was between 7.1–8.7 mg Zn L⁻¹ for the 100 mg L⁻¹ treatments and 7.1–12.5 mg Zn L⁻¹ for the 1000 mg L⁻¹ dispersions. These solubility figures are in the same range as the values reported in the literature⁷⁴. Albeit the ZnO nanoparticle concentrations employed in this study may be considered high compared to the estimated values found in the environment (from 1 × 10⁻⁶ up to 0.01 mg L⁻¹)⁷⁵, the concentration of Zn in the solution was in the same order of magnitude as that found in agricultural soils.

Figure 4 - Solubility of nano ZnO dispersions used in the present study and recovery test for ZnSO_{4(aq)}



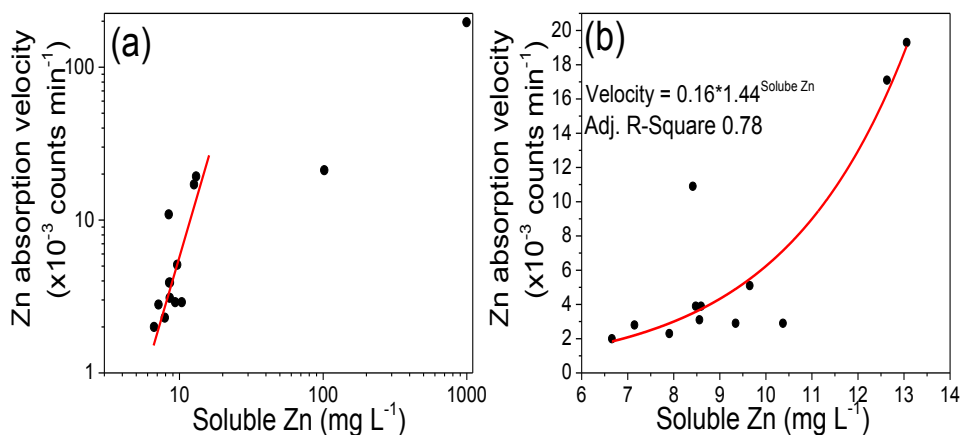
The content of Zn in soils considered uncontaminated ranges from 10–300 mg Zn kg⁻¹ soil⁷⁶. Although, it can naturally reach 1500 mg Zn kg⁻¹ soil, depending on the parent rock³⁶. From the plant nutritional point of view, the concentration of nutrients must be assessed in terms of their availability. A survey employing 38151 soil samples from Brazilian

agricultural areas showed that the concentration of Zn available to plants (extracted using a Mehlich 1 solution) varies from 0.1 to 92.1 mg Zn L⁻¹ soil. The median value was 3.2 mg L⁻¹.⁴⁸

There are literature reports that state that the solubility of nano ZnO is inversely proportional to the particle size^{73,74}. It is also known that the aggregation can decrease the solubility of nano ZnO⁷⁷. As expected, the solubility of coated ZnO nanoparticles was inversely proportional to the particle size at both concentrations. However, for the ZnO nanoparticles dispersed only in water, the concentration and particle size trends could not be associated with the dissolution.

Figure 5 displays the uptake velocity as a function of the content of soluble Zn in the dispersion. For the ZnO nanoparticles, the uptake rate could be adjusted as an exponential function of the concentration of soluble Zn. The low adjusted R-square value (0.78) suggests that the uptake velocity depends on additional factors, besides the measured Zn solubility. The Zn solubility in the presence of the roots might not be the same as the one determined in water. It was previously shown that humic acids can increase ZnO solubility⁷⁷, thus the root organic exudates are expected to cause the same effect. Also, in soil experiments, it was revealed that the organic coating, such as the one provided by surfactants, increased both solubility and diffusion of CeO₂ nanoparticles in a soil solution⁷⁸. Other parameters that might be considered for modeling the uptake velocity are the activity of Zn transporters and the channels of transport. These factors are also influenced by the concentration of Zn in solution.

Figure 5 - (a) Log-Log uptake velocity as function of the concentration of soluble Zn; (b) uptake velocity as function of the concentration of soluble Zn released by the nanoparticles

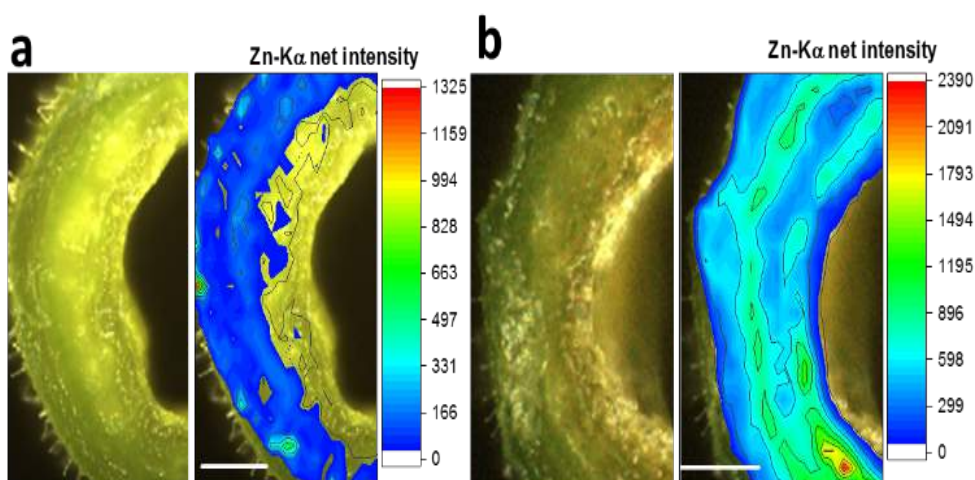


Hence, by defining the ZnO nanoparticle size and adding surfactants, one can potentially control the rate of Zn uptake by plants. This concept can be extended and tested under soil conditions. If successful, it ultimately may lead to the production of better fertilizers since there is a trade-off between nutrients readily available that may intoxicate the plant or leach, and sources that do not release it and therefore cause nutrient deficiency.

2.3.3. Spatial distribution of the absorbed Zn

Figure 6 presents cross section pictures and chemical images of stems exposed for 48 h to 100 mg L^{-1} (a) 40 nm ZnO dispersed with surfactants and (b) $\text{ZnSO}_{4(\text{aq})}$.

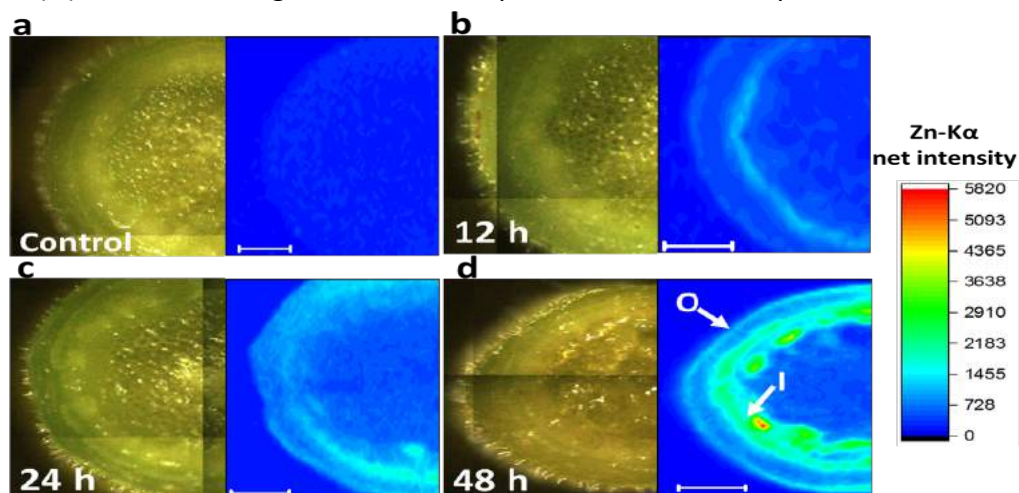
Figure 6 - *In vivo* monitoring of the Zn uptake in *Phaseolus vulgaris* by μ -XRF. The number of counts represent the Zn content in the stem of plants whose roots were exposed to 100 mg L^{-1} (a) 40 nm ZnO and (b) $\text{ZnSO}_{4(\text{aq})}$. The images contain 800 pixels each and the number of counts represent the net intensity of Zn. Scale bar: $400 \mu\text{m}$



In agreement with the rate of absorption shown in Table 2, the qualitative inspection of the images shows that the amount of Zn in the stem that received $\text{ZnSO}_{4(\text{aq})}$ was higher than that for the one that received 40 nm ZnO. Both images have a resolution of 800 pixels. The integration of the graphs showed that the content of Zn, in terms of the 3D projection volume, was six times higher for the $\text{ZnSO}_{4(\text{aq})}$ treated plant than that of the 40 nm ZnO treated plant. The median number of counts was equal to one for the plant treated with 40 nm ZnO. It means that in half of the pixels, there is no Zn signal. The median was equal to 376 counts for $\text{ZnSO}_{4(\text{aq})}$.

Figure 7 presents images of the cross sections and the corresponding Zn maps for the control plant (a), and plants exposed to 1000 mg L^{-1} 40 nm ZnO dispersed with surfactants for 12 h (b), 24 h (c), and 48 h (d). These images show how the spatial distribution of Zn evolved as a function of time. The increasing Zn content is in agreement with the kinetic data presented in Figures 2 and 3 since the amount of Zn accumulated in the stem was as function of time. The pattern of distribution pointed out that Zn was mainly concentrated in two annular regions highlighted by I (inner) and O (outer) in Figure 7(d).

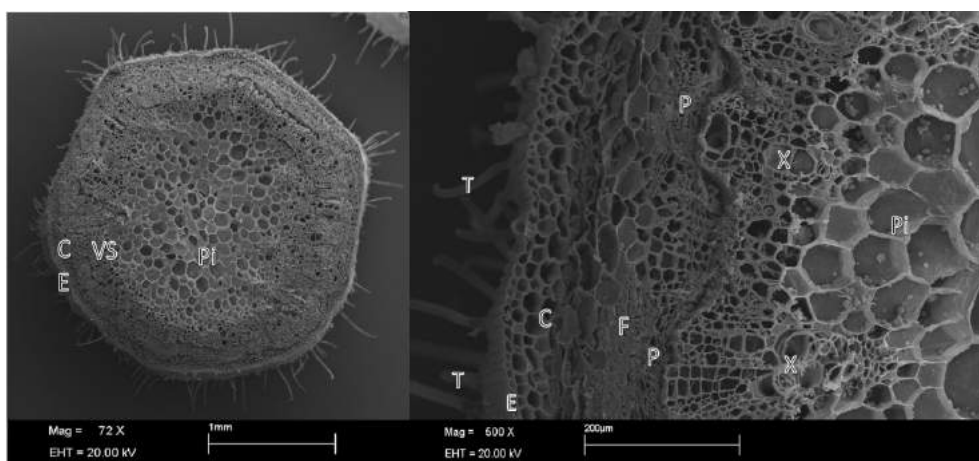
Figure 7 - *Phaseolus vulgaris* stem images and corresponding chemical images presenting the transversal spatial distribution of Zn in the stem of plants as a function of time of exposure to a $1,000 \text{ mg L}^{-1}$ 40 nm ZnO dispersion with surfactant. The Zn content increased as a result of time of exposure: (a) control, (b) 12 hours, (c) 24 hours, and (d) 48 hours. Higher concentrations of Zn were observed in two annular regions, the inner (I) vascular region, and the outer (O) cortex. All images contain 3200 pixels. Scale bar: $500 \mu\text{m}$



μ -XRF images present some important advantages over those that can be obtained by SEM-EDS. One can highlight the lower detection limits since excitation with X-rays generates lower X-ray scattering background, and therefore an improved signal-to-noise ratio. Additionally, sample preparation for μ -XRF is simpler. Since it does not require vacuum, the plants can be analysed in vivo or still fresh as shown in Figures 6 and 7. Nevertheless, conventional benchtop μ -XRF equipment offers poorer space resolution than SEM. In the present study, the elliptical X-ray spot was nearly $30 \mu\text{m}$ wide. Although, one can see the spatial distribution of the elements in Figures 6 and 7, it is difficult to make the corresponding histological assignments.

To circumvent this issue and identify the tissues in which Zn was found, an SEM micrograph of a sample equivalent to those shown in Figure 7 is presented in Figure 8. The SEM images allowed identifying the trichomes, the epidermis single cell layer, the cortex, and the vascular bundles composed by xylem and phloem. In spite of its higher lateral resolution, the chemical fixation process required to prepare samples for SEM can induce changes in the spatial distribution of the elements⁷⁹.

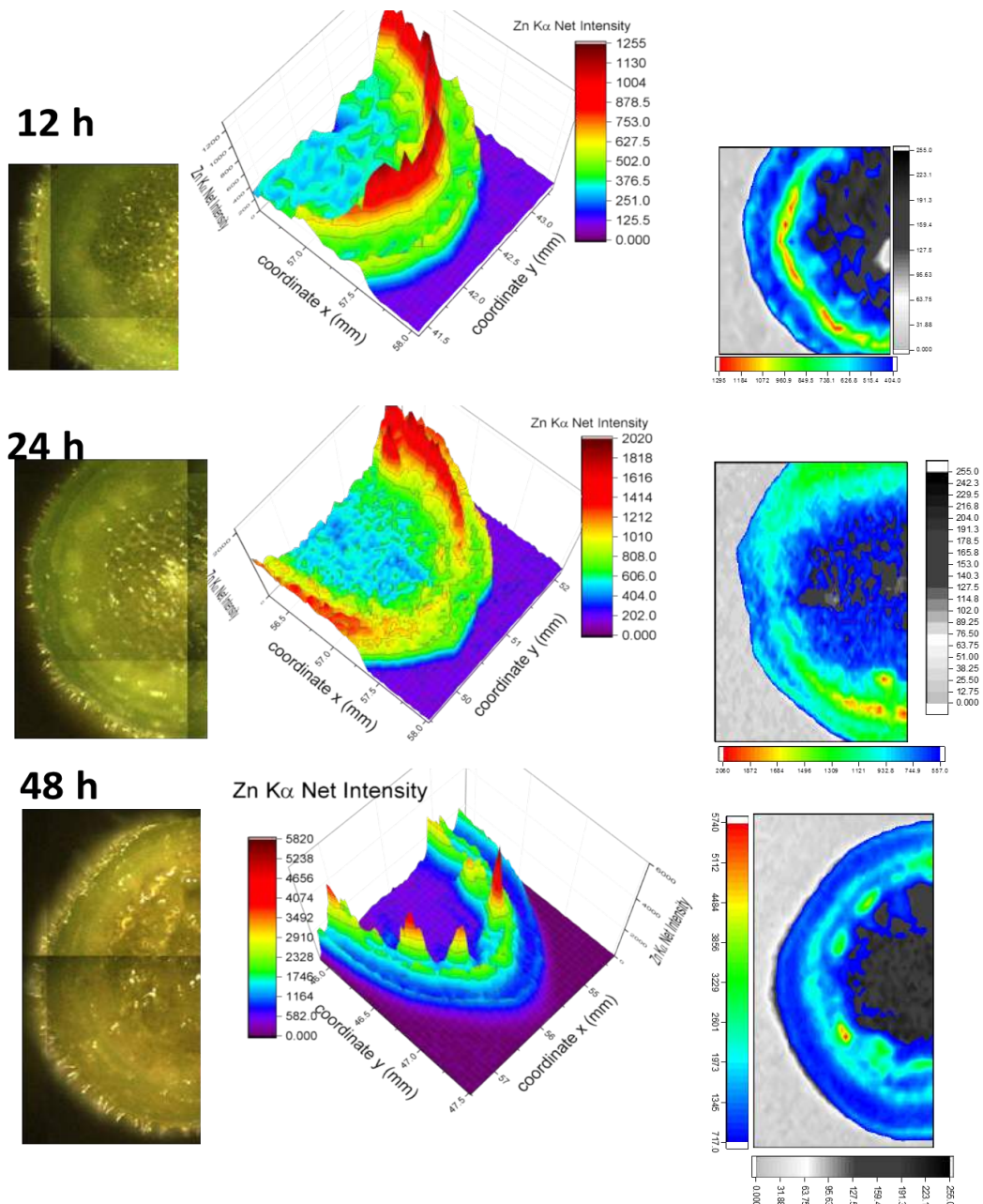
Figure 8 - Cross section of a *Phaseolus vulgaris* main stem, at 2 cm above the root crown, observed under the scanning electron microscope. T= trichome, C = cortex, E = epidermis, F = fibers, Pi = Pith, P = Phloem, VS = vascular system, X = xylem



Exploring the complementarity of μ -XRF and SEM imaging tools, one can conclude that the maximum intensity of the inner ring corresponds to the vascular region, composed of xylem and phloem. The maximum number of counts of the outer halo was found in the cortex–epidermis region.

Figure 9 presents the 3D plots and overlaps between Zn and the Rh-K α Compton scattering maps corresponding to Figure 7. Surprisingly, there was no gradient of Zn concentration from the inner vascular bundles to the outer parenchymatic region that discards diffusion between them. Conversely, one can see that there is a valley between the two Zn intensity maxima. Since it is well known that the transport from roots to shoots takes place through the xylem vessels, one would not expect to observe increasing Zn concentration in the outer cortex–epidermis without an outward gradient. The superposition of the Zn and Compton maps shows that the outer ring is close to the epidermis.

Figure 9 - 3D plots showing the spatial distribution of Zn in the stem of *Phaseolus vulgaris*. The roots of the plants exposed to 1000 mg L^{-1} 40 nm ZnO dispersion with surfactant for 12 h, 24 h and 48 h. It is also presented overlays between XRF and Compton maps. These images correspond to the same data shown in Figure 3



Roots have a structure called Casparian strip, which corresponds to a layer of cells with a lignified band that blocks the apoplastic movement of solutes and water. The two crests of Zn concentration, separated by a valley with no gradient (see Figure 9), suggest that

Zn found in the cortex was transported vertically upwards through an apoplastic route from the roots to shoots, bypassing the Casparian strip barrier in the endodermis. Therefore, Zn was transported to the aerial part by an alternative pathway to the xylem. This movement might be driven by the high Zn concentration gradient and mass flow induced by transpiration. To the best of our knowledge, this Zn translocation course has never been reported before and this topic deserves further investigation.

2.3.4. *In vivo* chemical speciation of Zn

Once it was clear that Zn was incorporated in the stem, a key question remained regarding its chemical species. As mentioned, reports in the literature do not agree on whether plants do or do not take up ZnO nanoparticles. Hence, the roots of the plants were exposed to the nano ZnO dispersion and XAS was employed to investigate the chemical state of Zn in roots and stems.

The XRF signals obtained for the experiments with the 100 mg L⁻¹ dispersions were not intense enough to yield satisfactory XANES spectra in terms of the signal-to-noise ratio. Therefore, in view of the experimental limitations, the speciation was carried out only to the 1000 mg L⁻¹ nano ZnO dispersions, even though this value may be above the concentrations to which plants might be exposed considering environmental concern to nanomaterials or the content of Zn employed in soil fertilization.

Appendix B (a) presents the XANES spectra for the ZnO nanoparticles used in the present study, while Appendix B (b) shows the XANES spectra for several Zn coordination compounds used as references to identify the chemical form of Zn inside the plants. Although malate, citrate, succinate and acetate present the same carboxyl functional group, their XANES spectra are considerably different.

A critical step in XAS speciation is the sample preparation. One has to prevent structural changes in the neighborhood of the analyte prior to the measurement, *e.g.* during sample preparation or preservation⁷⁹. To avoid this problem, the chemical environment of Zn absorbed by the plant was probed *in vivo*. Even if this approach is not as widespread as the measurement of freeze-dried, fixed, or frozen tissues, there are a few reports about this in the literature⁸⁰⁻⁸². To the best of our knowledge, this is the first report of *in vivo* XAS aiming at the speciation of absorbed nanomaterials.

One of the main difficulties of *in vivo* XAS measurements concerns the risk of radiation-induced damage, which can break chemical bonds, leading to membrane rupture, and changes in the chemical environment of targeted elements. According to the literature, radiation doses of 10^7 Gy can induce photoreduction and therefore damage on tissues⁸³⁻⁸⁵. In the present study, it was calculated that the dose that each plant received was in the order of 1.9×10^4 Gy (see the Appendix C). Moreover, no spectral changes for subsequent spectra (ca. 6 min for each spectrum) recorded in the same x-y coordinates were detected, therefore no induced chemical changes were observed.

Figure 10(a) presents the XAS spectra recorded for Zn-malate and 300 nm ZnO reference compounds, and for the stem of plants exposed to nano ZnO dispersions. The linear combination analysis of the spectra allows identifying the ratio of components in a mixture. The data show that Zn in the stem of plants treated with 40 and 60 nm ZnO was a mixture of ZnO and Zn-malate (see Table 3 and Appendix D; for the experimental setup used, refer to Appendix E). Two pathways for root absorption are known (Figure 10(b)). The symplastic transport takes place through cell connections called plasmodesmata. In this type of transport, solutes necessarily have to cross the plasma membrane to enter the cell. In apoplastic transport, solutes travel by diffusion or mass flux through the pores of the cell wall. Therefore, to be normally admitted into the xylem and consequently transported to the shoots, solutes such as nanoparticles or regular ions must, at some point, travel via the symplastic route.

Figure 10 - (a) Zn-K edge XAS spectra for Zn-malate and pristine 300 nm ZnO + surfactant reference compounds and spectra recorded at the stem of treated *Phaseolus vulgaris* plants whose roots were exposed to the different dispersions of nano ZnO. In this experiment, Zn was found as mixtures of ZnO and Zn-malate. When roots were intentionally damaged, ZnO was detected mostly in the stem; (b) the symplastic and apoplastic transport routes, the latter one is blocked by the Casparian strip in the endodermis; (c) image of an unintentionally injured secondary root during the initial XAS experiment using the setup shown in Figure S10

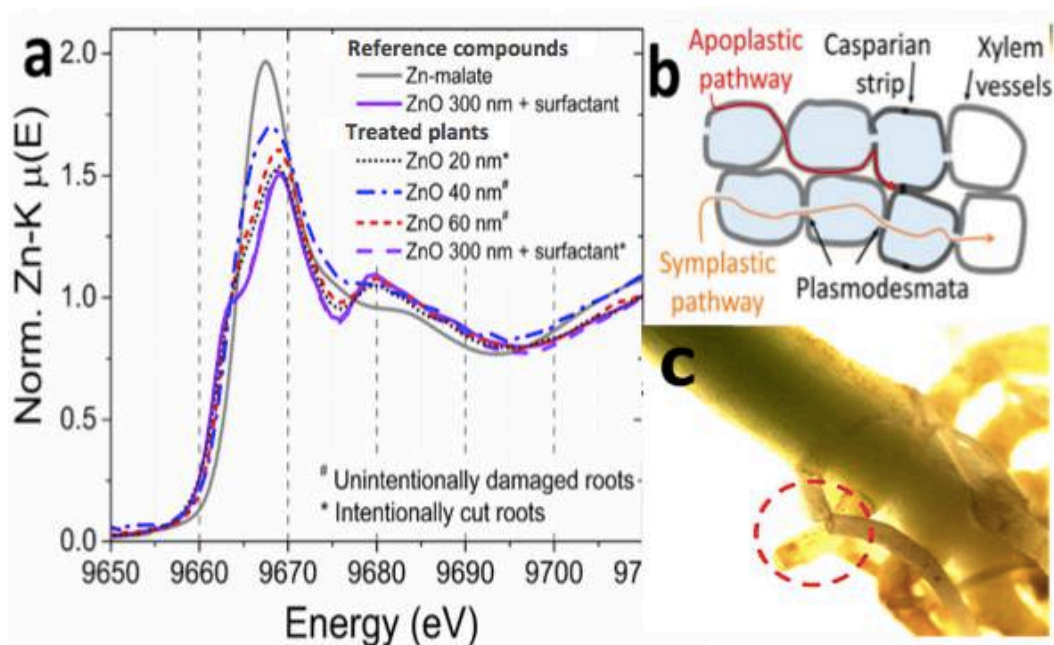


Table 3 - Linear combination analysis of XANES spectra *in vivo* recorded at the stem and roots *Phaseolus vulgaris* plants exposed to nano ZnO. Each spectrum corresponds to an average of three to five spectra

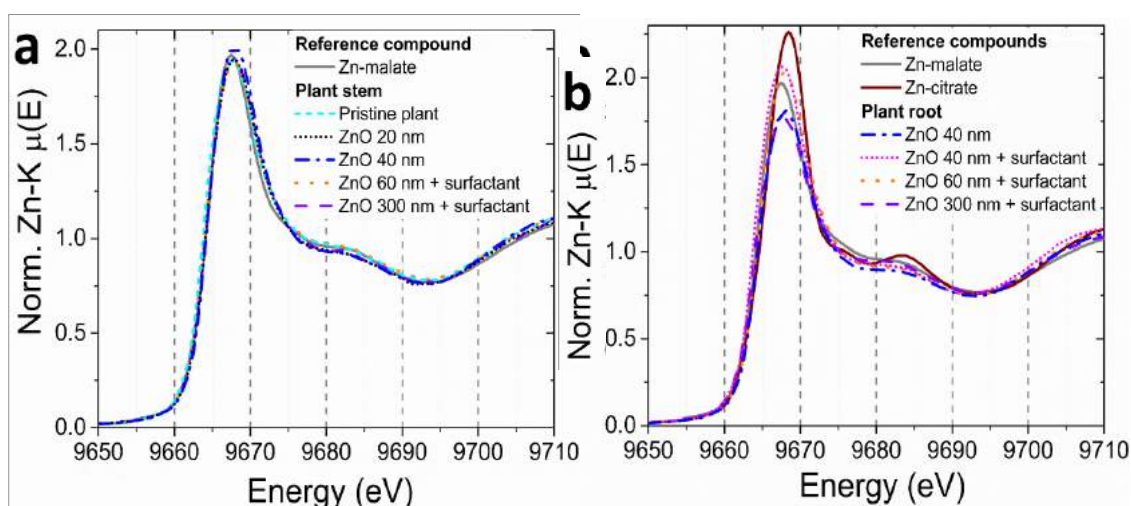
Treatment	Plant tissue	Fraction (%)			Fit disagreement (%)	
		ZnO	Zn-Malate	Zn-Citrate		Zn-Histidine
Pristine plant	Stem		95±2		5±2	0.56
ZnO 300 nm + surfactant	Stem		100			0.39
ZnO 60 nm + surfactant	Stem		100			0.43
ZnO 40 nm	Stem		67±4	33±4		0.36
ZnO 20 nm	Stem		84±2	16±2		0.26
ZnO 300 nm + surfactant	Root		71±4	8±5	21±2	0.50
ZnO 60 nm + surfactant	Root		66±4	34±4		0.33
ZnO 40 nm + surfactant	Root		62±6	38±7		0.46
ZnO 40 nm	Root		68±8	20±6	12±11	1.33
Damaged root ZnO 60 nm	Stem	74±2	27±2			0.34
Damaged root ZnO 40 nm	Stem	38±4	62±4			0.95
Damaged root ZnO 300 nm + surf.	Stem	96±2	4±2			0.06
Damaged root ZnO 20 nm	Stem	82±2	18±2			0.14

No nanoparticle specific membrane transporters have been so far identified in plants. However, researchers claim that nanoparticles can damage the membranes, enter the cell and be transported through plasmodesmata channels²⁸. Hence, there was an investigation on why ZnO was preliminarily detected in the stem by XAS (Figure 10(a)). A thorough inspection of the roots after the experiments unravelled tissue damages, as shown in Figure 10(c). A suggestion is that these injuries allowed nano ZnO to enter directly in the xylem. The injuries may have been caused by the sample holder (Appendix E). It is important to highlight that these first observed damages were not deliberated, they were caused during transferring the plants to the sample holder.

Thus, portions of the roots were intentionally damaged, including the primary root, and these were immersed in the 20 nm and 300 nm ZnO dispersions for 3 h. The spectra (Figure 10(a)) show that for the 300 nm dispersion, 96% of the Zn in the stem was nano ZnO. This happened because the barriers that prevent particles to have access to the xylem were removed. Therefore, nano ZnO was transported to the shoot through mass flux.

Additional XAS spectra recorded for stems and roots are presented (Figure 11(a) and (b), respectively) using another sample holder shown in Appendix F. The linear combination analysis of the spectra elucidated that Zn was mainly found as mixtures of Zn-malate and Zn-citrate, which are two organic compounds reported to transport Zn to vacuole^{86–88}. For some treatments, small contributions of Zn-histidine were observed in the roots. The proportion of citrate seemed to be higher in the roots than in the stem. No ZnO was found neither in the roots nor in the stem (see Table 3, Appendix G and H). A similar chemical environment was previously reported for *Noccea caerulea*⁸¹.

Figure 11 - Zn-K edge XAS spectra recorded at the roots and stem of common bean (*Phaseolus vulgaris*) plants which roots were not damaged. In (a) spectra recorded at the stem where Zn was found mainly as Zn-malate. In (b) spectra recorded at the roots, Zn was found as mixture of Zn-citrate, Zn-malate; Data recorded using the setup shown in Figure S11



Differently from Sarret *et al.* who reported contributions of Zn-phosphate in hyperaccumulator *Arabidopsis halleri*⁸⁹ and Lv *et al.* who noted that a major fraction of Zn binds to phosphorus in roots of *Zea mays*⁶¹, in the present study, Zn was not found associated to phosphorus forms. Hence, one can infer that the Zn chemical environment varies from one plant species to another.

Although the present study did not find any evidence of the uptake of entire nanoparticles in entire roots, still one has to keep in mind the rather low sensitivity of XAS to distinguish between different chemical species. The uptake of Zn in ionic form rather than the nanoparticulate form was also shown by Lv *et al.* in *Z. mays*⁶¹. Nevertheless, if only a small fraction of nano ZnO was present, e.g. <5%, it would be difficult to capture it in the linear combination analysis⁹⁰. Considering soil or hydroponic solution media, root injuries can be caused by mechanical impact, microorganisms, nematodes or insects.

The *in vivo* XAS speciation shows that Zn was transported as soluble Zn-organic complexes. Inside the roots, it was coordinated to citrate, malate and histidine, whereas along the stem, it was associated mostly to malate. *In vivo* measurements were only possible because of the relatively low photon flux supplied by the bending magnet XAFS2 beamline. Therefore, undulator based high brilliance beamlines may not be the best option for this type of study. In the latter case, the use of attenuators might be required.

A hypothesis that may explain why researchers have reported nano ZnO in the shoot system^{16,17} may be the consequence of its reconstitution inside the vacuole. In addition, nano ZnO could have been transported through the xylem due to root injuries caused either by the harshness of the medium, such as the typical high nanoparticle concentration employed in these experiments, or inadvertently by root fracture.

Additionally, the Zn distribution uncovered by μ -XRF implies that the parenchymal apoplastic alternative transport route is not negligible. Since the cell wall pore size is in the order of 10–20 nm⁹¹, particles smaller than that could travel across these pores and be transported from roots to shoots, circumventing the xylem route. The share of this route of transport to the total nutrient uptake deserves deeper investigation.

It is still not clear whether the dissolution of ZnO nanoparticles and the complexation of Zn by malate and citrate take place exclusively in the rhizosphere or also inside the root. The presence of ZnO inside the plant when roots are intentionally injured indicates that the ZnO dissolution and further complexation were not a fast processes.

2.4. Conclusions

Altogether, the results here presented showed that by choosing the size of the nanoparticle and the dispersion medium, either water or aqueous media plus surfactants, one can manage the rate of nutrient supply.

The *in vivo* X-ray spectroscopy approach was suitable to investigate the transport and chemical environment of Zn. It can be extended to other elements allowing the monitoring of metabolic processes while they are happening.

The higher absorption of Zn supplied by the particles dispersed with surfactants has been attributed to the higher solubility of the Zn dispersions, although the negative zeta potential may also have an influence. The rate of absorption along the 48 hours followed a linear function of time. The uptake velocities were positively correlated to the solubility through an exponential function. Therefore, it indicates that the velocity of absorption is governed, among other factors, by the concentration of Zn in solution.

The root to shoot transport takes place mainly through the xylem vascular bundles. Nevertheless, the μ -XRF images taken from freshly cut tissues unraveled that the root to shoot solute movement through the outer tissues, such as the cortex, also plays a meaningful role.

In vivo XAS showed that Zn is not transported as ZnO nanoparticles. It is rather associated to organic molecules such as malate and citrate. The proportion among these components binding to Zn varies from the roots to the shoots. ZnO was only found in the stem when roots were injured. Finally, these results suggest that ZnO nanoparticles are firstly dissolved and then Zn ions are transported to plant shoots.

3. PHYSIOLOGICAL EFFECTS AND ROOT-TO-SHOOT ZINC TRANSPORT FROM ZnSO₄ AND ZnO NANOPARTICLES ON *Phaseolus vulgaris* PLANTS

Abstract

New technologies are necessary to improve plant nutrient uptake and decrease nutrient losses. The knowledge about how NPs are uptake and its physiological effects on plants are required to use this technology in agriculture. In this study, *Phaseolus vulgaris* plants had their roots in contact with nanoparticles ZnO dispersions and ZnSO₄ solution for 48 hours. Zn absorption was *in vivo* monitored in different points of the plants by X-ray fluorescence spectroscopy. X-ray absorption spectroscopy was used to analyze the chemical environment of Zn in ZnO dispersion and ZnSO₄ solution after root contact. Energy dispersive X-ray fluorescence measured the Zn content of shoots from plants exposed to ZnO dispersions and ZnSO₄ solutions. Physiological effects of plants exposed to NPs and ZnSO₄ were determined by infrared gas analyser compared to a control treatment. Zn kinetics uptake presented a gradient on root to shoot Zn content, exception for ZnSO₄ at the highest concentration. XAS presented a difference on the chemical environment of ZnO dispersion after root contact. Regardless concentration, both ZnO NPs presented similar Zn content on shoot tissues, and also presented smaller Zn content compared to ZnSO₄ source. Water conductance, transpiration and photosynthetic rates decreased after 48 hours of exposure to ZnO NPs and ZnSO₄ relatively to the control plant.

Keywords: XRF. XAFS. Zn absorption. Zn transport.

3.1. Introduction

The application of nanotechnology is emerging as a new method to increase crop yields. One of the advantages that nanomaterial-related fertilizers might present over conventional ones is the high uptake efficiency^{92,93}. In principle, nanofertilizers could dispense nutrients according to the plant growth demand, releasing an environmental friendly dosage and reducing the amount of leaching into the soil and water bodies^{94,95}.

Zinc (Zn) is the micronutrient with the most common deficiency in soils around the world⁹⁶. For the supply of this micronutrient, scientists and companies research different sources of Zn to achieve the greatest fertilizer. Zn sulphate is known to be the commonly used inorganic source of Zn⁹⁷⁻⁹⁹, specifically because of its higher solubility comparing with other sources, like synthetic chelates and complexes¹⁰⁰. The Zn chelates forms are known to decrease the metal ion immobilization by soil particles, being greater sources to move Zn ions into the plant roots through the soil, but the leaching is a point of concern¹⁰¹.

Nanometric zinc oxide is one of the promising alternatives to enhance yields and growth of plants⁹³. Previous studies showed that it can increase the stem and root biomass in peanuts¹⁰², tomato¹⁰³ and positively impact the photosynthesis efficiency in *rabidopsis*¹⁰⁴. However, the lack of knowledge on metal NP delivery, assimilation, transport, biotransformation and accumulation^{20,105} in plant tissues and along the food chain, is a bottleneck to expand the application of the fertilizers based on nanomaterials.

It is reported that Zn is transported from root external cells to the xylem via cytoplasmic cells, linked by plasmodesmata where Zn moves through the symplastic pathway⁵⁰. On the other hand, apoplastic pathway also contributes on the transport of Zn from root to shoot tissues, especially when the environment concentration of Zn is high¹⁰⁶.

In the nanoparticle subject, the driving paths that NPs travel in plant are not fully clear. The dynamics of absorption and behavior of nanoparticles from roots to shoots are associated with their size, type, chemistry, composition and stability²¹. It can adhere to the root surface, physically attaching to the plant via sticky exudates in the rhizosphere¹⁰⁷, or decompose forming ions in soils and being absorbed by the common way in the soil solution, by metal transporters, ion channels, protein carriers or aquaporins²⁰.

The altered Zn levels activate genes to avoid the excessive or the poor absorption and accumulation in plant tissues such as transcriptional factors, enzymes, channels and transporters¹⁰⁸. The Zn transporter avoid its toxicity by modulating the influx and efflux of extracellular and intracellular membranes, controlling the metal concentration and distribution¹⁰⁹.

Zn intoxication has implications in many vital processes, because it is a constituent of special proteins related to DNA and RNA stabilization, causing genetic related disorders in presence of Zn excess^{41,110,111}; it is also component of enzymes and ribosomes. In addition to this, Zn direct participates in root development, chlorophyll and carbohydrates formation, affecting structure and growth parameters when found in excess on plant tissues¹¹².

In this study we investigated how young *Phaseolus vulgaris* plants transported and physiologically responded to different sizes and concentrations of ZnO nanoparticles (40 nm and 300 nm). Aqueous ZnSO₄ was employed as a positive control. The Zn concentration was traced in three points of the stem and in the petiole. XAS was employed to explore the dynamics of dissolution of nano ZnO in contact with roots and to evaluate the chemical

species of Zn in the leaves. The plant physiology was monitored by the water and CO₂ exchange behavior.

3.2. Experimental

3.2.1. Characterization of ZnO NPs

The characterization with XRD, DLS and SEM of 40 nm dispersed on distilled water and 300 nm with surfactants dispersed on distilled water ZnO NPs followed the same procedures described in section 2.2.1.

It was used the same sample preparation for evaluate the solubility, the only difference is that ZnO NPs dispersions and ZnSO₄ solutions were left in contact with roots for 48 hours before take the aliquot.

3.2.2. *In vivo* Zn monitoring in plants

The same conditions applied in section 2.2.2. were used for this evaluation. The only difference consisted in the analyzed parts of the plants. Here, we evaluate three points at the stem and one point at the petiole, as indicated on Appendix I

3.2.3. Zn quantifying in plants shoots

Shoots of *Phaseolus vulgaris* plants exposed to 40 nm ZnO NPs, 300 nm ZnO NPs with surfactants dispersions and ZnSO_{4(aq)} solution were dried at 60°C in an oven for 72 hours. The shoot (leaves and stem) were ground in a porcelain mortar and sieved with a 100 mesh sieve. Then, 50 mg of shoot tissue was deposited and gently pressed with a glass stick in a XRF cuvette, covered in the bottom with 5 µm polypropylene film.

Standard addition method was used to evaluate Zn content in this tissue with a benchtop EDXRF operating at 50 kV, 1000 µA, under vacuum and beam spot of 3 mm. In the same matrix and same mass of the samples were added standard solution of Zn, and after drying it was fully homogenized in a porcelain mortar, and it follows the same procedure described above for the samples.

3.2.4. Zn chemical speciation in dispersions and solution

The Zn-K edge X-ray absorption near edge spectroscopy (XANES) measurements were carried out at the same beamline described in section 2.2.4. There we analyzed the leaves of plants exposed to $\text{ZnSO}_{4(\text{aq})}$, 40 and 300 nm ZnO NPs; ZnO dispersion and ZnSO_4 solution after remaining in contact with roots for 48 h. Each XANES spectra was acquired in 20 minutes and three spectra per point per sample were measured. These spectra were merged, energy calibrated and normalized using Athena program within the IFEFFIT package.

Additionally to the samples, it was also recorded data for the reference compounds, pristine nano ZnO and ZnSO_4 as mentioned in topic 2.2.4.

3.2.5. IRGA

Gas exchanges were measured in the middle leaflet of the expanded trefoil, 5 times, with no exposure (t0) to treatments, after 15 minutes of exposure (t0.4), after 60 minutes after exposure (t1), after 24 hours of exposure (t24) and after 48 hours after exposure (t48).

For this purpose, evaluations of gas exchange consisted of non-destructive analyses using a portable gas exchange device (Infra Red Gas Analyzer – IRGA, Li-6400XT, LICOR Inc.). The following were determined: CO_2 assimilation rate expressed by area (A - $\mu\text{mol CO}_2 \text{ m}^{-2} \text{ s}^{-1}$), transpiration (E - $\text{mmol H}_2\text{O m}^{-2} \text{ s}^{-1}$), stomatal conductance (gs - $\text{mol H}_2\text{O m}^{-2} \text{ s}^{-1}$), and internal CO_2 concentration in the substomatal chamber (Ci - $\mu\text{mol mol}^{-1}$). The initial conditions imposed for measurements were $1000 \mu\text{mol m}^{-2} \text{ s}^{-1}$ of photosynthetically active radiation (PAR), provided by LED lamps, air CO_2 concentration of $400 \pm 20 \mu\text{mol mol}^{-1}$, and a chamber temperature of $25 \text{ }^\circ\text{C}$, according to the others studies^{113,114}.

3.3. Results and Discussion

3.3.1. Zn kinetics in different parts of *Phaseolus vulgaris* plants

The Zn content was monitored in three points of the stem and in the petiole of the central leaf as shown in Figure 1 (a). Figure 1(b-d) presents the Compton normalized counts of Zn in these four above mentioned regions for *P. vulgaris* plants exposed to $\text{ZnSO}_{4(\text{aq})}$, 40 nm and 300 nm ZnO dispersions at 100 and 1000 mg Zn L^{-1} . The Compton scattering

normalization intends to correct thickness effects, making the detected X-ray fluorescence proportional to Zn concentration instead of capturing the total amount of Zn. This is important because the diameter of the stem can slightly vary from one part of the plant to another.

One can observe that the Zn concentration decreases from P1 to the petiole, i.e. from root to shoot. The only exception was the $\text{ZnSO}_{4(\text{aq})}$ at $1000 \text{ mg Zn L}^{-1}$ that presented anomalous behavior, for example by the end of the experiment the concentration of Zn in the P3 point was higher than in P1, moreover the concentration of Zn in P2 was the same as in the petiole. This different trend was confirmed in the second biological replicate, where once again, plants were wilted, with clearly visual symptoms.

Figure 1(b-d) also reveals that the concentration of Zn in the different points along the stem was more homogenous for 40 nm and 300 nm ZnO than for ZnSO_4 . The amplitude of the gradient of concentration from root to shoot decreased as follows $\text{ZnSO}_{4(\text{aq})} > 40 \text{ nm ZnO} > 300 \text{ nm ZnO}$.

Although the concentration of the dispersion in which the roots were immersed was 10-fold a part, i.e. 100 and $1000 \text{ mg Zn L}^{-1}$, it presented only a slight effect on the concentration of Zn found in the stem regions. This was in agreement to the solubility data, since it also did not present great changes with the concentration rise. The exception were the treatments with $\text{ZnSO}_{4(\text{aq})}$, after 48 h exposure the number Zn counts for the $1000 \text{ mg Zn L}^{-1}$ solution was four fold higher than that measured for the 100 mg Zn L^{-1} solution. In the case of the petiole, this figure was 100 times higher for the $1000 \text{ mg Zn L}^{-1}$ than for the 100 mg Zn L^{-1} .

Figure 12 - *In vivo* monitoring of the concentration of Zn in three points of the stem and in the petiole of *Phaseolus vulgaris* whose roots were immersed in 100 and 1000 mg Zn L⁻¹; (a) the location in which the measurements were performed, (b) uptake of Zn in plants exposed to (b) ZnSO_{4(aq)}, (c) 40 nm ZnO, (d) 300 nm ZnO

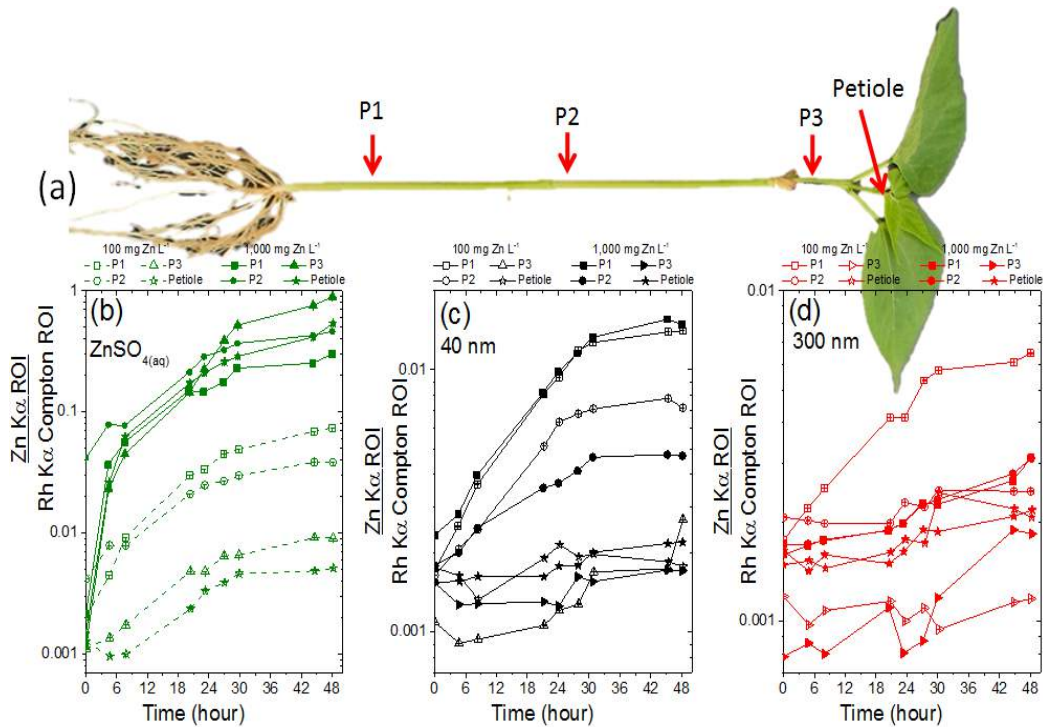


Figure 13 presents the uptake velocity along the shoot for plants exposed to (a) 100 mg Zn L⁻¹ and (b) 1000 mg Zn L⁻¹ treatment, the corresponding fitted slopes and correlation coefficients are presented in Appendix I.

Regardless the point of measurement and the concentration of the treatment, the Zn content followed a linear function of time. This finding is in agreement with the previous experiment involving more ZnO particles sizes and only single point of the stem reported in section 2.0. above. It shows that, for most treatments, not only the content of Zn decreased from root to shoot, but also the uptake velocity diminished, i.e. the uptake decelerates from root shoot. It shows that the plant trended to store Zn in the lower tissues. Again, a divergent behavior was observed for ZnSO_{4(aq)} at 1000 mg L⁻¹, for this treatment the uptake velocity increased in the upper tissues. The high concentration of Zn readily available might have saturated the lower tissues of the stem which gradually stopped accumulating whereas the upper were still be to keep storing Zn.

Figure 13 - Zn uptake velocity in three points of the stem and petiole of *Phaseolus vulgaris* whose roots were exposed to (a) 100 mg Zn L⁻¹ and (b) 1000 mg Zn L⁻¹

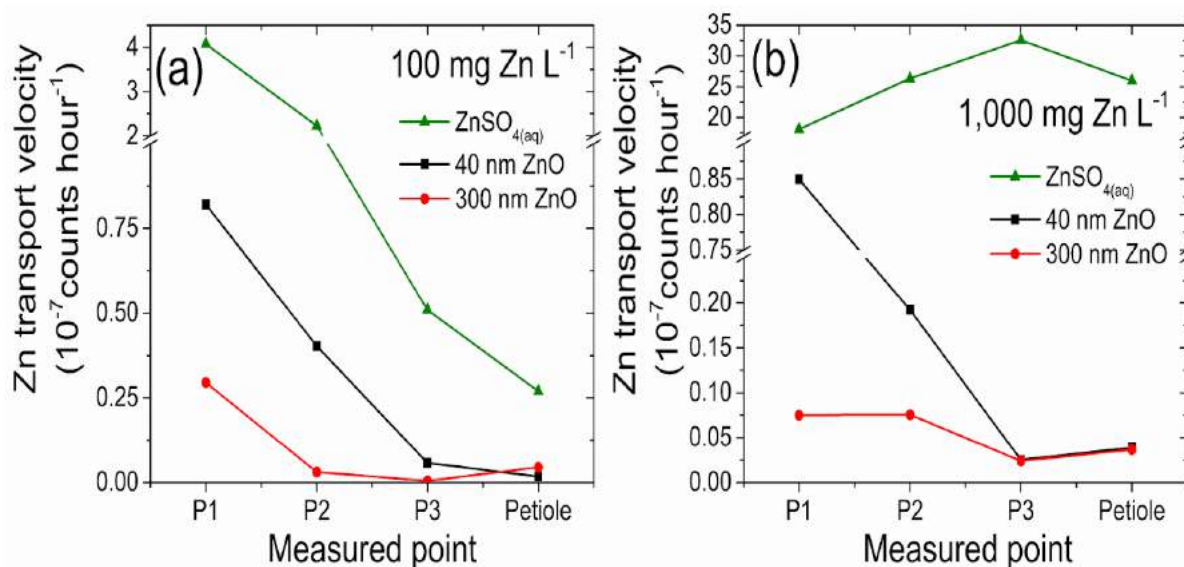


Table 5 presents the solubility of ZnO nanoparticles in the presence and absence of roots in the dispersions. The concentration of ZnO in the dispersion presented only a slight effect on the content of dissolved Zn. The amount of dissolved Zn for 40 nm ZnO NPs increased in the presence of roots, this effect is supposed to be caused by organic acids exudates produced by the roots, being a response consistent with other authors who reported some modifications in nanoparticles properties made by root exudates^{115–117}. Experiments analyzing the bioavailability of copper ions from soil exposed to synthetic root exudates and nano Cu revealed an increase in the Cu²⁺ concentration in the soil solution¹¹⁸. These molecules can both decrease the pH and chelate the Zn in solution shifting the equilibrium and therefore dissolving the ZnO.

Table 5 - Solubility of ZnO nanoparticles, with 100 and 1000 mg Zn L⁻¹, dispersions after 48 hours in presence and absence of *Phaseolus vulgaris* roots

Treatments		Solubility	
Root Contact	40 nm	30.1±4.5	
	100 mg L ⁻¹	300 nm	7.7±0.9
		ZnSO ₄	106.1±10.6
	1000 mg L ⁻¹	40 nm	20.7±4.1
		300 nm	8.2±1.2
		ZnSO ₄	1180.2±11.7
Water		40 nm	9.6±0.6
	100 mg L ⁻¹	300 nm	6.7±0.4
		ZnSO ₄	101.8±1.5
	1000 mg L ⁻¹	40 nm	8.4±0.3
		300 nm	8.6±0.5
		ZnSO ₄	995.2±23.3

3.3.2. Zn content in shoot tissues

EDXRF was used to quantify the Zn content in the shoot of plants exposed to ZnO dispersions and ZnSO₄ solution. Analyzing Table 6, it is possible to notice that for both concentrations, shoots of plants treated with ZnSO₄ presented higher Zn content those exposed to ZnO NPs. This can be explained by the solubility of sulphate source compared to ZnO NPs. The contents of Zn in the shoot of plants treated with 40 nm ZnO NPs and 300 nm ZnO NPs were similar. The greatest concentration of ZnSO₄ probably damaged the root cells with the high concentration of this salt and allowed the indiscriminate Zn uptake.

Table 6 - Zn content (mg kg^{-1}) and standard deviation on leaves of plants treated with ZnO nanoparticles and ZnSO_4 , in 100 and 1000 mg L^{-1}

Concentration (mg L^{-1})	Treatment	Zn content (mg kg^{-1})
100	40nm	93.7±0.078
	300nm	99.5±0.015
	ZnSO_4	363.4±0.007
1000	40nm	111.2±0.002
	300nm	104.7±0.004
	ZnSO_4	19472.9±0.121

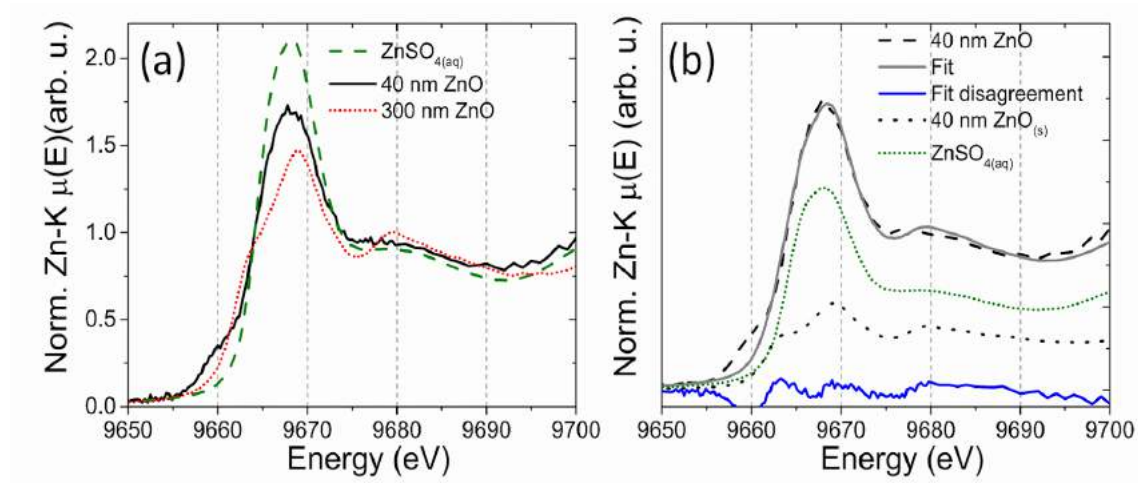
3.3.3. Chemical environment of Zn in root presence

XANES was employed to probe how roots influenced the chemical environment of dissolved and dispersed Zn. Figure 14(a) shows the XANES spectra recorded in aliquot collected from $\text{ZnSO}_{4(\text{aq})}$, 40 nm and 300 nm ZnO solution and dispersions that were let in contact with roots for 48 hours. The different spectral features indicated that Zn chemical environment was not the same for all treatments. The spectra suggested that the roots did not cause any measurable change in the chemical neighborhood of $\text{ZnSO}_{4(\text{aq})}$ and 300 nm ZnO. Conversely, the spectra for 40 nm ZnO was modified.

Figure 14(b) shows that after 48 hours in contact with roots, the 40 nm ZnO was partially dissolved, the linear combination analysis of the XANES spectrum unravels that Zn could be described a mixture of 63% soluble Zn and 37 % 40 nm ZnO. The linear combination was carried out using Zn-malate coordination compound, however the spectrum of Zn-malate in solution was very close to the given by aqueous ZnSO_4 , the only difference lied in the feature in 9675 eV. Thus, we could not assign the chemical nature of the soluble fraction.

Hence, the combination of *in vivo* X-ray probing of Zn concentration, Zn dissolution assays and chemical speciation of the dispersed/dissolved Zn shows that the key factor controlling the uptake of Zn is not the concentration of the nanoparticle, but the amount dissolved Zn. The uptake of Zn from the 300 nm ZnO was smaller due to its lowest solubility. The amount of dissolved Zn, in turn, varied only slightly with the concentration of the dispersed ZnO and depended more on the nanoparticle size. Therefore, by defining the nanoparticle size, one can control the rate of Zn absorption.

Figure 14 - XANES spectra recorded for liquid aliquots collected from the solution and dispersions that remained 48 hours in contact with plant roots; (a) XANES spectra highlighting the different chemical environment for $\text{ZnSO}_{4(\text{aq})}$, 40 nm and 300 nm ZnO and (b) linear combination analysis for 40 nm ZnO

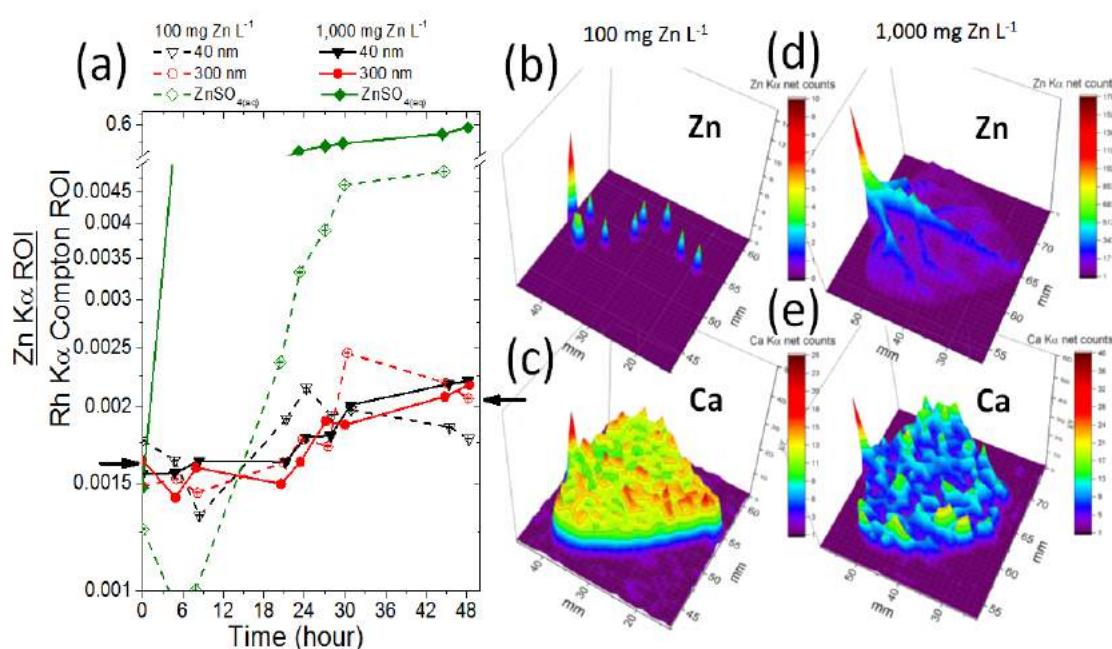


3.3.4. Zinc in the petioles, leaves and biological effects

Figure 15(a) shows that except for ZnSO_4 at 1000 mg L^{-1} , the concentration of Zn in the petiole was not affected by the nanoparticle size and concentration. As discussed above, the plant stem tissues acted as buffer storing Zn and thus preventing it from moving upwards. Since the intensity of an X-ray fluorescence signal holds a linear relationship with concentration of the analyte, one can state that the concentration in the petiole of the plant treated with ZnSO_4 at 100 mg L^{-1} increased nearly 4-fold during the 48 hours of exposure. On the other hand, the concentration of Zn in the petiole of plants whose roots were immersed in 40 nm and 300 nm ZnO at 100 and 1000 mg L^{-1} increased by a factor less than 1.5 fold.

Figure 15(b-e) shows the spatial distribution of Zn and Ca in the central leaflet of the first trefoil (the one held by the XRF monitored petiole), (b) and (c) present maps for the plant treated with ZnSO_4 at 100 mg L^{-1} , while (d) and (e) for the plants treated with 1000 mg L^{-1} . Since Ca is abundant and little mobile in the plant tissue, it was plotted here intending to assist the reader visualize the leaf. Figures 15(b) and (d) show that Zn concentration decreases from the petiole to the leaf tip, this behavior was similar to that found for the stem. Zinc is mainly concentrated in the midrib for the plant treated with $1000 \text{ mg Zn L}^{-1}$ (Figure 14(d)) it can also be observed in the lateral veins.

Figure 15 - (a) Content of Zn in the petiole as function of time for plants exposed to 100 and 1000 mg Zn L⁻¹ of ZnSO_{4(aq)}, 40 nm and 300 nm ZnO; (b) and (c) spatial distribution of Zn and Ca, respectively, in the leaf whose plant was exposed to 100 mg Zn L⁻¹ of ZnSO_{4(aq)}, (d) and (e) spatial distribution of Zn and Ca, respectively, in the leaf whose plant was exposed to 1000 mg Zn L⁻¹ of ZnSO_{4(aq)}. The chosen leaflet was the central one in the first trefoil that was attached by the XRF monitored the petiole

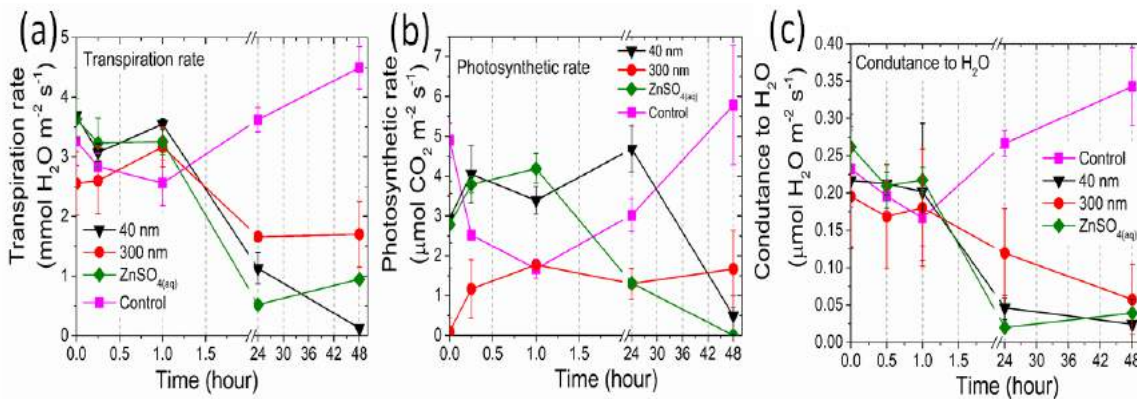


The capacity of cotyledon leaves to behave as a Zn sink preventing the intoxication was evaluated, however the content of Zn found in the cotyledon leaves was smaller than that observed in the trifoliolate leaves. Thus, this hypothesis was rejected.

The effects of Zn treatments on plant physiology were monitored using the infrared gas analyzer. Figure 16 presents the measured (a) transpiration and (b) photosynthetic rates as function of time for plants whose roots were immersed in 1000 mg L⁻¹ ZnO (40 nm and 300 nm), ZnSO_{4(aq)}, and a control plant that did not receive Zn. The data was acquired in the central leaflets of the first trefoil. The transpiration rate and conductance to H₂O were not affected during the first hour of treatment exposure. On the other hand, the measurement performed 24 hours later showed that transpiration rate decreased whereas the photosynthetic rate was only reduced in the plants treated with ZnSO₄. Finally, past 48 hours of exposure, the photosynthesis of the plants treated with 40 nm ZnO also decreased.

These results indicate that Zn coming from ZnO nanoparticles source takes more time to be absorbed by plants in toxic quantity, revealing to be released slower comparing with ZnSO_4 source.

Figure 16 - (a) transpiration - T, (b) photosynthetic rate - A and (c) stomatal conductance - g_s taken on the leaves in common bean plants exposed to $1000 \text{ mg Zn L}^{-1}$ 40 nm and 300 nm ZnO dispersions, $\text{ZnSO}_{4(aq)}$ and nutrient solution, for 48 hours

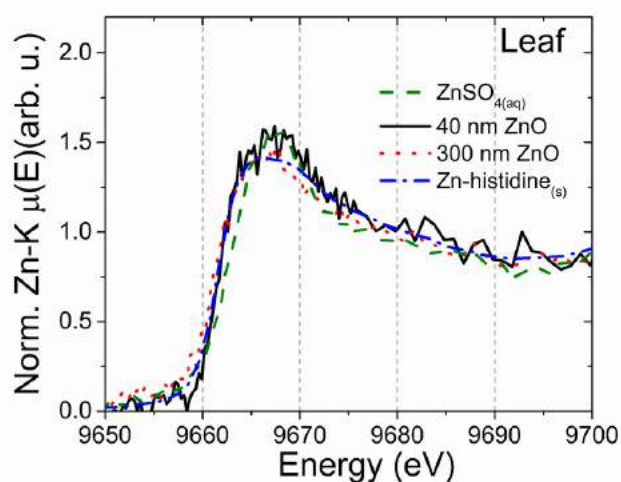


The data in Figures 15(a) and 16(a) shows a negative correlation between the Zn content in the petiole and the transpiration rate on leaves, what can be explained by the cortical cells plasmolysis and cell disruption¹¹⁹ which affects the photosynthetic rate and conductance to H_2O (Figure 16(b) and (c), respectively). For 300 nm ZnO, the lower concentration in the petiole (Figure 12 (d)) can explain the deleterious effects promoted by this treatments were less steep than those observed for ZnSO_4 and 40 nm ZnO.

Thanks to the control experiments, one can hold that the increasing concentration of Zn in the shoot was responsible for slowing down the plant metabolism, corroborating some authors that found reduction on photosynthesis rate and stomatal conductance in response to Zn^{+2} toxicity¹²⁰. The transpiration rate at leaves decreased before the Zn concentration in the petiole started to increase, it means that the transpiration might be a primary response to the increase of Zn content in roots and in the stem of plants. The photosynthesis, in the opposition, was impaired by Zn in the leaf. A surprising piece of information regards the amount of Zn necessary to trigger the deleterious effects on photosynthesis. The photosynthetic rate in the plants treated with ZnO was diminished by an increase of ca. of 50 % of the Zn concentration.

Figure 17 shows the XANES spectra recorded in the leaves of the plants exposed to 1000 mg Zn L⁻¹ of ZnSO_{4(aq)}, 40 nm and 300 nm ZnO, additionally this figure displays a spectrum for Zn-histidine reference compound. Regardless the source, Zn is stored in a chemical environment similar to Zn-histidine in *P. vulgaris* leaves. Zn excess is supposed to be stored in the cell vacuole as a detoxification mechanism, because this way, the Zn content on cytoplasm and nucleus decreased¹²¹. No induced chemical changes were observed on the leaves of the plants exposed to radiation.

Figure 17 - XANES spectra *in vivo* recorded in the leaf of plants exposed to 1000 mg Zn L⁻¹ of ZnSO_{4(aq)}, 40 nm ZnO and 300 nm ZnO, additionally it is presented the spectrum for Zn-histidine reference compound



3.4. Conclusions

Zn kinetics on different points of *Phaseolus vulgaris* plants indicated that exists a gradient of Zn content from root to shoot. Similarly, the uptake velocity decreases from root to shoot, except for sulfate source with the highest concentration.

The solubility of the NPs dispersion did not had great changes when the concentration of the dispersion increased 10 fold. On the other hand, the presence of roots slightly increased the Zn solubility, probably because of the exudates expelled by roots. The presence of roots also changed the chemical environment of 40 nm NPs.

Zn shoot content was almost the same for both NPs sources and concentrations. However, ZnSO_4 presented the higher Zn content for both studied concentrations.

XRF maps showed that Zn coming from sulfate source in the highest concentration was translocate in leaves mainly in its veins, and stem of the plants acted buffering the high Zn concentration. Regardless the Zn content and type of source, in the leaves it was found a chemical neighborhood similar to Zn-histidine.

The transpiration rate of leaves had a negative correlation with Zn content in the petiole. Photosynthetic rate and conductance to H_2O were also impaired by the presence of high amount of Zn on petiole and leaves.

4. MORPHOLOGICAL EFFECTS, SPAD INDEX AND NUTRIENT CONCENTRATION IN *Phaseolus vulgaris* PLANTS EXPOSED TO ZnO NANOPARTICLES: A LONG-TERM EXPOSURE EXPERIMENT

Abstract

Fertilizers are widely used and can boost plant development if used in the right moment and concentration. Many sources of nutrients are tested to reach the best performance, and NPs are one of them. This study verified the morphological effects, SPAD index and nutrient content in *Phaseolus vulgaris* hydroponically root exposed to ZnO NPs dispersion and ZnSO₄ solution. We evaluated the effects of three concentrations (1, 3 and 10 mg Zn L⁻¹) and four exposure periods (7, 14, 21 and 28 days for biometrics and nutrient concentration; and 4, 11, 18 and 25 days for SPAD). X-ray fluorescence microanalysis was employed to map the Zn location in the stem of plants. Energy dispersive X-ray spectroscopy measured the nutrient content in root and shoot tissues. Root length, shoot height, root dry mass, shoot fresh mass and leaf area were more impaired by Zn concentration than Zn sources. SPAD presented smaller indexes in treatments with 10 mg of Zn L⁻¹. Regardless Zn source and concentration, Zn apparently is found on the same regions of the stems. Zn content on both root and shoot tissues were directly related to Zn concentration of the dispersions/solutions. Zn content in roots was positively correlated with P and K content, and negatively correlated with S and Ca. In shoots, Zn content was positively correlated with K and Mn content, and negatively related with S, Ca and P.

Keywords: XRF. Nutrient correlation. Nanomaterial as fertilizers.

4.1. Introduction

Nanotechnology is a well-established in many fields like electronics¹²², clothing¹²³, paints¹²⁴ and civil engineer¹²⁵, but because of its unknown properties regarding effects on living beings metabolism, it is not widely spread in the agriculture . Since there is still no consensus about toxic effects of nanomaterials, their use in agriculture might suffer an initial rejection.

In this context, nanoparticulated ZnO can be employed as a Zn source for plants. It was shown in Chapter 2 that *Phaseolus vulgaris* only take up entire nanoparticles when roots are injured, otherwise ZnO is dissolved and the plant absorbs Zn²⁺ ions. On the other hand, other researchers reported that plant roots can incorporate entire nanoparticles^{69,19}. It seems to depend on plant species, nanoparticle size, shape and chemical composition²¹. Anyway, the driving paths that NPs travel in plants are not fully clear. It can adhere to the root surface, physically attaching to the plant via exudates in the rhizosphere¹⁰⁷,

or decompose forming ions in soils and being absorbed by the common way in the soil solution, or associate with metal transporters, ion channels, protein carriers or aquaporins²⁰.

The literature shows publications in which ZnO concentrations ranges from 100 to 4000 mg L⁻¹ ^{12,15,61–63,116}. Most of these studies were carried out in the context of nanotoxicology. Plant roots were exposed to nanoparticles in hydroponics^{20,61–63,107,126–128} and soil^{15,64,129}. Such concentrations are currently unlikely to be found in the environment, and they are also not practicable in the fertilizer framework because it is way above the used in agriculture. Generally, doses below 5 mg kg⁻¹ are used in agriculture¹³⁰.

However other studies showed that nanoparticle-mediated materials were associated with desirable agriculture traits, such as the promotion of seed germination^{31,10}, boosting plant defenses¹³¹ and enhancing soil conditions¹³². Additionally, they can potentially be used for plant nutrition^{92,93,133,134}.

This chapter compares the effect of ZnO NPs and ZnSO₄ on *P. vulgaris* development. The plants were grown the nutrient solution and exposed to 1, 3 and 10 mg Zn L⁻¹ for 1, 2, 3 and 4 weeks.

The aim of this topic is to test the hypothesis that NPs source of Zn can also bring benefits to *Phaseolus vulgaris* plants if used in the right concentrations. For that we evaluated some biometric parameters such as root mass and length, shoot mass and height, SPAD index and leaf area. We also measured the Zn content and correlated with others nutrients concentration in root and shoot tissues.

4.2. Material and Methods

4.2.1. NP Characterization

The NPs used in this experiment were the 40 nm, 60 nm and 300 nm ZnO NPs with surfactants cited in the topics above, and the characterization is described in topic 2.2.1.

These materials were used to prepare aqueous dispersions of 1, 3 and 10 mg Zn L⁻¹ dispersed in the modified Cakmak¹³⁵ solution without Zn.

4.2.2. *Phaseolus vulgaris* assay design

Phaseolus vulgaris seeds, BRS Estilo cultivar, were germinated in vermiculite until reaching the V3 stage. The germination room maintained plants under a photoperiod of 12 hours, at 27°C and LED illumination lamps, supplying 250 $\mu\text{mol photons m}^{-2} \text{s}^{-1}$.

Then, after reaching the V3 stage, 12 plants were transplanted to a set of three pots (two liters each), with different treatments, and each pot was one replicate. A stock solution pot (three liters) also participates in the recirculating system (Appendix K), where the nutrients and treatments were replaced when necessary.

4.2.3. Nutritive Solution Monitoring

Everyday the water volume of the solution was completed to the initial level (nine liters). Twice a week the nutrients were measured by energy dispersive X-ray fluorescence (EDXRF), by standard addition method, for the replacement of nutrients (Zn, Fe, K, P, S and Ca). The measurements conditions were 50 kV, 1000 μA , dwell time of 50 s, under vacuum and spot size of 3 mm. Standards solutions of Zn, Fe, P, K, S and Ca were added to a flask in different concentrations, in order to create a calibration curve for each element. 25 μL of each concentration were deposited five times, with intervals to dry the droplet, in a 0.5 μm thick polypropylene film, placed in a EDXRF cuvette. For nutrient concentration analysis, samples were deposited in the cuvettes in the same way for standards.

4.2.4. Morphological, SPAD analysis and $\mu\text{-XRF}$ maps

In order to verify the effects of these NPs on *P. vulgaris* plants development, 13 treatments were applied with three replicates, varying the source of Zn (ZnO NPs and ZnSO_4) and concentration (1, 3 and 10 mg of Zn L^{-1} of nutritive solution). The control plants were fed with the modified Cakmak solution¹³⁵. Further these different parameters, for biometrics analysis (root and shoot, mass and length, and foliar area) four times of exposure were analyzed (7, 14, 21 and 28 days), and for SPAD analysis it was used 4, 11, 18 and 25 days of exposure.

The treatments are described below:

- TC – Modified Cakmak solution (control);
- TS_1 - Modified Cakmak solution without Zn + ZnSO₄ at 1 mg of Zn L⁻¹;
- TS_3 - Modified Cakmak solution without Zn + ZnSO₄ at 3 mg of Zn L⁻¹;
- TS_10 - Modified Cakmak solution without Zn + ZnSO₄ at 10 mg of Zn L⁻¹;
- T40_1- Modified Cakmak solution without Zn + 40nm ZnO at 1 mg of Zn L⁻¹;
- T40_3- Modified Cakmak solution without Zn + 40nm ZnO at 3 mg of Zn L⁻¹;
- T40_10- Modified Cakmak solution without Zn + 40nm ZnO at 10 mg of Zn L⁻¹;
- T60_1- Modified Cakmak solution without Zn + 60nm ZnO at 1 mg of Zn L⁻¹;
- T60_3 - Modified Cakmak solution without Zn + 60nm ZnO at 3 mg of Zn L⁻¹;
- T60_10 - Modified Cakmak solution without Zn + 60nm ZnO at 10 mg of Zn L⁻¹;
- T300_1- Modified Cakmak solution without Zn + 300nm ZnO at 1 mg of Zn L⁻¹;
- T300_3- Modified Cakmak solution without Zn + 300nm ZnO at 3 mg of Zn L⁻¹;
- T300_10- Modified Cakmak solution without Zn + 300nm ZnO at 10 mg of Zn L⁻¹

After each time of exposure, one plant from each pot was collected, and their roots were washed in a 0.1 M of HNO₃ solution to remove any particle adhered in these tissues. Then shoots and roots were measured with a ruler, and weighted with a semi analytical scale.

One piece of the stem was collected, frozen with liquid N₂ and stored in a freezer at -18°C for μ-XRF maps. Then, the frozen stems were cut near to the roots using a scalpel yielding 1.5 mm thick cross sections. The sections were placed on the top of a Kapton thin film and assembled in a 20 mm XRF cuvette. The cuvette with the sample was loaded inside the μ-XRF Orbis PC. Maps were recorded using a 30 μm X-ray beam focused on the sample by a polycapillary optical element. Matrix of 32 × 25 pixels were employed in the mapping. X-rays were generated by a Rh anode operating at 40 kV and 300 μA. The XRF photons were detected by a 30 mm² SDD detector, the dwell time was 1000 ms per point, the total time of analysis was at a maximum of 15 min and the dead time was smaller than 2%.

For leaf area analysis, it was used a leaf area meter, model Li-3100, LICOR (Nebraska, USA), to measure it from each treatment after 7, 14, 21 and 28 days of exposure.

A SPAD-502, from Minolta (Osaka, Japan), was used to verify the leaves chlorophyll content of all the treatments cited above after 4, 11, 18 and 25 days of exposure.

4.2.5. Nutrient content in *Phaseolus vulgaris* tissues

Root and shoot of *Phaseolus vulgaris* plants were dried at 60°C in an oven for 72 hours, grounded in a porcelain mortar and sieved at 100 mesh. For shoot nutrient quantification it was used 50 mg and 30 mg of shoot and root tissues, respectively. The sample was deposited and gently pressed with a glass stick in a XRF cuvette, covered in the bottom with 5 µm thick polypropylene film.

Two EDRX methods were used to evaluate the nutrient concentrations in the samples. The first one was the standard addition (SA) method to evaluate Zn in both tissues. A series of standard solutions of Zn were added to samples and fully homogenized in a porcelain mortar. Then, the same sample procedure described above was performed. The second method was the fundamental parameter (FP) provided by the Shimadzu software considering a matrix made of 100% cellulose. This was used to evaluate Mn, Fe, P, S, K and Ca, except for roots, where it was not possible to evaluate Fe content. The matrix powders and cuvettes were prepared in the same way as described above.

For the trueness evaluation of the methods cited above, it was used certified reference materials, prepared in the same way mentioned above, and the recoveries were accepted if the result from equation on appendix L was nearly 20%.

4.2.6. Data analysis

These experiments were conducted as a complete randomized distribution with three replicates and results were reported with the means and standard deviation (bars in charts and numbers in tables). Analysis of variance (ANOVA) followed by Tukey test, with probability lower than 0.05 ($p < 0.05\%$), were performed using the R statistic program¹³⁶.

4.3. Results and Discussion

4.3.1. Effects on morphological aspects and SPAD index

Some morphological aspects were evaluated and Figure 18 presents the result for (a) root length, (b) shoot height, (c) root dry mass, (d) shoot fresh mass, (e) SPAD index and (f) leaf area. Figure 18 presents the mean values and error bars corresponding to the standard deviation. SPAD index measures the green color of the leaves. This parameter is highly correlated with the chlorophyll content¹³⁷.

For root length (Figure 18(a)), after seven days of exposure, TC and T60_3 presented the longest root length and the TS_10, the shortest. This last treatment with a low time of exposure was harmful to root length development.

After 14 days of exposure, we observed that T300_1 had the longest roots, and T300_10 and TS_10 presented the shortest ones. It confirmed that the concentration is a most important matter than the source of the nutrient, since the same NPs source, on this time of exposure, showed the longest and the shortest root length. It also corroborates other study that compared ZnO NPs and ionic Zn sources, where root length was impaired by the concentration and not the source¹³⁸. For 21 days of exposure, T300_1 continued to present longer roots, and TS_10, shorter.

After 28 days of exposure, it was observed that T300_10 together with TS_10 presented the smallest root length. The treatments with the highest root elongation on this last time of exposure were T40_1, all treatments with 60 nm ZnO NPs, T300_1, T300_3 and TS_1. One can notice that when the plants were older, most treatments presented similar results after 28 days of exposure, and it may be a defensive response from more developed plants. Another point to think about is that maybe roots become more resistant to elevated Zn content than shoots.

It was already reported that non hyper accumulator plants tend to store the excess of micronutrient in the roots, and restrict the transport to aerial parts¹³⁹. This mechanism was shown by study involving Norway spruce where roots showed greater resistance to toxicity than shoot tissues⁴⁷. Similar result was observed in ryegrass plants, where authors concluded that the susceptibility of a plant to nanoparticles depends on the development stage¹⁰⁷. In this experiment the smaller differences among results on the last time of exposure may be due to its greater resistant to Zn toxicity.

We also investigated which treatments promoted the largest shoot height (Figure 18(b)). In the 7 days harvest, T60_1 showed the highest shoot and the T60_10, the lowest. Here, the same source promoted the greatest and the smallest shoot development, changing just the concentration. It was also observed for root length with 14 and 28 days of exposure. At 14 days of exposure, the treatments with greater shoot height were T60_1 and T300_1. T300_10 presented smaller shoot development. These results reinforce that, in this study, concentration is more important than source.

For the last two exposure times, T40_1 was the treatment that presented longer shoot height, and all treatments containing 10 mg Zn L⁻¹ exhibited the worst shoot development. The stunted growth is the most common symptom related to Zn toxicity⁴⁷. There are cases reporting the reduced shoot growth in different plant species as peach, soybeans and cotton¹⁴⁰. Another point is the importance of Zn on auxin synthesis, which is involved on plants growth and development^{138,141}. Thus, the excess of Zn can deregulate this synthesis, disturbing the proper plant development.

Analyzing root dry mass (Figure 18(c)), it is possible to verify that T40_1 was the treatment with greater root dry mass for all the exposure times. This result indicates that ZnO NPs can enhance root development with the right concentration. TS_10 was the treatment that most negatively influenced the root dry mass at 7 and 21 days of exposure. The higher solubility of the source affected faster the root development than less soluble sources.

Both T300_3 and TS_3 were the treatments with smaller root dry mass at 14 days of exposure. However, this changed at 21 and 28 days of exposure. It may have happened as a defense mechanism after the plant reached older vegetative stages^{138,141}. The plant age can influence how plants pass through unfavorable events. For 28 days of exposure the treatment with smaller root dry mass was T300_10. It shows again, the importance of the concentration when working mainly with micronutrient. The literature^{107,138} described as evident the toxicity increase with the increasing of concentration coming from ZnO NPs or Zn⁺² sources. Other study also found that elevated Zn content in the growing medium can decrease the root dry mass¹⁴².

It was not possible to get data of shoot dry mass because after collecting the fresh plants, part of the stem was frozen and reserved in a freezer to make the u-XRF maps.

As it was observed in the root dry mass parameter, for shoot fresh mass (Figure 18(d)) the T40_1 had the greatest masses in all the periods of exposure. The smallest masses were found in TS_10 after 7 days of exposure. This was probably caused by the faster absorption of soluble sources. Together with T300_10, it also showed lower shoot fresh masses after 14 days of exposure.

At 21 days of exposure, all treatments containing 10 mg Zn L^{-1} presented low shoot fresh masses. It demonstrates again the importance of the concentration. It also raises the possibility that NPs can injure the superficial area of the roots on this greater concentration, allowing the easy absorption of Zn. The fact that T300_10 presented the lowest shoot dry mass at 28 days of exposure reinforces the latter hypothesis. This treatment was more harmful to the plant development than sulphate, which is a more soluble source, known to be readily absorbed by roots. A study⁶² with a 100 mg L^{-1} of ZnO NPs on rapeseed showed a toxic effect on plant biomass. It confirms that in higher concentrations, this material can decrease plant development according to the concentration, composition and plant species.

For the first two times of exposure, TC presented the greatest SPAD index (Figure 18(e)). This resulted from the adequate nutrient balance of the control. Still on these times of exposure, T60_10 showed to be the treatment with lowest SPAD index, together with TS_10 at 14 days of exposure. However, this same treatment presented the highest SPAD index in the last two times of exposure. This is was kind of trick because SPAD does not measure directly the chlorophyll content, it measures the intensity of green on the leaves, and one symptom of Zn toxicity is the darker green color of the leaves (Appendix M). Therefore, one has to pay attention to not be fooled by results coming from SPAD equipment.

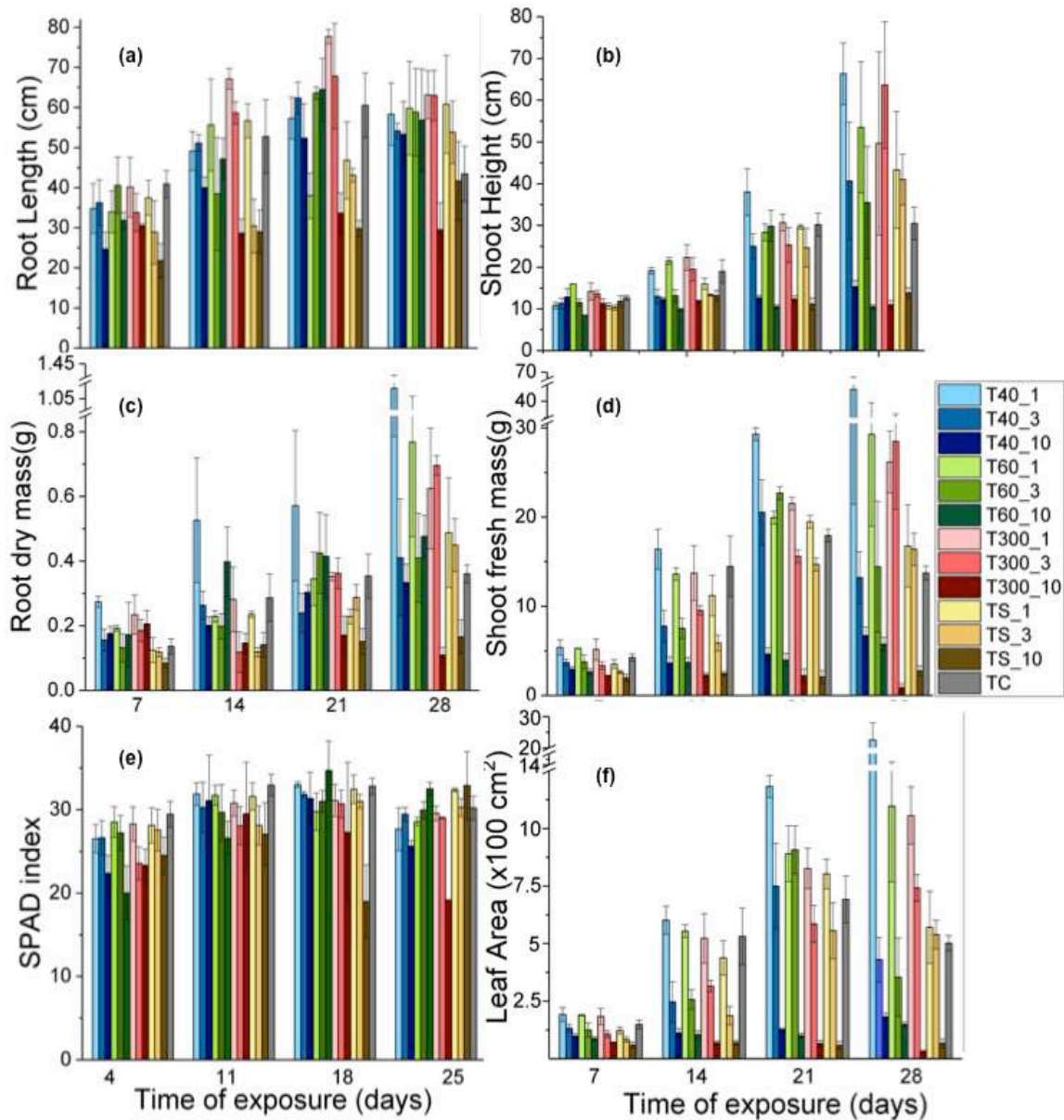
At 21 days of exposure, TS_10 presented the smallest SPAD index, and at 28 days of exposure it was observed for TS300_10. One can notice that for all exposure times, independently of the source of Zn, the greatest concentration tested presented the smallest SPAD index. However, this same concentration presented the highest SPAD index in some exposure times because of the intensity of green in the leaves. It may be caused

by the increase of the number of plastoglobuli in the chloroplasts with the increase of Zn in plant tissue¹¹², as a response to the stress caused Zn content in leaves. The plastoglobuli are known to be involved in many metabolic functions, being one of them the regulation of the photosynthesis¹⁴³.

At 7 days of exposure, T40_1 and T60_1 presented the greatest leaf area (Figure 18(f)), and TS_10 the smallest. These results exposed the faster toxicity response in plants with a soluble source. They also revealed the capacity of some ZnO NPs to accelerate the foliar development on initial stages, what enhances the photosynthetic area. Figure 18(f) also shows that for this first time of exposure the differences among treatments were in a smaller scale than for the others exposure times. After 14 days of exposure, greater foliar areas were observed on TC and treatments with nanoparticles at 1 mg Zn L⁻¹. TS_10 and T300_10 presented the smaller leaf areas.

At 21 and 28 days of exposure, the T40_1 continued to present a greater leaf area than others treatments. Conversely, treatments containing 10 mg Zn L⁻¹ presented smaller foliar areas. These results confirmed that apart the source of Zn, what seems to most induce the reduction of the foliar area is the concentration. It confirms published results that reported the dissolution of Zn from NPs can be more deleterious than the NPs itself⁶².

Figure 18 - *Phaseolus vulgaris* (a) root length, (b) shoot height, (c) root dry mass, (d) shoot fresh mass, (e) SPAD index and (f) leaf area of all treatments for different times of root exposure. Means were analyzed with ANOVA and Tukey test with $p < 0.05\%$



The tables with means and statistic differences of the analyzed parameters cited above are on Appendix N, O, P, Q, R and S.

4.3.2. Zn content on shoot and root tissues

For all exposure times, T300_10 presented the highest Zn content in shoot tissues (Table 7). TS_10 followed the same behavior, but only in the first two periods. Since Zn from

300 nm was slowly released, the plant might have better assimilated it. On the other hand, the Zn from ZnSO₄ is readily available and might triggered defense mechanisms that prevented the Zn uptake after 14 days of exposure. T40_10 and T60_10 were not statistically different in any exposure time for Zn content in shoot tissues. In agreement with Figure 3 of Chapter 2, this might be a consequence of the close particle size and surfactants.

As expected, TC presented, for all exposure times, the smallest Zn content in shoot tissue. It can be explained by the concentration of this micronutrient in Cakmak modified nutritive solution that is 0.065 mg of Zn L⁻¹, which was smaller than the others treatments. However, in the last exposure time, all treatments composed by NPs at 1 mg of Zn L⁻¹ exhibited results statistically equals to TC. Thus, these NPs had a smaller Zn release, uptake and accumulation, since the concentration of Zn on TC is lower than on these treatments.

Table 7 - Shoot Zn content (mg kg⁻¹) after different exposure times (7, 14, 21 and 28 days) for all treatments

Treatments	7 days*	14 days*	21 days*	28 days*
T40_1	107.7 h	106.9 e	84.9 f	69.7 fg
T40_3	325.6 d	329.1 c	215.9 d	156.1 d
T40_10	759.3 b	1130.3 b	1149.2 c	1074.4 b
T60_1	109.2 gh	102.9 e	84.9 f	67.0 fg
T60_3	231.3 e	232.5 d	157.0 e	283.9 c
T60_10	764.4 b	1030.7 b	1136.6 c	1174.3 b
T300_1	189.9 ef	106.2 e	102.2 f	59.0 fg
T300_3	432.9 c	311.2 cd	198.2 d	112.3 de
T300_10	1288.5 a	1620.2 a	2277.8 a	2224.4 a
TS_1	144.9 fg	113.0 e	95.2 f	80.7 ef
TS_3	410.7 cd	326.7 c	216.6 d	153.0 d
TS_10	1212.8 a	1824.7 a	1700.5 b	1594.5 ab
TC	54.0 i	54.9 f	46.6 g	51.2 g

*data transformed log(Y)

Comparing the first and the last exposure times (Table 7), the Zn contents on shoot tissues trend to decrease in the treatments with 1 mg L⁻¹. It may be a consequence of the leaves development stage. The leaf area (Figure 18 (f)) from these treatments presented a greater increase from 7 to 28 days of exposure. Thus, Zn was diluted in this plant tissue. However, the same comparison for treatments exposed to 10 mg L⁻¹ shows that Zn content

on shoot tissues increased. This can be explained by the stunted growth of these plants, where the Zn uptake does not stop and the development was retarded.

As for shoot, TC was also the treatment with smaller Zn content in root tissues (Table 8) for all exposure times. It worthy highlighting that for every treatment, root tissue accumulated more zinc than shoot tissue. This response was previously observed in non hyper accumulator plants, whose tends to store Zn in roots⁶². Another hypothesis states that the root secretion increase NPs adsorption on root surface¹⁰⁷, accumulating it on these tissues.

As described in the literature, the Zn content coming from ZnO NPs increase as the concentration of the medium also increases⁶². In Chapter 3, we reported the importance of root exudates on Zn ionic dissolution. These substances can increase the solubility in the medium around roots¹¹⁶.

Table 8 - Root Zn content (mg kg⁻¹) after different exposure times (7, 14, 21 and 28 days) for all treatments

Treatments	7 days*	14 days*	21 days*	28 days*
T40_1	185.3 h	288.1 e	407.4 f	472.1 d
T40_3	551.1 de	858.6 bc	1189.5 bc	1163.0 bc
T40_10	1507.1 aba	3337.2 a	2850.6 a	3241.4 a
T60_1	272.0 fgh	574.8 cd	652.8 def	548.5 d
T60_3	443.3 def	736.6 bcd	832.0 cde	1621.6 ab
T60_10	830.5 bcd	1568.2 ab	1835.7 ab	1569.5 ab
T300_1	367.0 efg	571.3 cd	657.1 def	494.2 d
T300_3	649.6 cde	803.6 bc	835.8 cde	826.6 bcd
T300_10	1880.7 a	3116.6 a	3432.6 a	1345.2 bc
TS_1	210.2 gh	409.4 de	484.7 cd	648.4 cd
TS_3	549.7 de	885.8 bc	883.7 dc	1413.4 abc
TS_10	1294.8 abc	2125.5 a	3483.1 a	3198.5 a
TC	165.3 h	270.3 e	211.6 g	210.7 e

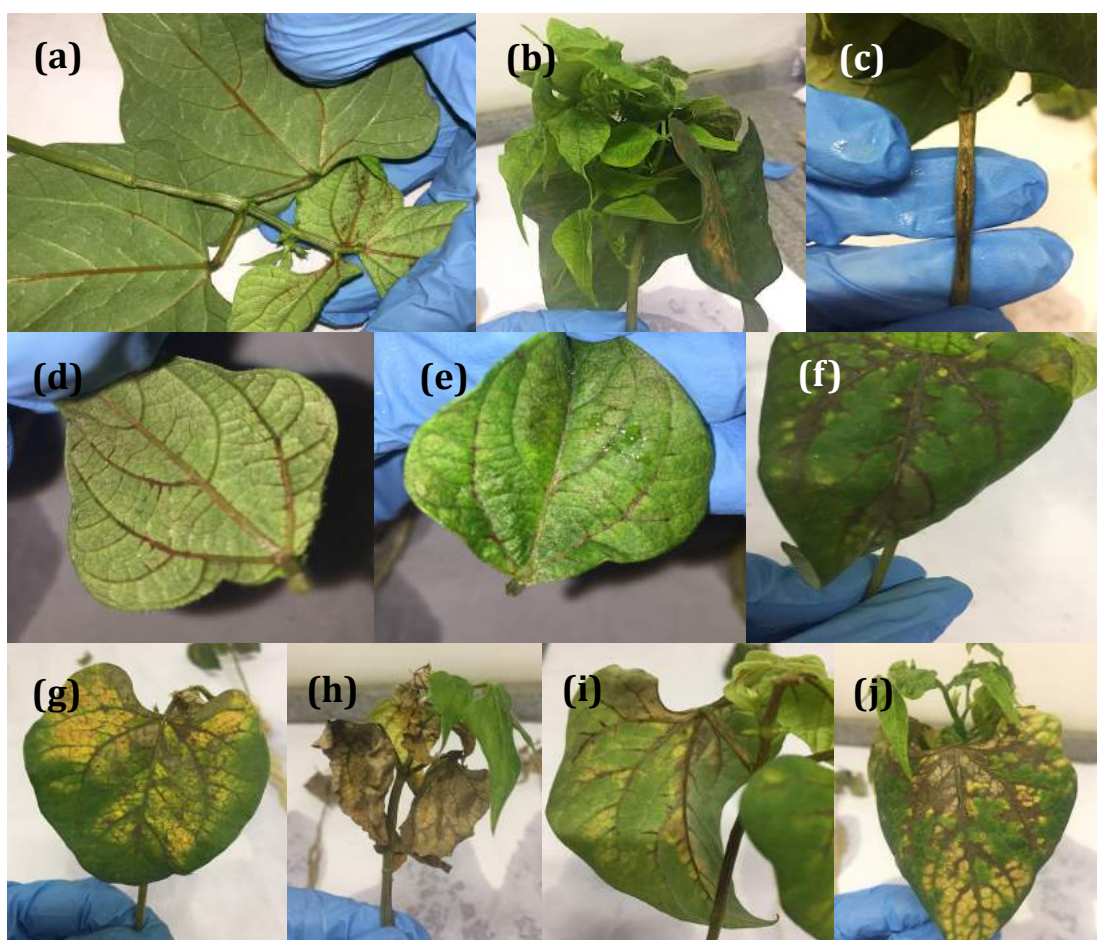
data transformed $Y^{-0.2}$ *

4.3.3. Zn toxicity symptoms

Previous studies indicated that different species have different tolerance to any micronutrient toxicity⁶⁹. Generally Zn toxicity can occur when Zn levels in plant dry matter are above 400 ppm¹⁴⁴. Zn Toxicity may happens because the high amount of Zn content on plant cell can disturb the antioxidant defense structure¹⁴⁵.

Figure 19 below shows some symptoms observed in plants exposed to 10 mg Zn L^{-1} . One can notice the presence of a purple brownish color in the veins of the leaves in Figure 19(a), (d) and (e). Figure 19(f), (g), (i) and (j), correspond to the treatments that presented the greatest Zn content in shoot tissues. The same symptom happened, but in an advanced stage. The purple brownish color evolved to necrosis in veins and parts of the limb around the veins. Figure 19(b) clearly shows the decrease on internodes, what was previously reported as symptom of Zn toxicity⁴⁰. Figure 19(c) shows a stem damage probably caused by the toxic concentration of Zn inside stem tissues.

Figure 19 - Symptoms on *Phaseolus vulgaris* shoots in T40_10 after (a) 7 and (b) and (c) 28 days of exposure; (d) and (e) T60_10 after 28 days of exposure; (f) T300_10 with 14, (g) 21 and (h) 28 days of exposure, and TS_10 with (i) 14 and (j) 21 days of exposure



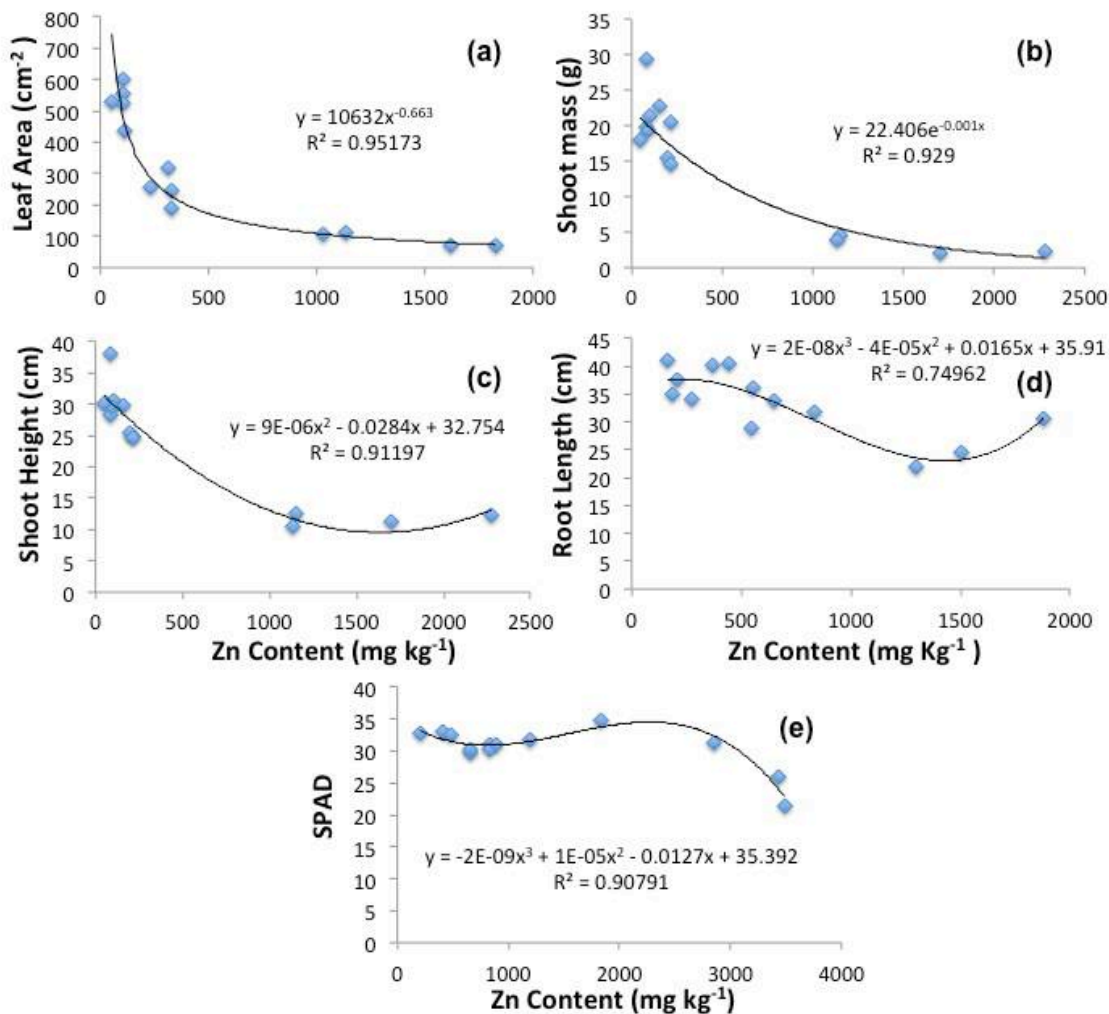
4.3.4. Correlations between Zn content and morphological effects

Figure 20 displays the biometric parameters as function of Zn shoot content. The leaf area (Figure 20 (a)) and shoot fresh mass (Figure 20(b)) were inversely proportional to Zn content on shoot tissues. Reinforcing that concentration and solubility are the main matters for foliar area.

Shoot height (Figure 20(c)) and root length (Figure 20(d)) presented polynomial correlations. After Zn content on root and shoot tissues reached 1500 mg kg⁻¹ the root and shoot elongation returned to increase.

The SPAD analysis presented also a polynomial correlation (Figure 20(e)). Initially, the SPAD index did not change until Zn reached a maximum in approximately 2500 mg Zn kg⁻¹ in shoot tissues, then started to decrease continuously as the Zn concentration increased.

Figure 20 - Correlation between Zn content in shoots and (a) foliar area, (b) shoot fresh mass, (c) shoot height, (d) root length and (e) SPAD index



4.3.3. Nutrient content analysis

Additionally to the biometrics analysis, nutrient content was accessed in order to check any possible correlation between Zn uptake and the absorption of others nutrients.

There are many studies indicating that excess of one nutrient can promote the deficient absorption of other nutrients. Thus, this experiment compared the Zn content on shoots and roots with Ca, S, P, K, Mn and Fe content in roots and shoot tissues (Figures 21 and 22). Iron could not be analyzed on root tissues. Figure 21 below shows the correlation equation and R^2 of the curves. It was not possible to verify any correlation with Mn and Zn in roots tissues, and Fe and Zn content in shoot tissues.

Figure 21 presents the correlation found between Zn content with S, Ca, P and K in root tissues. In roots, the concentration of S and Ca (Figure 21(a) and (b), respectively) decreased when the Zn content increased. The same result was observed for S, P and Ca (Figure 22(a), (b), and (c), respectively) in shoot tissues. The negative correlation between Zn and P^{146} and Ca^{147} was previous described in plants. Positive correlation between Zn and Ca was also reported in maize¹⁴⁸.

The K presented similar correlation both for root and shoot tissues (Figures 21(d) and 22(d), respectively). It looks like that the response on K concentration fluctuates. In root tissues, this macronutrient started to decrease as the Zn concentration increase. After 1000 mg Zn kg^{-1} in root tissue, K content started to increase showing a positive correlation with Zn. This trend agrees with other experiments on maize that verified positive correlation between these nutrients¹⁴⁸.

Mn content presented a different type of correlation (Figure 22(e)). In the beginning of the curve, this micronutrient concentration increased as Zn concentration increased, but after Zn reached 1500 mg kg^{-1} , the Mn content start to decrease. A previous experiment reported a decrease in Mn uptake with the excessive Zn content on plant tissues¹⁴⁶.

Figure 21 - Correlation of Zn content with (a) S, (b) Ca, (c) P and (d) K content in root tissues

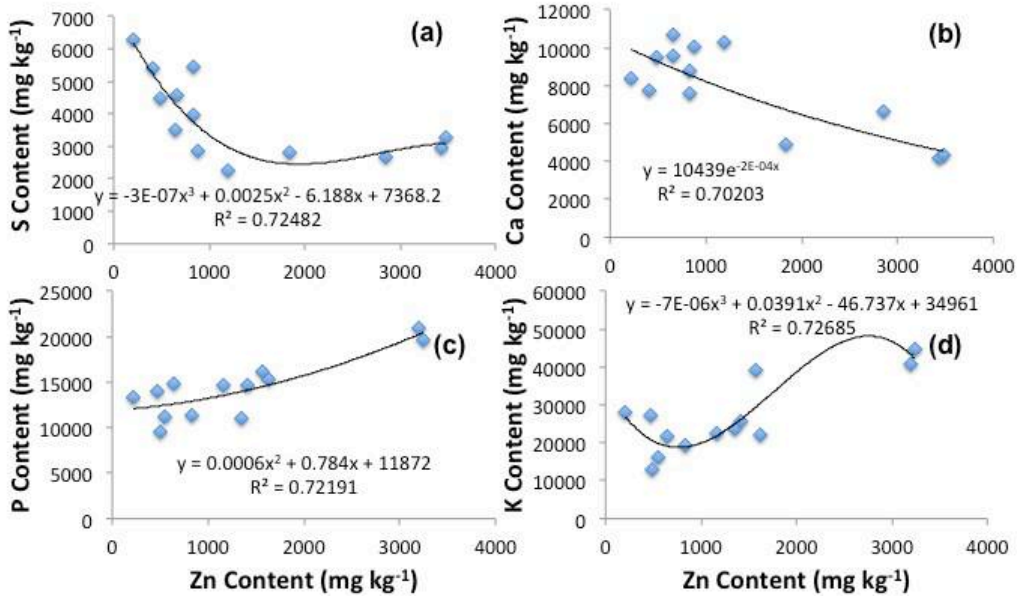
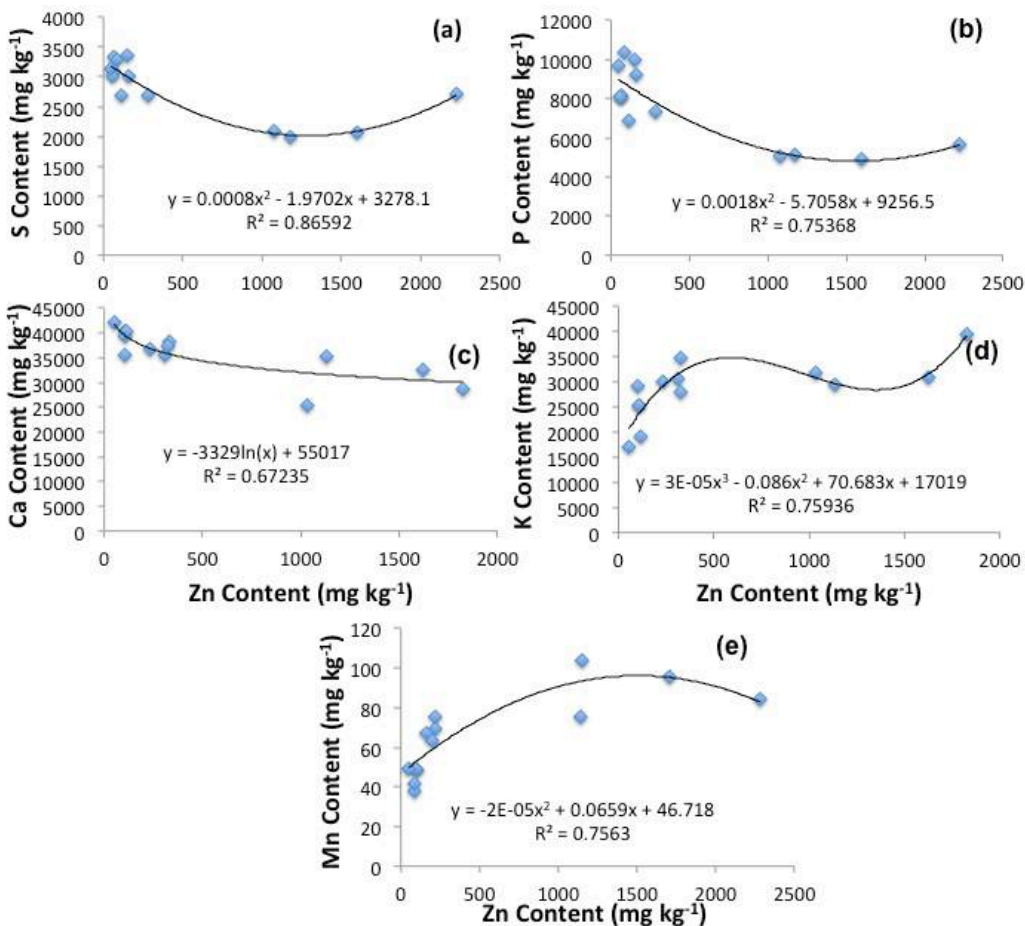


Figure 22 - Correlation of Zn content with (a) S, (b) P, (c) Ca, (d) K and (e) Mn content in shoot tissues



4.3.4. μ -XRF Zn maps

The μ -XRF images were recorded for ZnO 40 nm and ZnSO₄ treatments. Although the images shown here are not quantitative maps, the Zn counts measured are directly proportional to the Zn content.

Its resolution does not allow one to verify in which specifically tissue, cells or organelles Zn is stored. In spite of that, Figures 23 and 24 below, allowed us to verify that Zn is mainly found in the external part of *Phaseolus vulgaris* stems, independently of the exposure time and concentration. Apparently, in both Figures 23 and 24, the Zn content in the stems increased with the rise of concentration and time of exposure.

Another observed pattern in Figure 24 (images from stems treated with ZnSO₄) is the dilution of Zn concentration coming from external part to internal part of the stem. Observing the SEM images in Figure 8, one can suggest that the Zn is present in the cortex and vascular bundles of these stems.

Figure 23 - *Phaseolus vulgaris* stem images and corresponding chemical images presenting the transversal spatial distribution of Zn as function of time of exposure and concentration: (a) T40_1 with 7 days of exposure; (b) T40_1 with 28 days of exposure; (c) T40_3 with 14 days of exposure; (d) T40_3 with 28 days of exposure; (e) T40_10 with 14 days of exposure and (f) T40_10 with 28 days of exposure

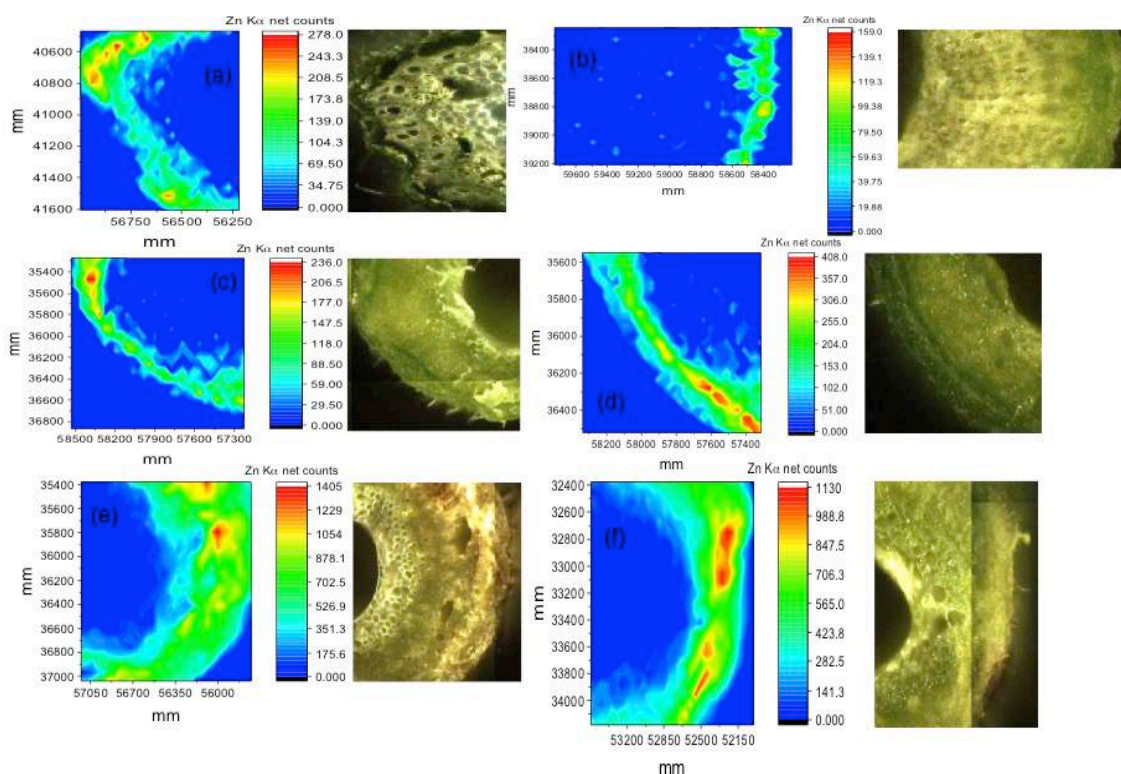
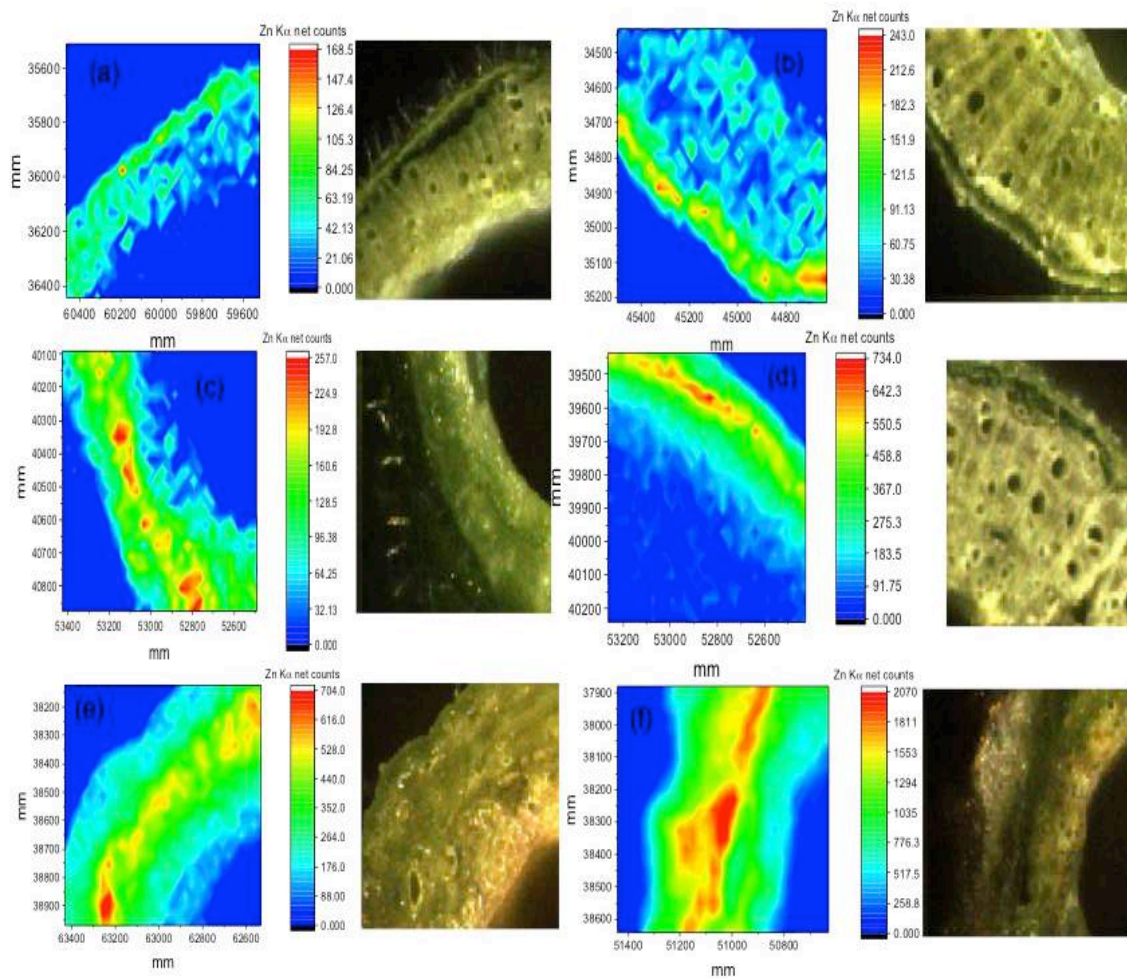


Figure 24 - *Phaseolus vulgaris* stem images and corresponding chemical images presenting the transversal spatial distribution of Zn as function of time of exposure and concentration: (a) TS_1 with 14 days of exposure; (b) TS_1 with 28 days of exposure; (c) TS_3 with 7 days of exposure; (d) TS_3 with 28 days of exposure; (e) TS_10 with 7 days of exposure and (f) TS_10 with 28 days of exposure



Both treatments used to make μ -XRF maps allow one to notice that the stems exposed to 10 mg Zn L^{-1} , presented damaged areas in brown color. This is likely a symptom of Zn intoxication.

4.4. Conclusion

The biometrics parameters analyzed: root length, shoot height, root dry mass, shoot fresh mass and leaf area showed to be more affected by the concentration than the source of Zn. This result suggests that, regarding these parameters, ZnO NPs can be a source of Zn to plants if used in the right concentration, respecting the exposure time and the solubility of the NPs.

It was observed correlation between Zn content in shoot tissues and S, P, Ca, K and Mn content on these same tissues. In roots, it was observed correlation between Zn content only with macronutrients content.

The maps recorded by μ -XRF showed that regardless of the source and concentration of Zn, it was found in the external part of this tissue. It looks like the sulfate source migrated also towards the inner part of the stems. Except from that, we did not notice other differences on the absorption of these two analyzed sources.

5. FINAL CONSIDERATIONS AND OUTLOOK

Considering all aspects discussed in this study, working with ZnO NPs as a source of Zn to *Phaseolus vulgaris* plants can be practicable. Some characteristics need to be evaluated before its use, as: nutrient concentration, solubility, composition (presence of surfactants or not), crystallite size, hydrodynamics radius and zeta potential. The ZnO NPs released Zn ions in growth medium slower than ZnSO₄. NPs with surfactants on its compositions trended to release Zn faster than NPs without it. However, NPs solubility did not presented a proportional increase with the dispersion concentrations.

X-ray fluorescence and X-ray absorption spectroscopy are suitable to investigate *in vivo* the uptake and chemical environment of Zn in plants. It can be extended to other elements, allowing monitoring metabolic processes while they are happening. XRF indicated that exists a gradient on Zn content and on its uptake velocity from root to shoot, except for ZnSO₄ with the highest concentration. XAS showed that Zn is mainly coordinated by citrate and malate in the *Phaseolus vulgaris* stem, and by histidine in leaves. Entire NPs were only absorbed when roots were injured, proving that Zn was dissolved by roots before the uptake.

μ-XRF images revealed that Zn transport from root to shoot happened through xylem and cortex. This technique also disclosed that independently of source and concentration, Zn is present in the same stem regions. Zn from ZnSO₄ at 1000 mg L⁻¹ was mainly present in the veins of the leaves.

EDXRF showed that Zn shoot content, after 48 hours of exposure, was almost the same for 40 and 300 nm ZnO NPs. ZnSO₄ presented the highest Zn content in both studied concentrations. However 300 nm ZnO NPs, with smaller concentration but longer exposure time seems to be more absorbed. It also trended to accumulate more Zn in plant tissues.

Physiological and morphological effects presented to be more impaired by the presence of high Zn content than the type of Zn source. The nutrient correlation varied as function of the analyzed plant tissue.

The most important challenges in this type of experiments are related to the development methods and the maintenance of the growing conditions. In order to verify NPs interaction with plants, it was necessary to control all possible variables. *In vivo* analysis just could be done in the initial stages, because of the limited space inside of the μ-XRF equipment.

The expectations regarding the employment of engineered nanomaterials in the mineral nutrition of plants are great. There are many fields on agriculture to be explored. The interaction of nanomaterials with soil, water, plants, microorganisms, animals and humans must be meticulously studied. It is important to verify the toxic and possible benefic effects. Such as in regular fertilizers, one has to find out the right concentrations of each type of NPs to each plant species. The scientific community must ensure that nanomaterials are safe and only then one can explore their properties towards crop production.

REFERENCES

1. WANG, P. et al. Nanotechnology: A New Opportunity in Plant Sciences. **Trends in Plant Science**, Kidlington, v. 21, p. 699–712, 2016.
2. GIRALDO, J. P. et al. Plant nanobionics approach to augment photosynthesis and biochemical sensing. **Nature Materials**, London, 13, 400–408 (2014).
3. MUKHERJEE, A. et al. Carbon Nanomaterials in Agriculture: A Critical Review. **Frontiers in Plant Science**, Lausanne, v. 7, p. 172, 2016.
4. FRACETO, L. F. et al. Nanotechnology in Agriculture: Which Innovation Potential Does It Have? **Frontiers in Environmental Science**, Lausanne, v. 4, p. 20, 2016.
5. RODRIGUES, S. M. et al. Nanotechnology for sustainable food production: promising opportunities and scientific challenges. **Environmental Science. Nano**, London, v. 4, p. 767–781, 2017.
6. MIRALLES, P.; CHURCH, T. L.; HARRIS, A. T. Toxicity, Uptake, and Translocation of Engineered Nanomaterials in Vascular plants. **Environmental Science & Technology**, Easton, v. 46, p. 9224–9239, 2012.
7. DIETZ, K.-J.; HERTH, S. Plant nanotoxicology. **Trends in Plant Science**, Kidlington, v. 16, p. 582–589, 2011.
8. ALLEN, C. et al. Research highlights: investigating the role of nanoparticle surface charge in nano-bio interactions. **Environmental Science. Nano**, London, v. 4, p. 741–746, 2017.
9. VALSAMI-JONES, E.; LYNCH, I. NANOSAFETY. How safe are nanomaterials? **Science**, Washington, DC, v. 350, p. 388–389, 2015.
10. DURAN, N. M. et al. X-ray spectroscopy uncovering the effects of Cu based nanoparticle concentration and structure on *Phaseolus vulgaris* germination and seedling development. **Journal of Agricultural and Food Chemistry**, Washington, DC, v. 65, p. 7874–7884, 2017.
11. SUTARIYA, P. G. et al. A simple and rapid creatinine sensing via DLS selectivity, using calix[4]arene thiol functionalized gold nanoparticles. **Talanta**, Oxford, v. 147, p. 590–597, 2016).
12. KUMARI, M. et al. Cytogenetic and genotoxic effects of zinc oxide nanoparticles on root cells of *Allium cepa*. **Journal of Hazardous Materials**, Amsterdam, v. 190, p. 613–621, 2011.
13. DIMKPA, C. O. et al. Fate of CuO and ZnO nano- and microparticles in the plant environment. **Environmental Science & Technology**, Easton, v. 47, p. 4734–4742, 2013.

14. SERVIN, A. D. et al. Synchrotron micro-XRF and micro-XANES confirmation of the uptake and translocation of TiO₂ nanoparticles in cucumber (*Cucumis sativus*) plants. **Environmental Science & Technology**, Easton, v. 46, p. 7637–7643, 2012.
15. HERNANDEZ-VIEZCAS, J. A. et al. In Situ Synchrotron X-ray Fluorescence Mapping and Speciation of CeO₂ and ZnO Nanoparticles in Soil Cultivated Soybean (*Glycine max*). **ACS Nano**, WASHINGTON, DC, v. 7, p. 1415–1423, 2013.
16. BANDYOPADHYAY, S. et al. Comparative phytotoxicity of ZnO NPs, bulk ZnO, and ionic zinc onto the alfalfa plants symbiotically associated with *Sinorhizobium meliloti* in soil. **Science of the Total Environment**, Amsterdam, v. 515–516, p. 60–69, 2015.
17. GHOSH, M. et al. Effects of ZnO nanoparticles in plants: Cytotoxicity, genotoxicity, deregulation of antioxidant defenses, and cell-cycle arrest. **Mutation Research. Genetic Toxicology and Environmental Mutagenesis**, Amsterdam, v. 807, p. 25–32, 2016.
18. PENG, C. et al. Translocation and biotransformation of CuO nanoparticles in rice (*Oryza sativa* L.) plants. **Environmental Pollution**, Barking, v. 197, p. 99–107, 2015.
19. CAPALDI ARRUDA, S. C. et al. Nanoparticles applied to plant science: A review. **Talanta**, Oxford, v. 131, p. 693–705, 2015.
20. ANJUM, N. A. et al. Transport phenomena of nanoparticles in plants and animals/humans. **Environmental Research**, New York, v. 151, p. 233–243, 2016.
21. RICO, C. M. et al. Interaction of nanoparticles with edible plants and their possible implications in the food chain. **Journal of Agricultural and Food Chemistry**, Washington, DC, v. 59, p. 3485–3498, 2011.
22. WANG, P. et al. Fate of ZnO Nanoparticles in Soils and Cowpea (*Vigna unguiculata*). **Environmental Science & Technology**, Easton, v. 47, p. 13822–13830, 2013.
23. BRAYNER, R. et al. Toxicological Impact Studies Based on *Escherichia coli* Bacteria in Ultrafine ZnO Nanoparticles Colloidal Medium. **Nano Letters**, Washington, DC, v. 6, p. 866–870, 2006.
24. KUREPA, J. et al. Uptake and Distribution of Ultrasmall Anatase TiO₂ Alizarin Red S Nanoconjugates in *Arabidopsis thaliana*. **Nano Letters**, Washington, DC, v. 10, p. 2296–2302, 2010.
25. LARUE, C. et al. Accumulation, translocation and impact of TiO₂ nanoparticles in wheat (*Triticum aestivum* spp.): Influence of diameter and crystal phase. **Science of the Total Environment**, Amsterdam, v. 431, p. 197–208, 2012.
26. ECKHARDT, S. et al. Nanobio Silver: Its Interactions with Peptides and Bacteria, and Its Uses in Medicine. **Chemical Reviews**, Easton, v. 113, p. 4708–4754, 2013.

27. TAYLOR, A. F. et al. Investigating the Toxicity, Uptake, Nanoparticle Formation and Genetic Response of Plants to Gold. **PLoS One**, San Francisco, v. 9, e93793, 2014.
28. SCHWAB, F. et al. Barriers, pathways and processes for uptake, translocation and accumulation of nanomaterials in plants. Critical review. **Nanotoxicology**, London, v. 10, p. 257–278, 2016.
29. ZHANG, Z. et al. Uptake and distribution of ceria nanoparticles in cucumber plants. **Metalomics**, Cambridge, v. 3, p. 816–822, 2011.
30. DE LA ROSA, G. et al. Effects of ZnO nanoparticles in alfalfa, tomato, and cucumber at the germination stage: root development and X-ray absorption spectroscopy studies. **Pure and Applied Chemistry**, London, v. 85, p. 2161–2174, 2013.
31. RASKAR, S. V.; LAWARE, S. L. Effect of zinc oxide nanoparticles on cytology and seed germination in onion. **International Journal of Current Microbiology and Applied Sciences**, Kancheepuram, v. 3, p. 467–473, 2014.
32. CASTIGLIONE, M. R. et al. The effects of nano-TiO₂ on seed germination, development and mitosis of root tip cells of *Vicia narbonensis* L. and *Zea mays* L. **Journal of Nanoparticle Research**, Dordrecht, v. 13, p. 2442–2449, 2011.
33. XIANG, L. et al. Effects of the size and morphology of zinc oxide nanoparticles on the germination of Chinese cabbage seeds. **Environmental Science and Pollution Research International**, Landsberg, v. 22, p. 10452–10462, 2015.
34. ZHANG, R. et al. Phytotoxicity of ZnO nanoparticles and the released Zn(II) ion to corn (*Zea mays* L.) and cucumber (*Cucumis sativus* L.) during germination. **Environmental Science and Pollution Research International**, Landsberg, v. 22, p. 11109–11117, 2015.
35. NAIR, P. M. G.; CHUNG, I. M. The responses of germinating seedlings of green peas to copper oxide nanoparticles. **Biologia Plantarum**, Praha, v. 59, p. 591–595, 2015.
36. MONTALVO, D. et al. Chapter five - Agronomic effectiveness of zinc sources as micronutrient fertilizer. **Advances in Agronomy**, New York, v. 139, p. 215–267. 2016.
37. SLLANPAA, M. **Micronutrient assessment at the country level: a global study**. Rome: FAO, 1990. (Soils Bulletin, 63).
38. KUMSSA, D. B. et al. Dietary calcium and zinc deficiency risks are decreasing but remain prevalent. **Scientific Reports**, London, v. 5, p. 10974, 2015.
39. BEAL, T. et al. Global trends in dietary micronutrient supplies and estimated prevalence of inadequate intakes. **PLoS One**, San Francisco, v. 12, e0175554, 2017.
40. ALLOWAY, B. J. **Zn in soils and crop nutrition**. 2. ed. Brussels: International Zinc Association; International Fertilizer Industry Association, 2008.

41. MOUSAVI, S. R.; GALAVI, M.; REZAEI, M. Zinc (Zn) importance for crop production - a review. **International Journal of Agronomy and Plant Production**, London, v. 4, p. 64068, 2013.
42. LIU, X. et al. Soil properties and microbial ecology of a paddy field after repeated applications of domestic and industrial sewage sludges. **Environmental Science and Pollution Research International**, Landsberg, v. 24, p. 8619–8628, 2017.
43. FAGERIA, N. K. Níveis adequados e tóxicos de zinco na produção de arroz, feijão, milho, soja e trigo em solo de cerrado. **Revista Brasileira de Engenharia Agrícola e Ambiental**, Campina Grande, v. 4, p. 390–395, 2000.
44. TAKKAR, P. N.; MANN, M. S. Toxic levels of soil and plant zinc for maize and wheat. **Plant and Soil**, Heidelberg, v. 49, p. 667-669, 1978.
45. HARMENS, H. et al. Uptake and transport of zinc in zinc-sensitive and zinc-tolerant *Silene vulgaris*. **Journal of Plant Physiology**, Stuttgart, v. 141, p. 309–315, 1993.
46. FONTES, R. L. F.; COX, F. R. Effects of sulfur supply on soybean plants exposed to zinc toxicity. **Journal of Plant Nutrition**, New York, v. 18, p. 1893–1906, 1995.
47. PÅHLSSON, A.-M. B. Toxicity of heavy metals (Zn, Cu, Cd, Pb) to vascular plants. **Water, Air, and Soil Pollution**, Dordrecht, v. 47, p. 287–319, 1989.
48. PLENDERLEITH, R. W. An evaluation of the tolerance of a range of tropical grasses to excessive soil levels of copper and zinc. Brisbane: University of Queensland, 1984.
49. FONTES, R. L. F.; COX, F. R. Iron deficiency and zinc toxicity in soybean grown in nutrient solution with different levels of sulfur. **Journal of Plant Nutrition**, New York, v. 21, p. 1715–1722, 1998.
50. GUPTA, N.; RAM, H.; KUMAR, B. Mechanism of Zinc absorption in plants: uptake, transport, translocation and accumulation. **Reviews in Environmental Science and Bio/Technology**, Dordrecht, v. 15, p. 89–109, 2016.
51. GONZÁLEZ-GUERRERO, M. et al. Transition Metal Transport in Plants and Associated Endosymbionts: Arbuscular Mycorrhizal Fungi and Rhizobia. **Frontiers in Plant Science**, Lausanne, v. 7, p. 1088, 2016.
52. PALMER, C. M.; GUERINOT, M. Lou. Facing the challenges of Cu, Fe and Zn homeostasis in plants. **Nature Chemical Biology**, New York, v. 5, p. 333, 2009.
53. SWAMY, B. P. M. et al. Advances in breeding for high grain zinc in rice. **Rice**, New York, v. 9, p. 49, 2016.

54. YONEYAMA, T.; ISHIKAWA, S.; FUJIMAKI, S. Route and regulation of zinc, cadmium, and iron transport in rice plants (*Oryza sativa* L.) during vegetative growth and grain filling: Metal transporters, metal speciation, grain Cd reduction and Zn and Fe biofortification. **International Journal of Molecular Sciences**, Basel, v. 16, p. 19111–19129, 2015.
55. STOMPH, T. et al. Zinc allocation and re-allocation in rice. **Frontiers in Plant Science**, Lausanne, v. 5, p. 8, 2014.
56. SPEROTTO, R. Zn/Fe remobilization from vegetative tissues to rice seeds: should I stay or should I go? Ask Zn/Fe supply! **Frontiers in Plant Science**, Lausanne, v. 4, p. 464, 2013.
57. SUZUKI, M. et al. Accumulation of starch in Zn-deficient rice. **Rice**, New York, v. 5, p. 9, 2012.
58. STOMPH, T. J.; JIANG, W.; STRUIK, P. C. Zinc biofortification of cereals: rice differs from wheat and barley. **Trends in Plant Science**, Kidlington, v. 14, p. 123–124, 2018.
59. JIANG, W. et al. Uptake and distribution of root-applied or foliar-applied ⁶⁵Zn after flowering in aerobic rice. **The Annals of Applied Biology**, Wellesbourne, v. 150, p. 383–391, 2007.
60. HUSSAIN, D. et al. P-Type ATPase heavy metal transporters with roles in essential zinc homeostasis in Arabidopsis. **Plant Cell**, Rockville, v. 16, p. 1327–1339, 2004.
61. LV, J. et al. Accumulation, Speciation and Uptake Pathway of ZnO Nanoparticles in Maize. **Environmental Science. Nano**, London, v. 2, p. 68–77, 2014.
62. MOUSAVI KOUHI, S. M. et al. Long-term exposure of rapeseed (*Brassica napus* L.) to ZnO nanoparticles: anatomical and ultrastructural responses. **Environmental Science and Pollution Research International**, Landsberg, v. 22, p. 10733–10743, 2015.
63. ZHANG, D. et al. Phytotoxicity and bioaccumulation of ZnO nanoparticles in *Schoenoplectus tabernaemontani*. **Chemosphere**, Oxford, v. 120, p. 211–219, 2015.
64. ZHAO, L. et al. Influence of CeO₂ and ZnO Nanoparticles on Cucumber Physiological Markers and Bioaccumulation of Ce and Zn: A Life Cycle Study. **Journal of Agricultural and Food Chemistry**, Washington, DC, v. 61, p. 11945–11951, 2013.
65. ZHU, H. et al. Uptake, translocation, and accumulation of manufactured iron oxide nanoparticles by pumpkin plants. **Journal of Environmental Monitoring**, Cambridge, v. 10, p. 713–717, 2008.
66. NHAN, L. Van et al. Phytotoxic Mechanism of Nanoparticles: Destruction of Chloroplasts and Vascular Bundles and Alteration of Nutrient Absorption. **Scientific Reports**, London, v. 5, p. 11618, 2015.

67. HATAMI, M.; KARIMAN, K.; GHORBANPOUR, M. Engineered nanomaterial-mediated changes in the metabolism of terrestrial plants. **Science of the Total Environment**, Amsterdam, v. 571, p. 275–291, 2016.
68. REDDY, P. V. L. et al. Lessons learned: Are engineered nanomaterials toxic to terrestrial plants? **Science of the Total Environment**, Amsterdam, v. 568, p. 470–479, 2016.
69. LARUE, C. et al. Comparative uptake and impact of TiO₂ nanoparticles in wheat and rapeseed. **Journal of Toxicology and Environmental Health. Part A**, Washington, DC, v. 75, p. 722–734, 2012.
70. RAVEL, B.; NEWVILLE, M. ATHENA, ARTEMIS, HEPHAESTUS: data analysis for X-ray absorption spectroscopy using IFEFFIT. **Journal of Synchrotron Radiation**, Copenhagen, v. 12, p. 537–541, 2005.
71. HAN, F. et al. Organic acids promote the uptake of lanthanum by barley roots. **New Phytologist**, London, v. 165, p. 481–492, 2005.
72. CALVIN, S. **XAFS for everyone**. Boca Raton: CRC Press, 2013.
73. MUDUNKOTUWA, I. A. et al. Dissolution of ZnO nanoparticles at circumneutral pH: a study of size effects in the presence and absence of citric acid. **Langmuir**, Washington, DC, v. 28, p. 396–403, 2011.
74. REED, R. B. et al. Solubility of nano-zinc oxide in environmentally and biologically important matrices. **Environmental Toxicology and Chemistry**, New York, v. 31, p. 93–99, 2012.
75. MAURER-JONES, M. A. et al. Toxicity of engineered nanoparticles in the environment. **Analytical Chemistry**, Washington, DC, v. 85, p. 3036–3049, 2013.
76. ALLOWAY, B. J. **Heavy metals in soils**. 2. ed. Glasgow: Blackey Academic and Professional, 1995.
77. BIAN, S.-W. et al. Aggregation and dissolution of 4 nm ZnO nanoparticles in aqueous environments: influence of pH, ionic strength, size, and adsorption of humic acid. **Langmuir**, Washington, DC, v. 27, p. 6059–6068, 2011.
78. ZHAO, L. et al. Effect of surface coating and organic matter on the uptake of CeO₂ NPs by corn plants grown in soil: Insight into the uptake mechanism. **Journal of Hazardous Materials**, Amsterdam, v. 225–226, p. 131–138, 2012.
79. CASTILLO-MICHEL, H. A. et al. Practical review on the use of synchrotron based micro- and nano-X-ray fluorescence mapping and X-ray absorption spectroscopy to investigate the interactions between plants and engineered nanomaterials. **Plant Physiology and Biochemistry**, Paris, v. 110, p. 13–32, 2017.

80. SCHECKEL, K. G. et al. In Vivo Synchrotron Study of Thallium Speciation and Compartmentation in Iberis intermedia. **Environmental Science & Technology**, Easton, v. 38, p. 5095–5100, 2004.
81. MONSANT, A. C. et al. In vivo speciation of zinc in Noccaea caerulescens in response to nitrogen form and zinc exposure. **Plant and Soil**, Heidelberg, v. 348, p.167, 2011.
82. PICKERING, I. J. et al. Quantitative, chemically specific imaging of selenium transformation in plants. **Proceedings of the National Academy of Science of the USA**, Washington, DC, v. 97, p. 10717–10722, 2000.
83. YANO, J. et al. X-ray damage to the Mn4Ca complex in single crystals of photosystem II: a case study for metalloprotein crystallography. **Proceedings of the National Academy of Science of the USA**, Washington, DC, v. 102, p. 12047–12052, 2005.
84. GEORGE, S. J. et al. X-ray photochemistry in iron complexes from Fe (0) to Fe (IV)—Can a bug become a feature? **Inorganica Chimica Acta**, Amsterdam, v. 361, p. 1157–1165, 2008.
85. JAMES, S. A. et al. μ XANES: in vivo imaging of metal-protein coordination environments. **Scientific Reports**, London, v. 6, p. 20350, 2016.
86. MATHYS, W. The role of malate, oxalate, and mustard oil glucosides in the evolution of Zinc-Resistance in Herbage plants. **Physiologia Plantarum**, Lund, v. 40, p. 130–136, 1977.
87. GODBOLD, D. L. et al. Accumulation of zinc and Organic Acids in Roots of Zinc Tolerant and Non-tolerant Ecotypes of Deschampsia caespitosa. **Journal of Plant Physiology**, Stuttgart, v. 116, p. 59–69, 1984.
88. WANG, J. et al. Computer, Simulated Evaluation of Possible Mechanisms for Sequestering Metal Ion Activity in Plant Vacuoles. **Plant Physiology**, Rockville, v. 99, p. 621-626, 1992.
89. SARRET, G. et al. Forms of zinc accumulated in the hyperaccumulator Arabidopsis halleri. **Plant Physiology**, Rockville, v. 130, p. 1815–1826, 2002.
90. AJIBOYE, B.; AKINREMI, O. O.; JÜRGENSEN, A. Experimental Validation of Quantitative XANES Analysis for Phosphorus Speciation. **Soil Science Society of America Journal**, Madison, v. 71, p. 1288–1291, 2007.
91. MCCANN, M. C.; WELLS, B.; ROBERTS, K. Direct visualization of cross-links in the primary plant cell wall. **Journal of Cell Science**, London, v. 96, p. 323–334, 1990.
92. LIU, R.; LAL, R. Potentials of engineered nanoparticles as fertilizers for increasing agronomic productions. **Science of the Total Environment**, Amsterdam, v. 514, p. 131–139, 2015.

93. SABIR, S.; ARSHAD, M.; CHAUDHARI, S. K. Zinc Oxide Nanoparticles for Revolutionizing Agriculture: Synthesis and Applications. **Science World Journal**, London, v. 2014, art. ID 925494, 8 p., 2014. <http://dx.doi.org/10.1155/2014/925494>.
94. DUHAN, J. S. et al. Nanotechnology: The new perspective in precision agriculture. **Biotechnology Reports**, Amsterdam, v. 15, p. 11–23, 2017.
95. RALIYA, R. et al. Nanofertilizer for Precision and Sustainable Agriculture: Current State and Future Perspectives. **Journal of Agricultural and Food Chemistry**, Washington, DC, 2017. doi:10.1021/acs.jafc.7b02178.
96. BROADLEY, M. R. et al. Zinc in plants. **New Phytologist**, London, v. 173, 677-702, 2007.
97. GANGLOFF, W. J. et al. Mobility of Organic and Inorganic Zinc Fertilizers in Soils. **Communications in Soil Science and Plant Analysis**, New York, v. 37, p. 199–209, 2006.
98. AMRANI, M.; WESTFALL, D. G.; PETERSON, G. A. Influence of water solubility of granular zinc fertilizers on plant uptake and growth. **Journal of Plant Nutrition**, New York, v. 22, p. 1815-1827, 1999.
99. GANGLOFF, W. J. et al. Relative availability coefficients of organic and inorganic zn fertilizers. **Journal of Plant Nutrition**, New York, v. 25, p. 259–273, 2002.
100. GONZALEZ, D.; OBRADOR, A.; ALVAREZ, J. M. Behavior of Zinc from Six Organic Fertilizers Applied to a Navy Bean Crop Grown in a Calcareous Soil. **Journal of Agricultural and Food Chemistry**, Washington, DC, v. 55, p. 7084–7092, 2007.
101. ALVAREZ, J. M. et al. Mobility and leachability of zinc in two soils treated with six organic zinc complexes. **Journal of Agricultural and Food Chemistry**, Washington, DC, v. 49, p. 3833–3840, 2001.
102. PRASAD, T. N. V. K. V et al. Effect of nanoscale zinc oxide particles on the germination, growth and yield of peanut. **Journal of Plant Nutrition**, New York, v. 35, p. 905–927, 2012.
103. GARCIA-GOMEZ, C. et al. Comparative effect of ZnO NPs, ZnO bulk and ZnSO₄ in the antioxidant defences of two plant species growing in two agricultural soils under greenhouse conditions. **Science of the Total Environment**, Amsterdam, v. 589, p. 11–24, 2017.
104. WANG, X. et al. Zinc oxide nanoparticles affect biomass accumulation and photosynthesis in Arabidopsis. **Frontiers in Plant Science**, Lausanne, v. 6, p. 1243, 2015.
105. DA CRUZ, T. N. M. et al. Shedding light on the mechanisms of absorption and transport of ZnO nanoparticles by plants via in vivo X-ray spectroscopy. **Environmental Science. Nano**, London, v. 4, p. 2367–2376, 2017.

106. WHITE, P. J. et al. Does zinc move apoplastically to the xylem in roots of *Thlaspi caerulescens*? **New Phytologist**, London, v. 153, p. 201–207, 2002.
107. LIN, D.; XING, B. Root Uptake and Phytotoxicity of ZnO Nanoparticles. **Environmental Science & Technology**, Easton, v. 42, p. 5580–5585, 2008.
108. SINCLAIR, S. A.; KRAMER, U. The zinc homeostasis network of land plants. **Biochimica et Biophysica Acta**, Amsterdam, v. 1823, p. 1553–1567, 2012.
109. HALL, J. L. Cellular mechanisms for heavy metal detoxification and tolerance. **Journal of Experimental Botany**, Oxford, v. 53, p. 1–11, 2002.
110. GUPTA, S. K. et al. Comparative Analysis of Zinc Finger Proteins Involved in Plant Disease Resistance. **PLoS One**, San Francisco, v. 7, p. 1–15, 2012.
111. MISHRA, S.; DUBEY, R. S. Heavy metal toxicity induced alterations in photosynthetic metabolism in plants. **Handbook of Photosynthesis**, 2. ed. Boca Raton: CRC Press, 2005. p. 845–863.
112. TODESCHINI, V. et al. Effects of high zinc concentration on poplar leaves: A morphological and biochemical study. **Environmental and Experimental Botany**, Oxford, v. 71, p. 50–56, 2011.
113. SANTOS, E. F. et al. Physiological highlights of manganese toxicity symptoms in soybean plants: Mn toxicity responses. **Plant Physiology and Biochemistry**, Paris, v. 113, p. 6–19, 2017.
114. REIS, A. R. dos et al. A glimpse into the physiological, biochemical and nutritional status of soybean plants under Ni-stress conditions. **Environmental and Experimental Botany**, Oxford, v. 144, p. 76–87, 2017.
115. JUDY, J. D.; BERTSCH, P. M. Chapter One - Bioavailability, Toxicity, and Fate of Manufactured Nanomaterials in Terrestrial Ecosystems. **Advances in Agronomy**, New York, v. 123, p. 1–64, 2014.
116. MOUSAVI KOUHI, S. M. et al. Comparative Effects of ZnO Nanoparticles, ZnO Bulk Particles, and Zn²⁺ on *Brassica napus* After Long-Term Exposure: Changes in Growth, Biochemical Compounds, Antioxidant Enzyme Activities, and Zn Bioaccumulation. **Water, Air, and Soil Pollution**, Dordrecht, v. 226, p. 364, 2015.
117. LI, M. et al. Stability, Bioavailability, and Bacterial Toxicity of ZnO and Iron-Doped ZnO Nanoparticles in Aquatic Media. **Environmental Science & Technology**, Easton, v. 45, p. 755–761, 2011.
118. HUANG, Y.; ZHAO, L.; KELLER, A. A. Interactions, Transformations, and Bioavailability of Nano-Copper Exposed to Root Exudates. **Environmental Science & Technology**, Easton, v. 51, p. 9774–9783, 2017.

119. BAZIHIZINA, N. et al. Zn(2+)-induced changes at the root level account for the increased tolerance of acclimated tobacco plants. **Journal of Experimental Botany**, Oxford, v. 65, p. 4931–4942, 2014.
120. SAGARDOY, R. et al. Carboxylate metabolism in sugar beet plants grown with excess Zn. **Journal of Plant Physiology**, Stuttgart, v. 168, p. 730–733, 2011.
121. SRESTY, T. V. S.; MADHAVA RAO, K. V. Ultrastructural alterations in response to zinc and nickel stress in the root cells of pigeonpea. **Environmental and Experimental Botany**, Oxford, v. 41, p. 3–13, 1999.
122. VANCE, M. E. et al. Nanotechnology in the real world: Redeveloping the nanomaterial consumer products inventory. **Beilstein Journal of Nanotechnology**, Frankfurt, v. 6, p. 1769–1780, 2015.
123. JARVIS, D. S.; RICHMOND, N. Regulation and Governance of Nanotechnology in China: Regulatory Challenges and Effectiveness. **European Journal of Law Technology**, Belfast, v. 2, n. 3, 2011.
124. KAISER, J.-P.; ZUIN, S.; WICK, P. Is nanotechnology revolutionizing the paint and lacquer industry? A critical opinion. **Science of the Total Environment**, Amsterdam, v. 442, p. 282–289, 2013.
125. GOPALAKRISHNAN, K. et al. **Nanotechnology in Civil Infrastructure: A Paradigm Shift**. Heidelberg: Springer, 2011. doi: 10.1007/978-3-642-16657-0.
126. LEE, S. et al. Assessment of phytotoxicity of ZnO NPs on a medicinal plant, *Fagopyrum esculentum*. **Environmental Science and Pollution Research International**, Landsberg, v. 20, p. 848–854, 2013.
127. DE LA ROSA, G. et al. Toxicity and biotransformation of ZnO nanoparticles in the desert plants *Prosopis juliflora-velutina*, *Salsola tragus* and *Parkinsonia florida*. **Interanational Journal of Nanotechnology**, Bucks, v. 8, p. 492–506, 2011.
128. HERNANDEZ-VIEZCAS, J. A. et al. Spectroscopic verification of zinc absorption and distribution in the desert plant *Prosopis juliflora-velutina* (velvet mesquite) treated with ZnO nanoparticles. **Chemical Engineering Journal**, Amsterdam, v. 170, p. 346–352, 2011.
129. MUKHERJEE, A. et al. Physiological effects of nanoparticulate ZnO in green peas (*Pisum sativum* L.) cultivated in soil. **Metallomics**, Cambridge, v. 6, p. 132–138, 2014.
130. VITTI, G. C.; QUEIROZ, F. E. de C.; QUINTINO, T. A. Micronutrientes na cana-de açúcar: mitos e realidades. In: SIMPÓSIO TECNOLOGIA NA PRODUÇÃO EM CANA-DE-AÇÚCAR, 2., 2005, Piracicaba. **Anais...** Piracicaba: Potafos, 2005.
131. MAJUMDAR, S. et al. Exposure of cerium oxide nanoparticles to kidney bean shows disturbance in the plant defense mechanisms. **Journal of Hazardous Materials**, Amsterdam, v. 278, p. 279–287, 2014.

132. KANJANA, D. Advancement of Nanotechnology Applications on Plant Nutrients Management and Soil Improvement. In: PRASAD, R.; KUMAR, V.; KUMAR, M. (Ed.). **Nanotechnology: Food and Environmental Paradigm**. Singapore: Springer, 2017. p. 209–234. doi:10.1007/978-981-10-4678-0_12.
133. DIMKPA, C. O.; BINDRABAN, P. S. Fortification of micronutrients for efficient agronomic production: a review. **Agronomy for Sustainable Development**, v. 36, p. 7, 2016.
134. BINDRABAN, P. S. et al. Revisiting fertilisers and fertilisation strategies for improved nutrient uptake by plants. **Biology and Fertility of Soils**, v. 51, p. 897–911, 2015.
135. MARSCHNER, H.; CAKMAK, I. High light intensity enhances chlorosis and necrosis in leaves of zinc, potassium, and magnesium deficient bean (*Phaseolus vulgaris*) plants. **Journal of Plant Physiology**, v. 134, p.308-315, 1989.
136. R CORE TEAM. **R: A Language and environment for statistical computing**. 2017.
137. PÔRTO, M. L. et al. Índice SPAD para o diagnóstico do estado de nitrogênio na cultura da abobrinha. **Horticultura Brasileira**, Viória da Conquista, v. 29, p. 311–315, 2011.
138. NAIR, P. M. G. & CHUNG, I. M. Regulation of morphological, molecular and nutrient status in *Arabidopsis thaliana* seedlings in response to ZnO nanoparticles and Zn ion exposure. **Science of the Total Environment**, Amsterdam, v. 575, p. 187–198, 2017.
139. STEFANOWICZ, A. M. et al. The accumulation of elements in plants growing spontaneously on small heaps left by the historical Zn-Pb ore mining. **Environmental Science and Pollution Research International**, Landsberg, v. 23, p. 6524–6534, 2016.
140. FOY, C. D., CHANEY, R. L. & WHITE, M. C. The Physiology of Metal Toxicity in Plants. **Annual Review of Plant Physiology**, Palo Alto, v. 29, p. 511–566, 1978.
141. BARAN, A. Assessment of Zea mays Sensitivity to Toxic Content of Zinc in Soil. **Polish Journal of Environmental Studies**, Olsztyn, v. 22, 2013.
142. EBBS, S.; KOCHIAN, L. Toxicity of Zinc and Copper to Brassica Species: Implications for Phytoremediation. **Journal of Environmental Quality**, Madiosn, v. 26, p. 776–781, 1997.
143. VAN WIJK, K. J.; KESSLER, F. Plastoglobuli: Plastid Microcompartments with Integrated Functions in Metabolism, Plastid Developmental Transitions, and Environmental Adaptation. **Annual Review of Plant Biology**, Palo Alto, v. 68, p. 253–289, 2017.
144. FAGERIA, N. K. **Maximizing crop yields**. Boca Raton: CRC Press, 1992.
145. TIECHER, T. L. et al. Physiological and nutritional status of black oat (*Avena strigosa* Schreb.) grown in soil with interaction of high doses of copper and zinc. **Plant Physiology and Biochemistry**, Paris, v. 106, p. 253–263, 2016.

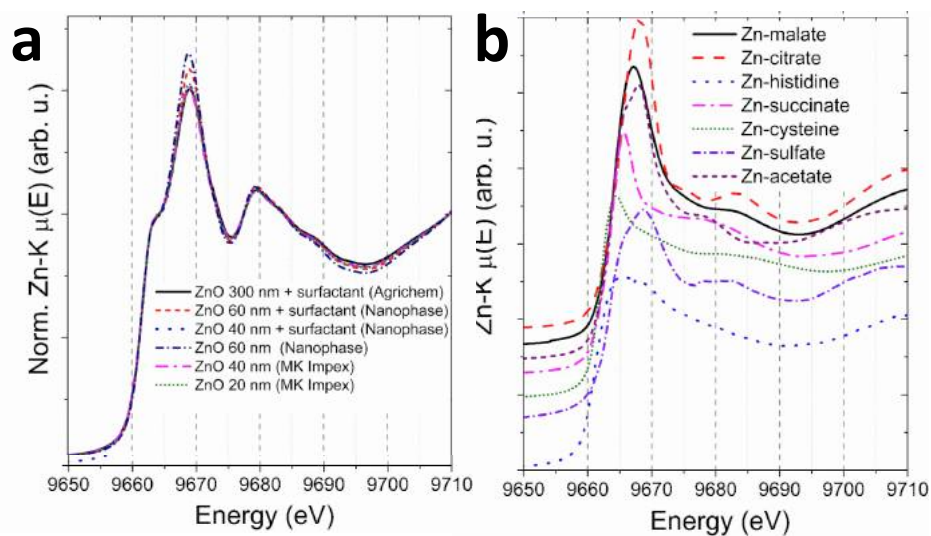
146. MALVI, U. R. Interaction of micronutrients with major nutrients with special reference to potassium. *Karnataka Journal of Agricultural Sciences*, Beijing, v. 24, p. 106–109, 2011.
147. HART, J. J. et al. Characterization of Zinc Uptake, Binding, and Translocation in Intact Seedlings of Bread and Durum Wheat Cultivars. ***Plant Physiology***, Rockville, v. 118, p. 219-226, 1998.
148. FURLANI, Â. M. C. et al. Efficiency of maize cultivars for zinc uptake and use. ***Scientia Agricola***, Piracicaba, v. 62, p. 264–273, 2005.

APPENDIX

Appendix A - Setup used to monitor *in vivo* Zn uptake using a 1 mm \varnothing X-ray beam. The red arrow illustrates the incoming X-ray beam and the yellow one the outgoing Zn X-ray fluorescence.



Appendix B - (a) XANES spectra for the ZnO nanomaterials employed in the present study; (b) XANES spectra for the Zn coordinate compounds synthesized in our laboratory. Since the shape of the curves are fingerprints of the chemical environment, these spectra were used in the linear combination analysis to identify the Zn forms inside of the living the plants.



Appendix C – Estimation of the radiation dose received by the samples

To estimate the radiation dose, which the samples were submitted, besides the photon flux input, the following assumptions and approximations were made:

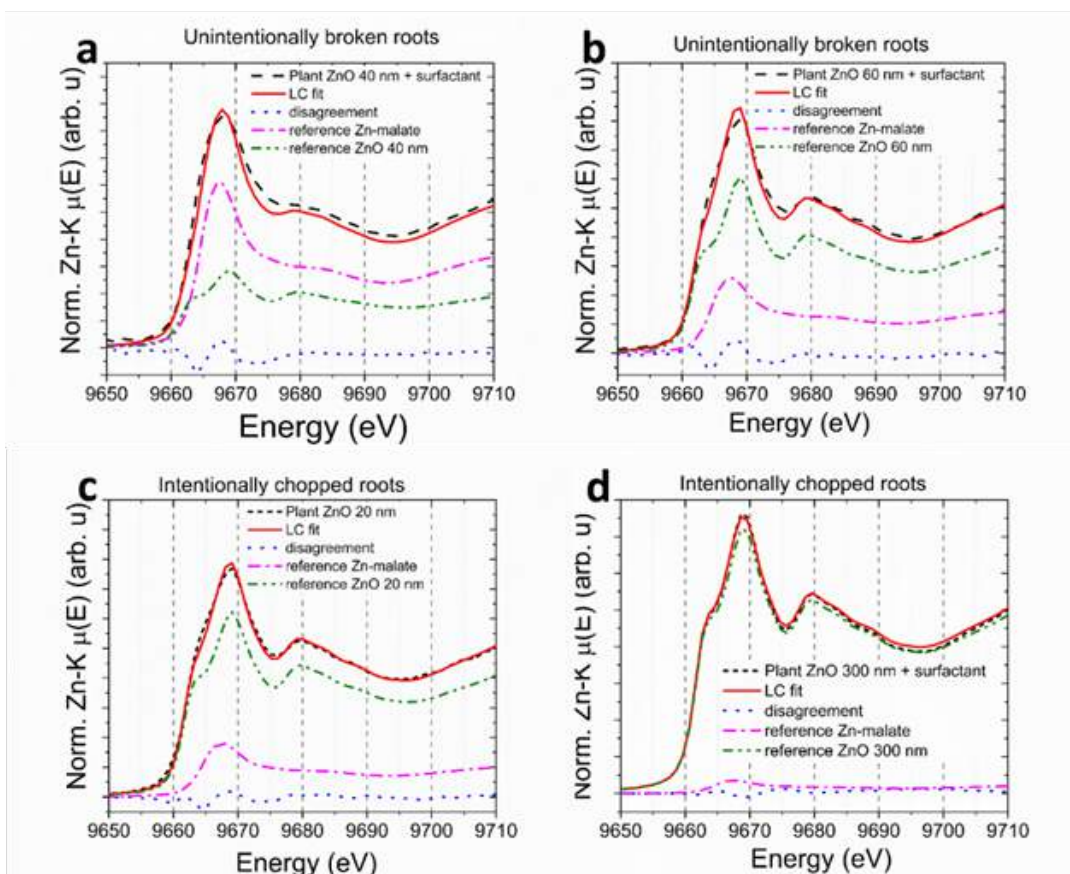
- i) Incident energy at 9,560 eV = 1.54×10^{-15} J
- ii) Time of exposure = 1800 s, considering the time employed to adjust the sample in front of the beam
- iii) Approximated mass of the irradiated volume = 4×10^{-7} kg

The absorbed radiation dose is expressed in Gray unity (Gy). Knowing that $\text{Gy} = \text{J kg}^{-1}$, we approximated the calculations as follows:

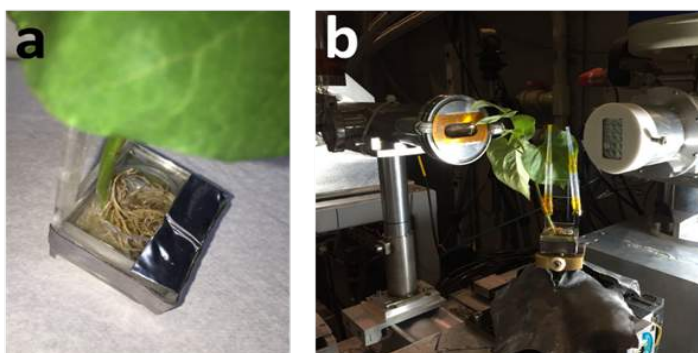
$$\text{Gy} = \frac{\text{number of photons per second (s}^{-1}) \times \text{time of exposure (s)} \times \text{energy of the incident photons (J)}}{\text{mass of the irradiated volume (kg)}}$$

The estimation of the radiation dose indicates that the samples received a dose lower than 1.9×10^4 Gy.

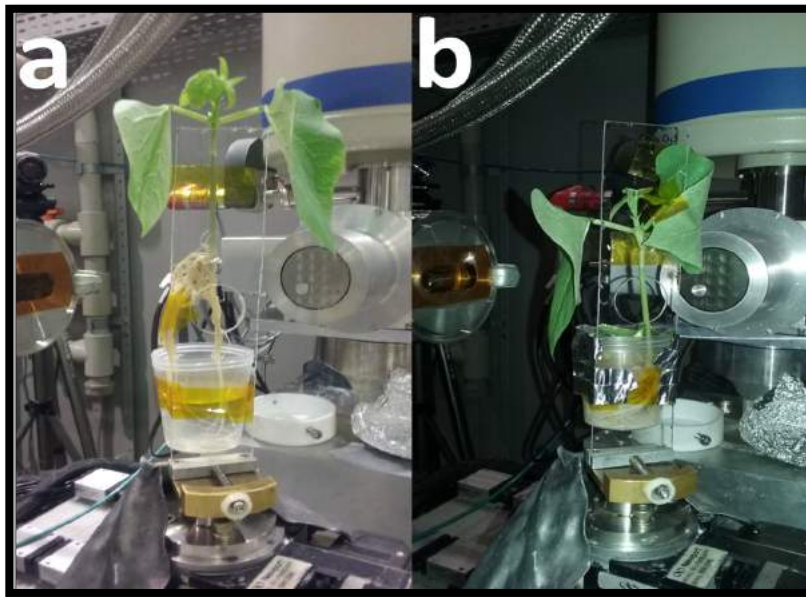
Appendix D - Zn-K experimental XANES spectra recorded *in vivo* at the stem of *Phaseolus vulgaris* plants treated with 20, 40, 60 and 300 nm ZnO NPs, linear combination fits and the weighted spectra for the reference compounds. (a) and (b) show the spectra for plants in which exhibited damage in the roots, whereas (c) and (d) show the spectra for plants in which roots were intentionally damaged.



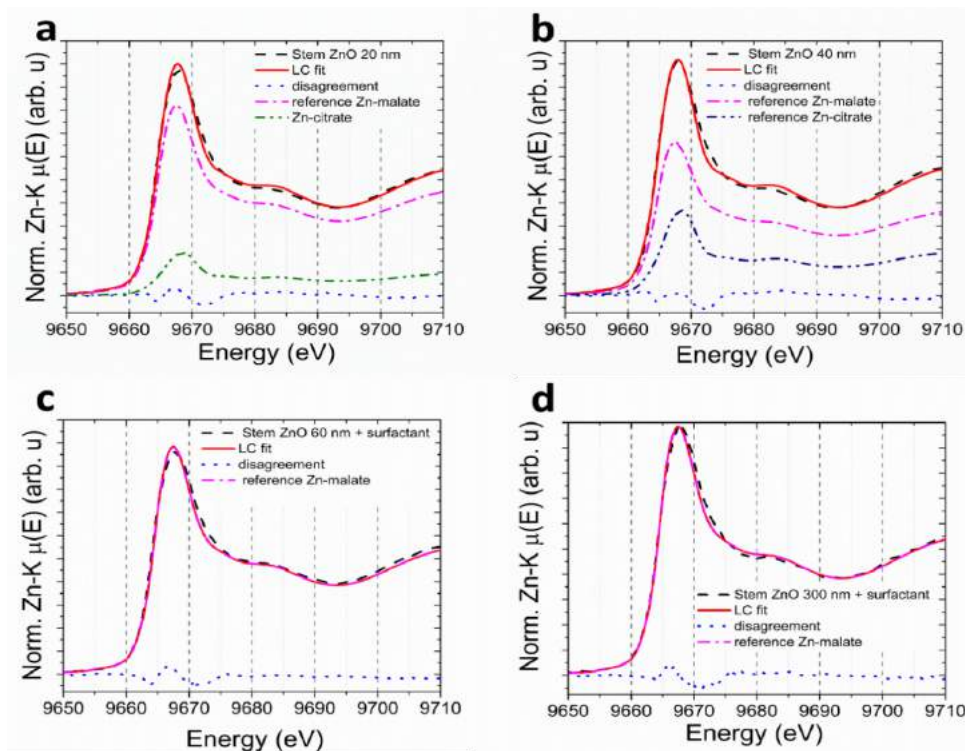
Appendix E - (a) Sample holder used to keep the roots of the bean (*Phaseolus vulgaris*) plant in contact with a dispersion of nano ZnO while recording XAS spectra in fluorescence mode; (b) Plant + sample holder assembled at XAFS2 beamline.



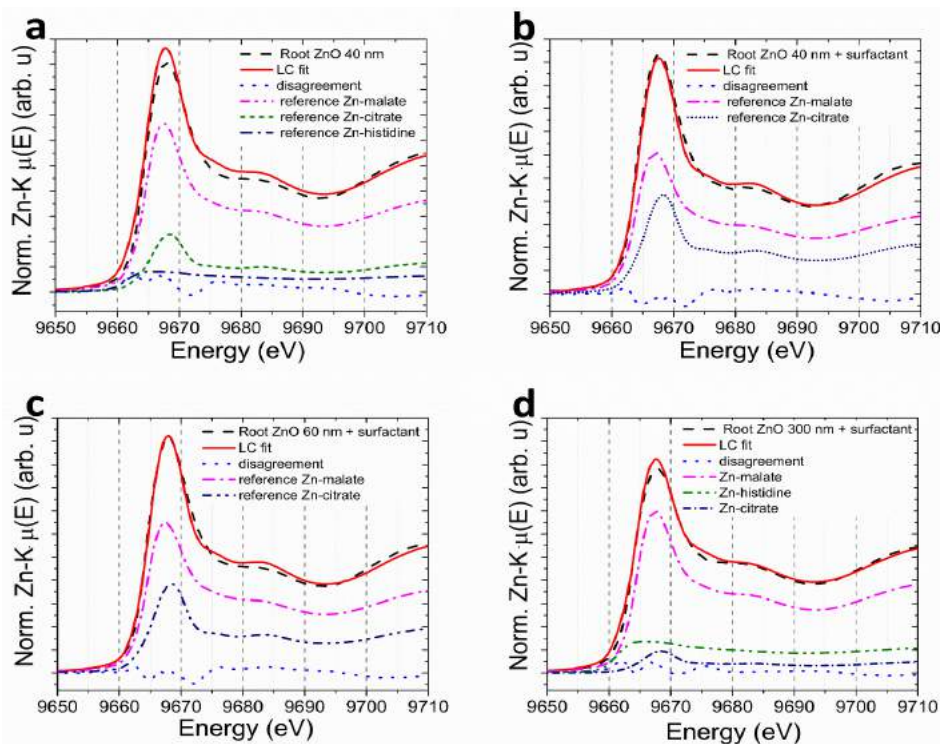
Appendix F - Setup for recording XAS spectra in fluorescence mode for (a) root and (b) stem at XAFS2 beamline.



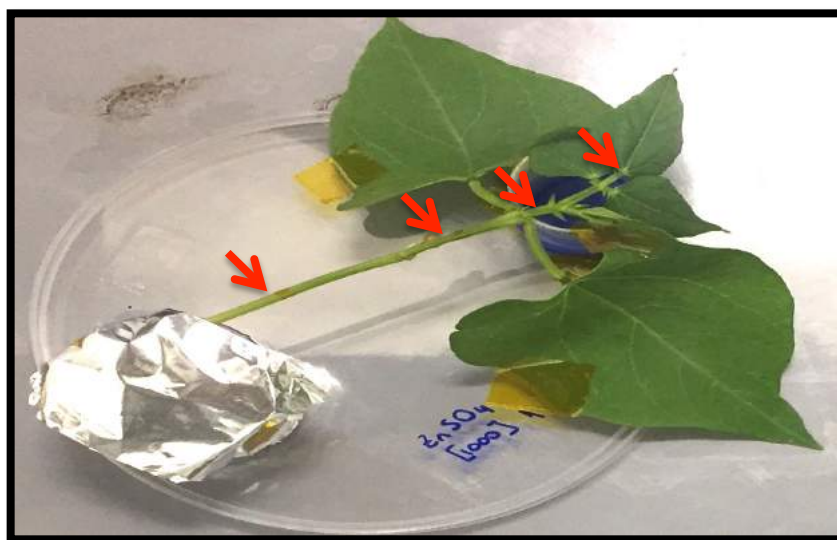
Appendix G - Zn-K experimental XANES spectra recorded *in vivo* at the stem of *Phaseolus vulgaris* plants whose roots were immersed in nano ZnO dispersed in water; (a) 20 nm ZnO, (b) 40 nm ZnO, (c) 60 nm ZnO + surfactant and (d) 300 nm ZnO + surfactant.



Appendix H - Zn-K experimental XANES spectra recorded *in vivo* at root of *Phaseolus vulgaris* plants whose roots were immersed in nano ZnO dispersed in water: (a) 40 nm ZnO, (b) 40 nm ZnO + surfactant, (c) 60 nm ZnO + surfactant, and (d) 300 nm ZnO + surfactant.



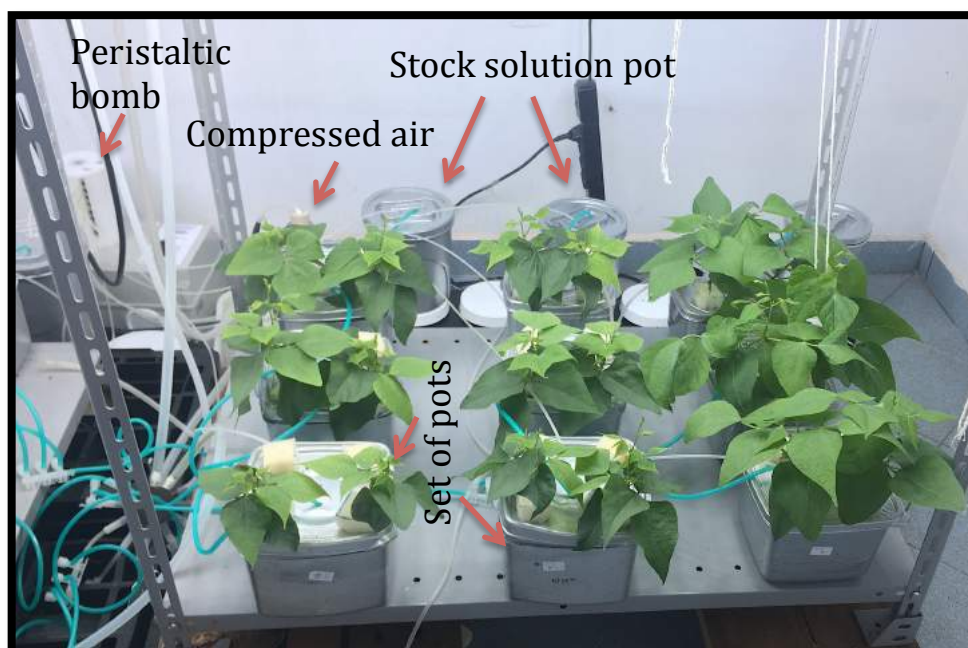
Appendix I - Red arrows indicate the analysed points to monitor *in vivo* Zn uptake with x ray fluorescence.



Appendix J - Zn uptake velocity by *P. vulgaris* and Person's R from adjusted slopes as function of nanoparticle size, concentration and analysed part of the plants. Treatments consisted of 4 different points in the plants, 100 and 1000 mg L⁻¹ of Zn from ZnO nanoparticles and aqueous ZnSO₄.

Treatments	100 mg L ⁻¹		1000 mg L ⁻¹		
	Slope	R ²	Slope	R ²	
Stem 1	40 nm	2,83E-06	0,9833	1,55E-06	0,98062
	300 nm	6,53E-07	0,9783	3,93E-07	0,78852
	ZnSO _{4(aq)}	2,41E-05	0,9723	1,19E-04	0,97912
Stem 2	40 nm	1,53E-06	0,905	5,28E-07	0,9541
	300 nm	2,59E-07	0,9706	4,08E-07	0,87257
	ZnSO _{4(aq)}	1,32E-05	0,9592	1,23E-04	0,98745
Stem 3	40 nm	1,40E-07	0,6798	2,12E-07	0,91167
	300 nm	-2,15E-08	-0,194	1,73E-07	0,88069
	ZnSO _{4(aq)}	2,06E-06	0,9576	5,03E-05	0,82798
Leaf	40 nm	1,44E-07	0,7762	2,84E-07	0,84036
	300 nm	1,43E-07	0,8475	6,82E-08	0,2569
	ZnSO _{4(aq)}	5,74E-07	0,8581	1,32E-04	0,95737

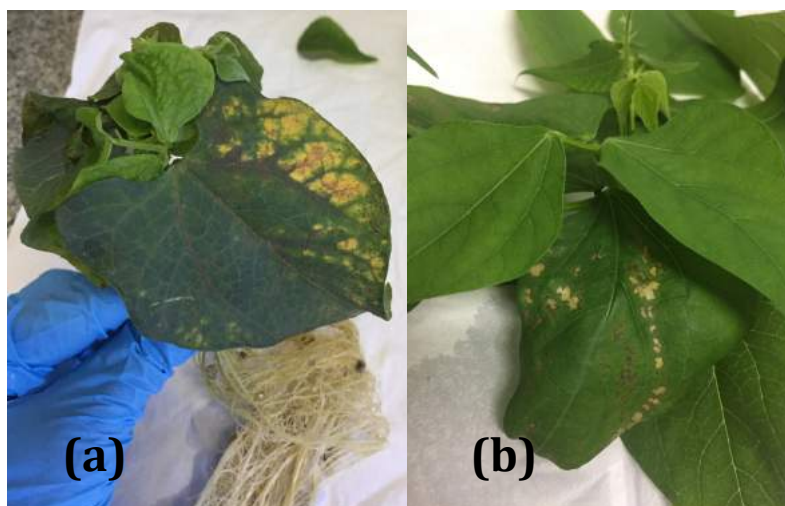
Appendix K – The cultivated system, with a set of three pots connected with a stock solution pot; the peristaltic bomb that recirculates the nutritive solution among pots and the compressed air that provides oxygen for the plants.



Appendix L – In order to certify the method, the equation below was used, where the certified reference material concentration or the known amount of analyte (Certified value) is divided by the EDXRF result measured and then it is multiplied by 100 to verify if the EDXRF result is between 80 and 120% of the certified value.

$$\text{Recovery (\%)} = \frac{\text{Certified value}}{\text{EDXRF measured}} * 100$$

Appendix M – Leaves of plants treated with 10 mg of Zn L⁻¹ (a) and Cakmak modified solution (b).



Appendix N – Root length (cm) of *Phaseolus vulgaris* plants after different times of exposure (7, 14, 21 and 28 days) to nanoparticles dispersions and ZnSO₄ solutions. Same letters in the same column indicates that means are statistically the same, by Tukey test with $p < 0.05$.

Treatments	Root Length (cm)							
	7 days		14 days		21 days		28 days	
T40_1	34.8	abc	49.2	abcd	57.3	bcde	58.3	a
T40_3	36.3	abc	51.2	abc	62.4	abcd	54.2	ab
T40_10	24.7	bc	40	bcde	52.3	bcdef	53.3	ab
T60_1	34	abc	55.7	abc	38	efg	59.8	a
T60_3	40.6	a	38.5	cde	63.6	abc	58.8	a
T60_10	31.8	abc	47.2	abcde	64.5	abc	56.3	a
T300_1	40.2	ab	67.2	a	77.7	a	63.2	a
T300_3	33.8	abc	58.7	ab	67.8	ab	63	a
T300_10	30.5	abc	28.7	e	33.7	fg	29.5	b
TS_1	37.5	ab	56.7	abc	46.8	cdefg	60.8	a
TS_3	28.9	abc	30.5	de	43.1	defg	53.8	ab
TS_10	21.8	c	29	e	29.8	g	41.7	ab
TC	40.9	a	52.8	abc	60.6	abcd	43.4	ab

Appendix O – Shoot height (cm) of *Phaseolus vulgaris* plants after different times of exposure (7, 14, 21 and 28 days) to nanoparticles dispersions and ZnSO₄ solutions. Same letters in the same column indicates that means are statistically the same, by Tukey test with $p < 0.05$.

Treatments	Shoot Height (cm)							
	7 days		14 days		21 days		28 days	
T40_1	10.8	cde	19.2	ab	38	a	66.3	a
T40_3	11.3	bcde	13	cd	25	b	40.7	abc
T40_10	12.8	abcd	12.3	cd	12.7	c	15.3	c
T60_1	16	a	21.5	a	28.3	b	53.5	ab
T60_3	11.5	bcde	13.2	cd	29.8	ab	35.5	abc
T60_10	8.5	e	9.8	d	10.5	c	10.5	c
T300_1	14.2	ab	22.3	a	30.7	ab	49.7	ab
T300_3	13.7	abc	19.5	cab	25.4	b	63.7	ab
T300_10	11.3	bcde	11.8	d	12.4	c	11	c
TS_1	10.7	cde	16	bc	29.7	ab	43.3	abc
TS_3	10.3	de	13.3	cd	24.7	b	41	abc
TS_10	11.8	bcd	13.2	cd	11.2	c	13.8	c
TC	12.7	bcd	19	ab	30.2	ab	30.5	bc

Appendix P – Root dry mass (g) of *Phaseolus vulgaris* plants after different times of exposure (7, 14, 21 and 28 days) to nanoparticles dispersions and ZnSO₄ solutions. Same letters in the same column indicates that means are statistically the same, by Tukey test with $p < 0.05$.

Treatments	Root dry mass (g)			
	7 days	14 days*	21 days*	28 days
T40_1	0.27 a	0.53 a	0.57 a	1.1 a
T40_3	0.16 abc	0.26 abcd	0.24 bcd	0.41 bc
T40_10	0.18 abc	0.2 bcde	0.3 abcd	0.33 bcd
T60_1	0.19 abc	0.23 bcde	0.34 abc	0.77 ab
T60_3	0.13 bc	0.2 bcde	0.42 ab	0.41 b
T60_10	0.17 abc	0.4 ab	0.41 ab	0.48 bcd
T300_1	0.23 ab	0.28 abcd	0.35 ab	0.62 abc
T300_3	0.18 abc	0.12 e	0.36 ab	0.7 ab
T300_10	0.21 abc	0.15 cde	0.17 cd	0.11 d
TS_1	0.12 bc	0.23 bcde	0.23 bcd	0.49 bcd
TS_3	0.12 bc	0.12 e	0.29 abcd	0.45 bcd
TS_10	0.08 c	0.14 de	0.15 d	0.17 cd
TC	0.14 bc	0.29 abc	0.35 ab	0.36 bcd

data transformed $\log(Y)^*$

Appendix Q – Shoot fresh mass (g) of *Phaseolus vulgaris* plants after different times of exposure (7, 14, 21 and 28 days) to nanoparticles dispersions and ZnSO₄ solutions. Same letters in the same column indicates that means are statistically the same, by Tukey test with $p < 0.05$.

Treatments	Shoot Fresh Mass (g)			
	7 days	14 days	21 days	28 days*
T40_1	5.39 a	16.4 a	29.29 a	43.58 a
T40_3	3.70 bcd	7.79 bcd	20.54 bc	13.23 bcd
T40_10	2.94 cde	3.64 ef	4.64 e	6.78 cde
T60_1	5.29 ab	13.62 ab	19.94 bcd	29.27 ab
T60_3	3.76 bcd	7.54 cde	22.69 b	14.44 bcd
T60_10	2.67 cde	3.71 ef	3.98 e	5.77 de
T300_1	5.15 ab	13.73 ab	21.52 b	26.18 ab
T300_3	3.36 cde	9.55 bcd	15.6 cd	28.5 ab
T300_10	2.23 de	2.27 f	2.24 e	0.88 f
TS_1	3.51 cde	11.21 bc	19.47 bcd	16.75 abc
TS_3	2.62 de	5.89 def	14.7 d	16.4 abc
TS_10	1.98 e	2.44 f	2.08 e	2.8 e
TC	4.26 i	14.47 f	17.93 bcd	13.74 bcd

data transformed $\log(Y)^*$

Appendix R – SPAD index of *Phaseolus vulgaris* plants after different times of exposure (7, 14, 21 and 28 days) to nanoparticles dispersions and ZnSO₄ solutions. Same letters in the same column indicates that means are statistically the same, by Tukey test with p<0.05.

Treatments	SPAD index			
	7 days	14 days	21 days*	28 days**
T40_1	26.5 abcde	21.9 ab	33 ab	27.7 bc
T40_3	26.6 abcd	30.3 ab	31.8 abc	29.5 ab
T40_10	22.4 ef	31.1 ab	31.3 abc	21.7 c
T60_1	28.5 ab	31.7 ab	29.8 abc	28.6 abc
T60_3	27.3 abcd	29.7 ab	31 abc	30 ab
T60_10	18.7 f	26.6 b	34.7 a	32.5 a
T300_1	28.3 ab	30.8 ab	30.2 abc	29.6 ab
T300_3	23.6 cde	28.1 ab	30.3 abc	29 abc
T300_10	23.3 de	29.5 ab	25.9 bc	19.2 d
TS_1	28.1 ab	31.6 ab	32.4 ab	32.4 ab
TS_3	27.6 abc	28.1 ab	31 abc	30.3 ab
TS_10	24.5 bcde	27.1 b	21.5 c	32.9 ab
TC	29.5 a	33 a	32.8 ab	30.2 ab

data transformed Y⁵* and Y⁻³*

Appendix S – Leaf area (cm²) of *Phaseolus vulgaris* plants after different times of exposure (7, 14, 21 and 28 days) to nanoparticles dispersions and ZnSO₄ solutions. Same letters in the same column indicates that means are statistically the same, by Tukey test with p<0.05.

Treatments	Leaf Area (cm ²)			
	7 dias	14 dias	21 dias	28 dias*
T40_1	192.2 a	601.8 a	1182.5 a	2255.0 a
T40_3	132.8 bcd	246.8 cde	750.1 bcd	430.3 cde
T40_10	98.4 cdef	112.2 de	126.4 e	182.0 efg
T60_1	189.4 a	554.2 a	890.8 b	1096.9 b
T60_3	125.1 cde	257.2 bcd	907.6 b	354.5 def
T60_10	87.4 def	104.7 de	100.9 e	148.8 fg
T300_1	183.4 ab	523.1 a	826.2 bcd	1056.2 b
T300_3	107.1 cdef	315.9 bc	585.7 cd	741.8 bc
T300_10	71.7 ef	68.5 e	66.3 e	30.9 g
TS_1	122.4 cde	437.9 ab	802.8 bcd	570.6 cd
TS_3	83.2 def	187.2 cde	555.4 d	538.9 cd
TS_10	59.5 f	69.4 e	58.3 e	67.6 g
TC	149.7 abc	531.1 a	692.4 bcd	501.8 cd

data transformed log(y)*